OBSERVATIONAL EXTRAGALACTIC ASTRONOMY: AN INVESTIGATION OF SOUTHERN QUASARS AND RELATED OBJECTS.

A thesis
submitted in partial fulfilment
of the requirements for the Degree
of
Doctor of Philosophy
in the
University of Canterbury
by

G. F. Gilmore

University of Canterbury
1979

ABSTRACT

An observational programme to monitor the optical variability of southern quasars has been established and operated at Mt. John University Observatory. This programme, which is the first in the southern hemisphere, involves systematic observations of a large sample (~130 sources) of both radio- and optically-selected quasars.

Because the observations are all obtained with a 61 cm telescope, broad-band photographic photometry is necessary to allow an adequate sample of sources to be studied. Because the observations are broad-band, standard methods of photographic data reduction are unsuitable. A generalised technique of data reduction has therefore been developed, tested and applied. This technique allows the detection of luminosity variations in a source with an accuracy limited only by the detective quantum efficiency of the photographic plate.

As a part of the application of the results of this programme to test the available source models, a generalised relation for the significance of inverse Compton scattering in an anisotropic source has been derived. The theory of incoherent synchrotron radiation in a source constrained by the inverse Compton scattering mechanism, has been applied to the source PKS 0537-441 to illustrate the application of this theory.

The observational results obtained have been applied as a test of the available quasar models. The simplest forms of the multiple independent-event (supernovae) and the spinar-giant pulsar models have been shown to be inconsistent with observation. The most active sources

observed are consistent with a model of a super massive black hole accreting mass at a rate determined by its Eddington luminosity.

CONTENTS

CHAPTER PAGE

CHAPTER PAGE

LIST OF TABLES

LIST OF FIGURES

PREFACE

The aim of the research programme described in this thesis is to obtain observational results which allow a critical analysis of the existing theories of quasar energy sources and radiation mechanisms.

The more plausible models of quasar energy generation are reviewed in Chapter 1, with special reference to their observational predictions.

In Chapter 2 the theory of incoherent synchrotron emission and inverse Compton radiation scattering is developed. This is applied in a derivation of the physical parameters of a typical very active source.

The observational programme is described in Chapter 3.

A new form of data reduction was necessary for this project. This is described in Chapter 4, which also contains a discussion of the corrections necessary for photometry of resolved sources.

The results obtained are presented in Chapter 5, and are applied in a critical test of the models summarised in Chapter 1.

The results obtained are presented in an appendix. A complete bibliography relevant to those sources studied here is also presented.

CHAPTER 1

QUASAR THEORIES

1.1 INTRODUCTION

For the purpose of this thesis, a quasar may be defined as a compact extragalactic source of non-thermal radiation, with an optical flux at least comparable to the integrated starlight of a typical galaxy. A variety of models of quasars have been proposed. The less speculative models available in the literature are reviewed here under five sections, corresponding to the mechanism of energy generation and/or release. The sections are:

a) Thermonuclear generation;

b) Conversion of bulk kinetic energy;

c) Stellar disruption;

d) Gravitational release by a non-collapsed object;

e) Gravitational release by a black hole.

Fundamentally, only gravitational or nuclear potential energy release is possible. This division however conveniently classifies the available models, even though the boundaries between these groups are often indistinct.

1.2 SUPER MASSIVE STAR MODELS

A single massive star could form in the potential well at the centre of a star cluster either by repeated coalescence of smaller stars, or by condensation of gas liberated during normal evolution of the cluster stars, and disruptive collisions between those stars (Sanders, 1970; Mathews, 1972, von Hoerner and Saslaw, 1976; and section 1.4 below).

Provided that the mass density in stars exceeds that in gas, objects of up to 10^7 $M_\odot$ can form. Such an object must lose angular momentum to avoid disruption by the bar-mode instability (Salpeter, 1971). If this can be achieved, it is possible for masses of up to $\sim 10^9$ $M_\odot$ to be stabilised by differential rotation. In this case, characteristic observable timescales would be the rotation period

$$T_R \sim 1.5.10^{-9}\left(\frac{2GM}{Rc^2}\right)^{-3/2}\frac{M}{M_\odot} \quad \text{days} \qquad 1.1a$$

and the period of fundamental pulsation

$$T_p \sim 10^{-7}\,\frac{M}{M_\odot} \quad \text{days} \qquad 1.1b$$

for radius R and mass M. The object's minimum radius is

$$R_{min} \sim 10\ R_{SCH} \qquad 1.2$$

where R_{SCH} is the Schwarzschild radius (Wagoner, 1969). For masses less than $\sim 3.10^6$ $M_\odot$ nuclear energy release can prevent collapse for some time, while for masses in the range 3.10^6 $M_\odot \leqslant M \leqslant 4.10^7$ $M_\odot$, collapse must continue in spite of nuclear burning (von Hoerner and Saslaw, 1976). Masses greater than 4.10^7 $M_\odot$ collapse inside the Schwarzschild radius before nuclear burning can begin. In this collapse, clouds with masses in the range 3.10^5 $M_\odot \leqslant M \leqslant 10^6$ $M_\odot$ could be expelled. This scenario is in agreement with the original analysis of Hoyle and Fowler (1963a, 1963b) who reached essentially the same conclusions.

The explosion of a massive object has been considered by Mollenhoff (1976), who noted that such an explosion into a mass distribution with a steep density gradient along the rotation axis would cause the ejecta to be focussed into oppositely directed jets. An injection of this type is consistent with the radio galaxy model of Ryle and Longair (1967).

The greatest limitation for models involving a super massive star is however not the stability restrictions but the efficiency of energy release. The gravitational potential energy of 10^9 $M_\odot$ in a sphere of 10 light hours diameter (required from the timescale for variability) is greater than the energy available from thermonuclear processes. It may also be released with considerably greater efficiency (up to 42% for a maximal Kerr black hole (Lynden-Bell 1971, 1978)) after collapse of the star than the thermonuclear energy can be before collapse (typically $\leqslant 0.5\%$). Therefore, even if a super massive star is stabilised for a time, its luminosity will be considerably greater after it becomes unstable and collapses, than during its stable evolution.

It is therefore unlikely that a super massive star releasing energy from thermonuclear processes is a viable model for the quasar phenomenon. It may however be relevant to less extreme forms of activity in galactic nuclei.

1.3 SHOCK WAVE MODELS

Shock waves may create energetic particles either by the conversion of bulk kinetic energy into particle thermal motions, or by direct acceleration in a relativistic blast. The former method was originally suggested in the context of quasar models by Osterbrock (1971), and was developed by Daltabuit and Cox (1972), Daltabuit and Cantó (1974) and Daltabuit et al, (1978).

The collision of two dense clouds with radii ~ 1 pc, mass ~ 10^6 $M_\odot$, and relative velocity ~ 10^8 cm s^{-1} would be required for a typical quasar luminosity. A pair of shock fronts would form, where the kinetic energy is thermalised, and absorbed in an adjacent H II region. While the details are model sensitive (density, velocity and radiation pressure being important parameters), the energy release would be from a low temperature black body and in emission lines.

The very large shock area (10^{38} cm^2 for a quasar luminosity) precludes short term variability. This, together with the dominance of thermal flux, makes this model untenable as an explanation of quasars' continuum emission. It does seem however to have some relevance to Seyfert galaxy emission line regions (Collin-Souffrin, 1978), and possibly therefore to quasar emission line regions as well.

A possible utilisation of shock heating by colliding clouds was presented by Fabian et al (1976), in their model of Centaurus A. They are able to explain the observed X-ray emission as thermal flux from a shock-wave-

heated accretion disk surrounding a 10^7 $M_\odot$ black hole. In this model infalling clouds undergo a velocity change $\geq$ 0.1c while shock-heating material in the disk. The heated material is that with angular momentum a in the range

$$a_{CR} < a < 30a_{CR}$$

where a_{CR} is the angular momentum limit at which direct accretion will form a disk ($a_{CR} = 2c \times R_{SCH}$).

A detailed study of the observational appearance of a propagating blast wave has been presented by Blandford and McKee (1976, 1977). They consider the evolution of an expanding, spherically symmetric, possibly relativistic shock wave. In this model, radiation is generated by synchrotron emission from electrons accelerated to relativistic energies behind the shock front. Because the acceleration is local to the emitting region, timescale and lifetime difficulties (cf. Chapter 2) with uniform spherical sources are alleviated.

Blandford and McKee provide expressions for the time dependence of both observables and the shock parameters. They illustrate their model for highly relativistic radiative blasts by numerically modelling the active sources 3C120, Centaurus A, and AO 0235+164. While these blasts are consistent with an origin from any of the energy release mechanisms considered here, they note that the 1975 outburst in AO 0235+164 released more than 1 $M_\odot c^2$ of energy. A normal supernova could not therefore be the source of this outburst.

Models of active sources involving shock waves

have also been presented by Christiansen and Scott (1977), Christiansen, Scott and Vestrand (1978), Marscher (1978a, 1978b), Mathews (1978), Rees (1978) and Blandford and Königl (1979). All these models involve the generation of a blast wave containing 10^{56} - 10^{57} ergs, from an unspecified origin. This energy is eventually radiated by relativistic particles accelerated in the shock front.

These models are able to account for the observed very rapid variations in total and polarised flux, as well as the short timescale decametric variations, while avoiding the inverse Compton inconsistencies inherent in most other models (Chapter 2).

The later evolution of the blast will result in fragmentation into $\sim 4\gamma^2$ fragments, each ram pressure confined, where γ is the blast wave Lorentz factor. This occurs because distant regions in a relativistically propagating shock are unable to communicate with each other. The effect of this fragmentation on the ability of the source to undergo rapid, large amplitude intensity changes has not been analysed. It is however likely that inhomogeneities in the ambient medium would produce a variety of evolutionary timescales in the fragments. If so, the intensity variations in the later stages of the evolution of an outburst should show low-level flickering superimposed on a slowing rate of decline, to a greater extent than the early evolution. A detailed analysis is however necessary to establish this prediction.

An interesting possibility in the earlier stages of shock propagation is the onset of pion pair production,

which will limit particle energies to 140 MeV. This value is significant in that a 140 MeV electron has a relativistic velocity, while a 140 MeV proton is a thermal particle. The source dynamics are therefore dominated by the inertia of the thermal protons, while the absence of thermal electrons produces a negligible Faraday depolarisation. This is consistent with the stringent limits on thermal electron content derived from depolarisation studies by Jones and O'Dell (1977).

Potentially the greatest relevance of shock wave models is to those sources which exhibit jet-like marc s structure and/or superrelativistic component separation velocities (Cohen et al, 1977; Readhead et al, 1978). In this scenario, rapidly variable and expanding sources are those in which the linear (jet) structure contains a blast wave which is propagating towards the observer. This leads to amplification of the luminosity and compression of the timescale of activity.

An example of a model of this type is that of Scheuer and Readhead (1970). In this model, radio emitting sources are irregularly ejected along a fixed direction from the source nucleus. These sources may be either blast waves (Blandford and Königl, 1979) or plasmons. Emission near the line of sight then corresponds to a radio emitting quasar, while emission at other angles corresponds to optically selected sources. This model is consistent with the observed value of ~1% of optically selected quasars which are radio detected. It is also consistent with a possible trend among non-radio

source quasars to be less optically variable than are radio source quasars (Faulkner and Gaskell, 1978).

The success of these models in explaining the observed activity in several active sources suggests that blast waves are a viable model for the luminosity variations in large amplitude variables. Their applicability to less active sources is however less clear. Kronberg and Clark (1978) for example were able to exclude blast waves as a possible model for the compact, non-variable source in M82. Similarly, the relevance of blast wave models to those sources which show rapid fluctuations without longer timescale variations is not clear.

1.4 STELLAR CLUSTER AND MULTIPLE SUPERNOVA MODELS

1.4.1 Multiple Pulsar Models.

An obvious endpoint of a stellar system which is dynamically stable for greater than the stellar evolutionary timescale is a cluster of pulsars. This situation was suggested as a quasar model by Kardashev (1970) and was developed by Arons et al, (1975). The justification of this model is the known ability of supernova remnants to emit high frequency power-law spectra. The superposition of many such sources might therefore reproduce quasar properties.

The Arons et al, model predicts the following observational properties:

a) Large outbursts are possible ($\Delta L > \frac{N+1}{N}$, L = luminosity, N = number of pulsars);

b) Doppler effects could allow rapid variations;

c) Outbursts should last longer in the red than the blue;

d) Soft X-ray bursts may occur;

e) The continuum in a flare will become redder, then bluer;

f) The spatial positions of detected bursts should be uncorrelated;

g) Outbursts will be more linearly polarised than average, and the degree will decline with time;

h) There should be no consistency in the position angle of polarisation in successive bursts.

Point f is a restatement of the "Christmas Tree" model of Dent (1972), but is not consistent with VLBI observations (Cohen et al, 1977). Similarly, the limited available data on polarisation variations (Schilizzi et al, 1975), and the observed continuity between nuclear and extended radio source structure (Readhead et al, 1978) suggest a fixed nuclear structure which is related to the extended components. This is not a natural feature of the Arons et al, model, and makes the model an unlikely explanation of the energy source in quasars.

1.4.2 Dense Stellar Cluster Models

A more plausible model is the earlier stage of evolution of a star cluster, when stellar interactions and supernovae may generate a significant luminosity. The dynamics of such a cluster have been reviewed by Saslaw (1973).

The general evolutionary scenario for a cluster of

10^8 solar mass stars is summarised below and in Figure 1.1. The details and references to recent work are available in, for example, Begelman and Rees (1978).

If the stellar density is sufficiently high for the rate of collisions to be significant, then there will be substantial liberated gaseous debris and/or many massive coalesced stars. The gaseous debris will condense to the centre of the cluster, and undergo new star formation. The stellar distribution will eventually settle into a cold disk distribution, which is globally unstable. Collisions will occur at an increasing rate, with energy release and the generation of more debris. This continues until the Eddington luminosity is reached, when radiation pressure prevents further new star formation. The debris will then form a massive cloud.

The later evolution of this system is dependent on the system angular momentum and its transport, and is therefore poorly understood. Possibilities include direct collapse to a single object (cf. Sections 1.2 and 1.5) or collapse to a black hole, possibly by way of fragmentation into many smaller objects (Section 1.6).

Stellar collisions leading to coalescence have been studied in detail by Colgate and his collaborators (Colgate, 1967; Colgate, Lee and Rosenbluth, 1970; Colgate, Colvin and Petschek, 1975; Petschek, Colgate and Colvin, 1976). These collisions lead to stars of $\sim 50\ M_\odot$, which rapidly evolve to supernovae, each releasing $\sim 3.10^{53}$ ergs. Ten such explosions per year would provide a quasar luminosity, with each supernova releasing ejecta

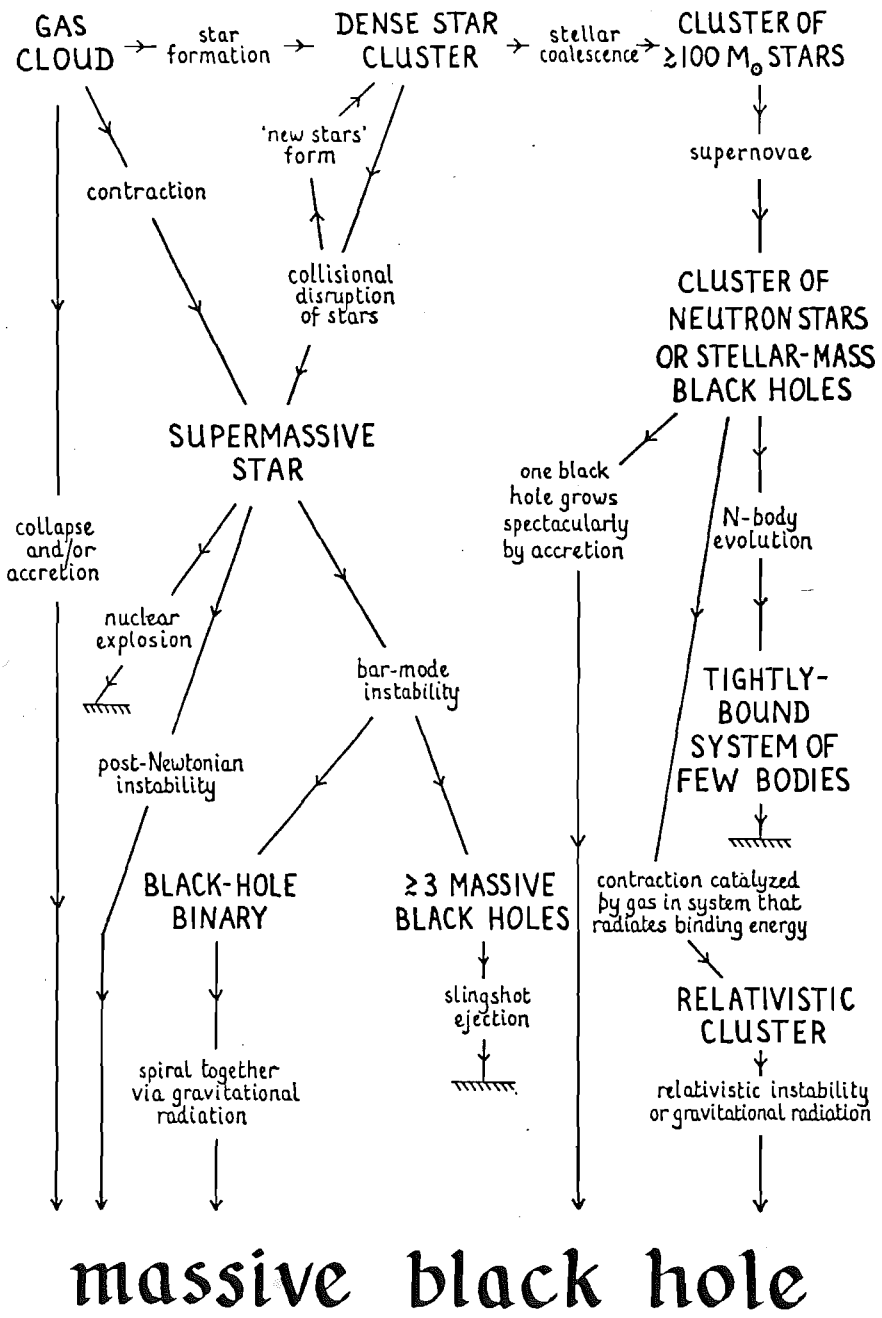

FIGURE 1.1 The evolution of a massive gas cloud to form a massive black hole. This diagram is taken from Rees, M.J., 1978 Observatory 98 210.

into an interstellar medium of electron density $\sim 10^6$ cm^{-3}.

Thermalisation of the ejecta would then lead to electron counterstreaming, and strong ion-acoustic waves, which drive plasma oscillations. Non-linear plasma wave interactions then generate many photons with frequency twice that of the plasma frequency. These are Compton scattered up in frequency until their number density exceeds four times the Planck distribution. Stimulated Compton scattering then takes over in the opposite sense. These 2 processes are in equilibrium when the photon frequency distribution is $N(\nu) \propto \nu^{-3}$.

Because higher energy photons are scattered low frequency photons, this model predicts that high energy variations occur one scattering time ($\sim 5.10^5$s) after the lower energy variations. It also follows that the characteristic time for a decrease in flux (which is controlled by the radiation energy loss rate) will be slower than the rate of increase (which is controlled by scattering in the source). These are also predictions of the multiple pulsar model (above, section 1.4.1).

A major limitation of Colgate's process of energy generation as described above is its inability to generate photons more energetic than microwaves. This limitation was confirmed in a detailed study by Jones and Kellogg (1972). Possible solutions to this problem involve photon scattering from coherent plasma waves (Ginzburg and Ozernoy, 1966), induced Compton scattering in a high radiation density environment (Levich and Sunyaev, 1970), or Cerenkov emission (Colvin, 1974).

This last possibility leads to the simple relation between luminosity L and Radius R:

$$L > 1.6 \times 10^{73} R^{-2} \text{ ergs } s^{-1} cm^{-2} .$$

Because source size determines the shortest timescale for significant variation, this implies that high luminosity sources should be the most rapidly variable. This correlation is tested in Chapter 5.

Tentative observational support for a multiple supernova model is provided by Fahlman and Ulrich (1975), who were able to decompose the light curve of 3C273 into a random superposition of supernova-like light curves. However, the pulse timescale they derive is an order of magnitude longer, and the energy release 3 orders greater than for a 1 $M_{\odot}$ explosion. Their analysis of the light curve has also been criticised by Ozernoy et al, (1976) who claim that the variations are periodic. If so, this would be inconsistent with the multiple independent-pulse model of this type.

A major conflict of the predictions of this model with observation is the constancy of position angle of polarisation from burst to burst. Schilizzi et al, (1975) for example report that the position angle of linear polarisation was constant from burst to burst to within 10^{o} for the source 3C120. A second difficulty with polarisation data is the required dominance of relativistic over thermal particle densities derived from Faraday depolarisation limits (Jones and O'Dell, 1977). If the plasma oscillation mechanism is to generate significant

photon fluxes, very high thermal particle densities ($\sim 10^{12}$ cm^{-3} for a source of quasar luminosity with a radius $\sim 10^{15}$ cm) are required. These are inconsistent with the depolarisation limits.

The prediction of high frequency activity one scattering time after low frequency variations was tested by Bekenstein and Rosencrantz (1978) who found that published data for OJ287 and BL Lac were consistent with delayed activity in U, relative to B and V. This however presumes that the model can be modified in some way to generate radiation at optical and infrared frequencies.

The lack of observational support for the predictions of the models discussed here makes them unlikely as viable models of the energy generation mechanism in quasars.

1.5 SPINAR AND MAGNETOID MODELS

A massive coherent object with energy release from angular momentum or gravitational potential energy conversion was first suggested as a quasar model by Morrison (1969). To stabilise such an object differential rotation, magnetic pressure or thermal pressure support is necessary.

The properties of an object of this type have been studied by many authors (Cavaliere, Pacini, and Setti, 1969); Cavaliere, Morrison and Pacini, 1970; Morrison and Cavaliere, 1971; Sturrock, 1971; Ozernoy and Usov, 1973; Ozernoy, 1974; Opher, 1975; Flasar and Morrison, 1976; Ozernoy, 1976; Ginzburg and Ozernoy, 1977; Ozernoy and Usov, 1977). For solid body rotation of an object of

mass M, radius R, angular velocity Ω, magnetic pole field strength Hp, and with magnetic axis inclined at angle χ to the rotation axis. The thermal (L_{TH}) and magnetic-dipole radiation (L_{MD}) luminosities are:

$$L_{TH} = 10^{46} \frac{M}{10^8 M_O} \quad \text{ergs s}^{-1}$$

and

$$L_{MD} = \frac{2}{3c^3} \, Hp^2 \, \Omega^4 \, R^6 \sin^2 \chi \quad .$$

Plasma surrounding the spinar at the light cylinder (defined as the radius $r = c/\Omega$) absorbs the low frequency radiation until the particles reach a Lorentz factor $\gamma \sim 10^3$. A magnetic field ~1 Gauss at this radius is postulated, in which these electrons will radiate at a frequency of 10^{13} Hz. Such a source would have a very steep spectrum at higher frequencies, and would be self-absorbed below $\sim 5.10^{12}$ Hz. Other possible energy release mechanisms include magnetic field line recombination (Sturrock, 1965; Piddington, 1970) or coherent emission by bunches of particles in the spinar magnetosphere (Cocke and Pacholczyk, 1975; Benford, 1977). Another possibility is synchro-Compton emission by particles accelerated into a cavity formed by the very low frequency (10^{-6} - 10^{-8} Hz) magneto-dipole radiation. In this case (Ozernoy, 1974) substantial infra-red emission will result, in agreement with observation. This model, however, also predicts that a decrease in flux will be less rapid than an increase. This is not supported by observations (Angione and Smith, 1972; and Chapter 5).

Independently of the emission mechanism, the spinar

will slowly contract to the radius

$$R \approx 4.10^{14} \left(\frac{z}{0.1}\right)^{-1} \frac{M}{10^8 M_\odot} \quad \text{cm}$$

with z the ratio of rotational to gravitational energy, at which it will collapse inside its Schwarzschild radius. Before this collapse three observational timescales are possible. The first is the rotational period

$$T_R = \frac{2\pi}{\Omega} \approx 800 \left(\frac{M}{10^8 M_\odot}\right)^{-1/2} \left(\frac{R}{10^{16} \text{cm}}\right)^{3/2} \quad \text{days.}$$

the second is the fundamental pulsational period

$$T_P = \sqrt{3/2} \quad T_R \ ,$$

and the third is the (semi-regular) mass-loss timescale

$$T_M \sim 100 \left(\frac{M}{10^8 M_\odot}\right)^{-3/2} \left(\frac{R}{10^{16} \text{cm}}\right)^{5/2} \quad \text{years.}$$

By identifying the short periods they derived from quasar and Seyfert galaxy light curves with T_R, and the longer quasiperiods with T_M, Ozernoy and Usov (1977) derive a typical spinar mass of $\sim 3.10^6$ $M_\odot$, and radius $\sim 10^{15}$ cm. A difficulty with such small masses is that very large energies ($\sim 10^{60}$ ergs = 10^7 $M_\odot c^2$) are stored in the extended radio components of radio-source quasars, and give every indication of having been supplied from the nucleus. Many spinars would therefore be required in a single quasar, and collimation of the compact and extended components becomes difficult.

A possible relevance of spinars to extended radio

sources is as an explanation of the 'hot spots' in the extended lobes (Flasar and Morrison, 1976). This suggestion is also consistent with the discovery of optical emission from compact components ($\leqslant$ 2 arc s) in the radio lobes (Saslaw, Tyson and Crane, 1978). In these sources, the electrons' radiative lifetime is very much less than the light travel time from the nucleus. In situ acceleration is therefore necessary. If spinars are present in extended radio components, a possible explanation is gravitational slingshot ejection from the nucleus (Burbidge, 1967; Saslaw, Valtonen and Aarseth, 1974).

Because a spinar is a single, rotating, coherent object, its most crucial observational test is the detection of periodicity in variable quasars. The presence of a true periodicity is a matter of some dispute. Some discussion and reference to the earlier literature is available in Chertoprud et al, 1973; Fahlman and Ulrich, 1975, Fahlman, 1977; and Belokon et al, 1978. In addition, Press (1978) provides some interesting cautionary remarks. If real periodicities can be found, it would a strong argument for a model of this type. Black hole models however would also be consistent with such an observation.

As in the case of the super massive star model (section 1.2), the inevitability of collapse to a massive black hole is a powerful argument against a spinar model for the dominant luminosity of a quasar. The efficiency of energy release from accretion onto this hole would be very much greater than the potential efficiency of the spinar, which is always much less than 1% (Opher, 1975).

This, together with the incorrect prediction of a luminosity decline which is more gradual than an increase, suggests that the spinar model of quasars is incorrect.

1.6 BLACK HOLE MODELS

All models of quasar energy sources require large masses (10^6 - 10^9 $M_\odot$) in small volumes (radii of 10^{13} - 10^{17} cm). The form in which this mass can generate the greatest luminosity with the greatest efficiency is as an accreting, rotating black hole. The necessary accretion rate is then

$$\dot{m} \approx 0.1\ \varepsilon^{-1}\ L_{TOT} \qquad M_\odot\ \text{year}^{-1}$$

to generate a total luminosity L_{TOT} (in units of 10^{46} ergs s^{-1}) for an efficiency ε. Spinar models have $\varepsilon << 0.01$, while thermonuclear processes have $\varepsilon < 0.01$. A maximal Kerr black hole has $\varepsilon = 0.42$. A given mass will therefore generate considerably more luminosity as an accreting Kerr black hole than in any other known form.

Excellent reviews of black hole accretion models have recently become available (Rees, 1977; 1978; Lynden-Bell, 1978) and contain details and references to the original literature. A summary of this model is presented below.

The prerequisite for this model is the formation of a black hole mass $\geqslant 10^3$ $M_\odot$. This might form by the direct collapse of a massive gas cloud, or the collapse of a precursor object (super massive star, spinar). The hole then accretes mass, part of which is radiated, either from the interstellar medium or from the capture

and/or tidal disruption of nearby stars.

This second possibility has received considerable recent attention because of its relevance to X-ray bursts from galactic globular clusters (Lewin and Joss, 1977). The most complete recent treatment is that of Shapiro and Marchant (1978) who Monte-Carlo modelled globular cluster and galactic nucleus stellar dynamics. Their study, which utilised a 2-dimensional simulation in energy-momentum phase space, also included the effects of a central black hole.

The effect of the hole is to modify the dynamics to a distance $r_h = GM_h/v_c^2$, where M_h is the hole mass, v_c the line of sight velocity dispersion $\approx (G\, m_* n_c r_c^2)^{1/2}$, with m_* a typical stellar mass, n_c the stellar density and r_c the core radius of the stellar distribution. A cusp will form in the stellar distribution, with $n(r) \propto r^{-7/4}$. Stars with low angular momentum orbits will occupy a "loss cone" in momentum space. Stars in this loss cone which orbit closer to the hole than $\sim 4.10^{13} \left(\frac{M_h}{10^7 M_\odot}\right)^{1/3}$ cm will be tidally disrupted, and their debris will be accreted. These orbits are repopulated by stellar dynamical relaxation interactions. Some of these interactions - those occurring closer to the hole than $\sim 7.10^{17} \left(\frac{M_h}{10^7 M_\odot}\right)$ cm - will involve physical collisions between the stars, which may lead to stellar disruption and/or coalescence.

Tidal disruptuon of stars by the hole will continue until the hole mass reaches $\sim 10^9\ M_\odot$, when the radius at which tidal disruption will occur is less than the

Schwarzschild radius ($\sim 3.10^{12}\left(\frac{M_h}{10^7 M_\odot}\right)$cm). Stars are then swallowed whole. This cutoff in the supply of debris for accretion is a natural cutoff to the highly luminous stage of a galactic nucleus.

Some indirect support for this suggestion is provided by the discovery of a central mass of $\sim 5.10^9 M_\odot$ in M87 (Sargent et al, 1978), which would then be a quasar nearing extinction. If this scenario is correct, giant radio galaxies with weak central components, such as Cygnus A, would typify a quasar's swan song.

The details of the accretion of this material, whether provided by normal stellar evolutionary mass-loss processes or by tidal disruption (the Black tide model) are well treated in the reviews mentioned above. The alternatives are either quasi-spherical accretion or via a disk. While the details of a specific model are sensitive to the assumed parameters, the general features of black hole accretion are fairly well established.

In an accretion disk, material slowly drifts inward to a radius r = 6x Schwarzschild radius, which is its last stable orbit, before it spirals into the hole. The particle's gravitational potential energy must be released, presumably through disk viscosity. The inner regions of the disk are unstable to small perturbations, especially so if the system luminosity is near the Eddington limit. This provides a natural explanation for variability among quasars, with the shortest timescale being the light travel time across the Schwarzschild radius. For a hole accreting at its Eddington limit this leads to the simple

relation between luminosity L and minimum timescale of variation (in the quasar's rest frame) t (Elliott and Shapiro, 1974)

$$t \geqslant 7.8.10^{-44} L \quad s.$$

this timescale limitation is considered for the sources studied in this thesis in Chapter 5.

A difficulty with simple accretion disk models is that the radiation should be thermal emission from the viscosity-heated disk, in contradiction to observations. The resulting spectrum should be the sum of the thermal spectra from all parts of the disk, none of which is likely to exceed $\sim 10^4$ ^{o}K, at which temperature radiative cooling is very efficient. If however the energy supply is sufficiently powerful so that this cooling limit is exceeded, the temperature will rise to $\sim 10^{10}$ ^{o}K, when non-thermal cooling mechanisms become significant.

If the disk-hole system is surrounded by a large, optically thick cloud, the radiation will be absorbed and thermalised. If not, line emission should be absent. This latter case was suggested by Rees (1977) as an explanation of the BL Lac type objects.

Other radiation processes which could be significant include magnetic field line winding and recombination, leading to particle acceleration and mass expulsion, non-linear plasma wave scattering, or particle acceleration in blast waves generated by bursts of supercritical accretion. This last possibility is considered in section 1.3, and appears the most likely explanation,

among those proposed to date, for large amplitude flares in active sources.

A possibly significant advantage of disk accretion models is their compatability with models to explain the observed linear structure and superluminal expansion in radio sources (Lynden-Bell, 1978; Blandford and Rees, 1978). A density gradient along the rotation axis would be expected, and this could allow the escape of hot plasma preferentially along oppositely directed beams, possibly those observed in recent VLBI studies (Readhead et al, 1978).

The other possible form of accretion is quasi-spherical infall. The interesting feature of this case is that the mass inflow can be sufficiently fast so that the radiation does not have time to diffuse out through it. This "one step forward, two steps back" model then provides a natural origin for a non-thermal spectrum. In the absence of efficient radiative cooling, the temperature must rise until significant non-thermal cooling intervenes near 10^{10} ^{o}K.

When this happens we can directly observe the regions near the Schwarzschild radius, and the Elliott-Shapiro timescale limitation becomes significant.

Indirect support for a model in which energy is released by accretion of mass lost by or tidally pulled from normal stars (Black Power Model) is obtained from the emission-line spectra. These are consistent in all cases with near-solar abundances of the heavy elements, as would be expected from matter which has been processed by stars.

This, together with the ability of the shock wave model to explain large amplitude variables, and the high radiative efficiency of a massive rotating black hole, make this model

the most likely of the available explanations of the quasar phenomenon. A more decisive conclusion must however await both greater refinement of the model, expecially the form of the expected radiation spectrum, and more detailed observations of a large sample of quasars.

CHAPTER 2

ANALYSIS OF SYNCHROTRON SPECTRA

2.1 QUASI-STATIC SYNCHROTRON SPECTRA

2.1.1 Uniform Source Spectra

The significant features of the continuous spectra of most quasars are:

i) a power law dependence of flux on frequency,

$$S_\nu \propto \nu^{-\alpha}$$

with α the spectral index, over much of the observed frequency range;

ii) a low frequency turnover; and

iii) a high frequency steepening.

These features are explicable in terms of synchrotron radiation from relativistic electrons which are distributed in energy as:

$$N(E)dE \propto E^{-\gamma},$$

where $\gamma \equiv 1+2\alpha$. (See O'Dell et al, 1978, for a discussion and several examples of spectra). Detailed discussions of the theory of synchrotron radiation are available in Ginzburg and Syrovatskii (1965; 1969), Pacholczyk (1970) and Moffet (1975). This theory then explains the high frequency steepening as due to depletion of high energy electrons by synchrotron radiation losses, and the low frequency steepening as due to self absorption. This latter effect will occur whenever the surface brightness temperature of the source is comparable to the kinetic temperature of the radiating electrons

(Williams, 1963). This becomes significant when the frequency is

$$\nu_m \approx 10\ S_m^{2/5}\ \theta_m^{-2/5}\ B^{1/5}\ (1+z)\ \text{GHz} \qquad 2.1$$

where S_m is the observed flux density at the self-absorption frequency ν_m, in Janskys (1 Jy = 10^{-26} W m^{-2} Hz^{-1} s^{-1}), θ_m is the source angular size at that frequency (arc s), B is the magnetic field strength (Gauss), and z is the redshift. For frequencies below ~0.5 ν_m the spectral index should be -2.5. The fact that this value is not observed is usually considered evidence of source structure, as in galactic HII regions.

2.1.2 Non-Uniform Source Spectra

The modifications to the spectrum of a source which is static but inhomogeneous have been discussed by Ozernoy and Sazonov (1971), Condon and Dressel (1973), Cavallo and Ventura (1975), de Bruyn (1976), and Marscher (1977).

These models are able to generate agreement with observed low frequency spectra by considering magnetic field and particle density gradients. They are also able to model complex spectra with a single component source, instead of the superposition of several compact components required under the assumption of uniformity. This modelling could be tested by multifrequency monitoring of a variable source which shows a complex spectrum.

The significant feature of these models is however a comparison of the physical parameters of the source

derived assuming both uniform and non-uniform sources (cf. section 2.2 for an example of such an analysis). Marscher (1977) finds that there is remarkably little difference in the values of these parameters. For non-uniform and uniform models with similar observational parameters, the derived physical parameters agree to within better than a factor of 2.7 for a typical case. This is considerably better than the uncertainty in determining most of these parameters, as a consequence of uncertainties in the observations.

An analysis of the type carried out in section 2.2 is therefore not critically dependent on the assumption of source uniformity.

2.1.3 Inverse Compton Scattering Constraints

The inverse Compton scattering process involves the scattering of a fast electron and a photon, with the subsequent production of a high energy photon and a corresponding decrease in electron energy. In a high radiation density environment these high energy photons may dominate the energy loss.

Hoyle, Burbidge and Sargent (1966) noted that the inverse Compton scattering of synchrotron radiation by the synchrotron emitting electrons could be used to constrain the angular sizes of compact radio sources, and therefore allow the determination of the source magnetic field by using equation 2.1. The ratio of the intensity of inverse Compton scattered radiation to synchrotron radiation is the ratio of the radiation energy density

to the magnetic field energy density. This ratio is conveniently expressed in terms of source brightness temperature, T_B, as

$$\frac{L_c}{L_s} \approx \frac{\nu_c}{2}\left(\frac{T_B}{10^{12}}\right)^5 \left\{1 + \frac{\nu_c}{2}\left(\frac{T_B}{10^{12}}\right)^5\right\} \qquad 2.2$$

where ν_c is the high frequency cutoff in the spectrum due to a finite maximum electron energy, and the second term represents second order scattering (Kellermann and Pauliny-Toth, 1969).

[Brightness temperature is defined as the temperature of the black body which would generate the same observed flux. It may be expressed conveniently as

$$T_B = 4.4 \times 10^{} \frac{S_\nu}{\theta^2 \nu^2} \ {}^oK \qquad 2.3$$

where S_ν is the flux (Jy) at frequency ν(GHz) from a source of angular size θ (milliarcsecs, ms).]

Equation 2.4 clearly shows the significance of a brightness temperature of $10^{12}{}^oK$. Below this value inverse Compton scattering is not important, while above it losses are proportional to $\left(T_B/10^{12}\right)^{10}$. Because the frequency of the scattered photon is increased by $\sim\gamma^2$, where γ is the electron Lorentz factor, a source of brightness temperature $\geqslant 10^{12}$ ^oK will emit a large flux of high energy photons. These may be scattered again, and so on. This continues until the unscattered photon frequency satisfies

$$\gamma h\nu > m_e c^2$$

when electron recoil in the collision becomes important. The electron cross section for further scattering is then no longer the Thomson cross section but the Klein-Nishina value, which effectively suppresses higher order collisions.

The time scale for an electron to lose 50% of its energy by synchrotron radiation is

$$T^{s}_{1/2} = \frac{422}{B^2 E} \text{ s (cgs units)} \qquad 2.4$$

where E is the energy of the electron, and H is the magnetic field strength perpendicular to the direction of the electron's motion. For typical source parameters, this time is $\sim 10^4$ years for an electron radiating at 1 GHz. In a source with $T_B = 10^{12}$ ^{o}K however, the inverse Compton timescale is ~1 day, and decreases as $\left({}^{T_B}/_{10^{12}}\right)^{-7}$.

It is therefore necessary that a viable source model allows the magnetic energy density to exceed the radiation energy density, or else is able to replenish the electron energies in times $\leqslant$ 1 day. The ability of the inverse Compton mechanism to generate high energy photons has led to a wealth of models of highly active sources in which the high frequency radiation is inverse Compton scattered from radio photons in a source with $T_B \sim 10^{12}$ ^{o}K.

An example is the variable radio, X-ray and γ-ray source in the nucleus of Centaurus A. Models of this source have been presented by Grindlay (1975), Beall et al, (1978) and Mushotzky et al, (1978). Grindlay assumes two synchrotron self absorbed components, with each supplying an inverse Compton scattered flux at higher frequencies. By allowing for synchrotron radiation and

adiabatic expansion losses, however, Mushotzky et al, require only a single component model.

Beall et al, present a model in which the scattered electrons are initially thermally generated, rather than by the synchrotron mechanism. They are then able to explain their observations by allowing for inverse Compton scattering of these photons off relativistic electrons, which are accelerated in situ in an adiabatically expanding plasma cloud.

The range of models for a single (relatively) well observed source often tells more about the observational uncertainties, and the allowable range of the adjustable parameters to permit an "acceptable" fit to those observations, than it does about the physics of the source. The success of synchrotron self-Compton models is then an indication that such models can be constructed to be consistent with observations, and is not conclusive evidence that the physical conditions in a particular source are well known.

The important feature of the inverse Compton process is that it provides a very tight limit on the allowable source size. Source sizes may also be measured interferometrically, or deduced from the time scale for significant variation, by simple causality arguments. In many cases this latter determination is inconsistent with the other values. This then indicates either relativistic effects or source anisotropy.

This latter possibility was considered by Woltjer (1966) who noted that the inverse Compton flux would

be reduced if the average pitch angle of the electron's velocity vector to the magnetic field direction was small. Defining this angle by ϕ, the ratio of equation 2.4 becomes

$$\frac{L_c}{L_s} = \frac{u_r}{2u_m}\left(\frac{1-\cos\phi}{\sin\phi}\right)^2 \qquad 2.5$$

integrated over all frequencies. This value however is based on an approximate derivation. More accurate derivations have been presented by Peterson and King (1975, for the isotropic source case) and Jones, O'Dell and Stein (1974a, for the general case). An independent derivation of the correct form of equation 2.7, obtained while the last two references were in press, is presented below.

This derivation follows the method outlined in Blumenthal and Gould (1970, ≡ BG).

The physical properties are defined in the figure, and there and below unprimed symbols refer to quantities evaluated in the observer's rest frame; primed values to those in the unscattered electron's rest frame.

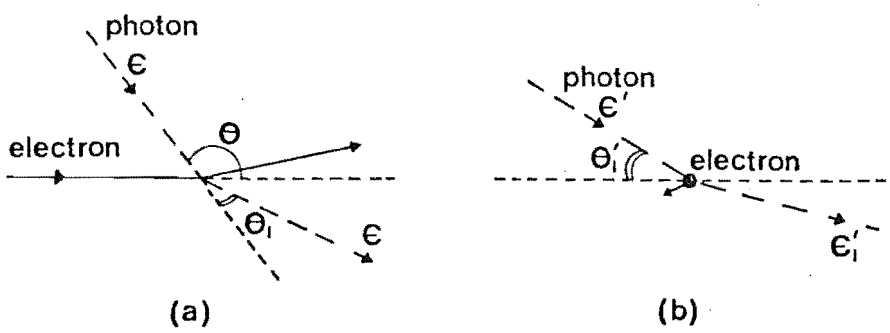

FIGURE 2.1: Inverse Compton scattering viewed by an external observer (a), and in the rest frame of the electron (b).

We have the usual relation for the energy of the scattered photon:

$$\varepsilon' = \gamma\varepsilon(1+\beta\cos\theta) \qquad 2.6$$

[Note: BG have $1-\beta\cos\theta$, which is incorrect], which gives a range of ε' of ($\beta \approx 1 - \frac{1}{2}\gamma^{-2}$) :

$$\left.\begin{aligned} \varepsilon'_{max} &= 2\gamma\varepsilon \quad (\theta=0) \\ \varepsilon'_{min} &= \frac{\varepsilon}{2\gamma} \quad (\theta=\pi) \end{aligned}\right\} \qquad 2.7$$

and

$$\varepsilon'_1 = \frac{\varepsilon'}{1+\left(\varepsilon'/mc^2\right)\left(1-\cos\theta'_1\right)} \qquad 2.8$$

and, for $\beta \approx 1$,

$$\varepsilon_1 = \gamma\varepsilon'_1(1-\cos\theta'_1) \qquad 2.9$$

We now assume a photon distribution which is isotropic within a cone of half angle ϕ, with axis along the electron velocity vector and zero elsewhere. This gives

$$\left.\begin{aligned} \varepsilon'_{max} &= \gamma\varepsilon(1-\cos\phi) \\ \varepsilon'_{min} &= \varepsilon/2\gamma \end{aligned}\right\} \qquad 2.10$$

and $\varepsilon' = \gamma\varepsilon(1+\cos\theta - \frac{1}{2}\gamma^{-2}\cos\theta)$

$$\pi \leqslant \theta \leqslant \pi - \phi.$$

We now use the invariant $\frac{dn}{\varepsilon}$, with dn the differential photon number density in the observer's rest frame. In this case it is:

$$dn = n(\varepsilon,x)\,d\varepsilon dx = \frac{n(\varepsilon)\,d\varepsilon dx}{1-\cos\phi} \qquad 2.11$$

where $x = \cos\phi$, and $n(\varepsilon)$ is the total differential density (integrated over angle). If $dn'(\varepsilon';\varepsilon)d\varepsilon'$ is the total differential photon density in the electron rest frame within $d\varepsilon'$ due to photons in the observer's rest frame within $d\varepsilon$, then:

$$\frac{n(\varepsilon)d\varepsilon dx}{\varepsilon(1-\cos\phi)} = \varepsilon'^{-1} dn'(\varepsilon';\varepsilon)d\varepsilon' \quad . \qquad 2.12$$

Equation (1) gives $\frac{d\varepsilon'}{dx} = \gamma\beta\varepsilon \approx \gamma\varepsilon$, which leads to:

$$dn'(\varepsilon';\varepsilon) = \frac{n(\varepsilon)\cdot\varepsilon'}{\gamma^2\varepsilon(1-\cos\phi)} \; S\left(\varepsilon';\ \frac{\varepsilon}{2\gamma}\ ,\ \gamma\varepsilon(1-\cos\phi)\right) d\varepsilon \qquad 2.13$$

where the step function S is defined as

$$S(x;a,b) = 1,\ a \leqslant x \leqslant b$$
$$= 0,\ x < a;\ x > b.$$

The distribution in angle and energy of the inverse Compton scattered photons, for fixed incident energy, is:

$$\frac{dN_{\gamma,\varepsilon}}{dt'\,d\varepsilon'\,d\varepsilon_1'\,d\Omega_1'} = dn'(\varepsilon';\varepsilon)\ \frac{c\cdot d\sigma}{d\Omega_1'\ d\varepsilon_1'} \qquad 2.14$$

where the scattering cross section is adequately approximated by the Thomson cross section in the case of interest. For an electron $\gamma \leqslant 10^4$, this is

$$\sigma_T = \frac{d\sigma}{d\varepsilon_1'\ d\Omega_1'} = \frac{1}{2}\, r_o^2(1 + \cos^2\theta_1')\,\delta(\varepsilon_1' - \varepsilon') \qquad 2.15$$

with $d\Omega_1'$ the element of solid angle.

The desired result is the distribution in energy of scattered photons, in the observer's rest frame, which is

$$\frac{dN_{\gamma,\varepsilon}}{dt\ d\varepsilon_1} = \iint_{(\varepsilon',\Omega_1')} \frac{dN_{\gamma,\varepsilon}}{dt'\ d\varepsilon'\ d\varepsilon_1'\ d\Omega_1'}\ \frac{dt'}{dt}\ \frac{d\varepsilon'\ d\Omega_1' d\varepsilon_1'}{d\varepsilon_1} \qquad 2.16$$

substituting $\eta_1' = 1-\cos\theta_1'$, we have ($\beta=1$):

$$\frac{dt'}{dt} = \gamma^{-1};\ \frac{d\varepsilon_1'}{d\varepsilon_1} = (\gamma\eta_1')^{-1};\ d\Omega_1' = 2\pi d\eta_1'$$

We now require the new limits on the step function S. For the Thomson scattering limit to be valid, $\varepsilon' << m_e c^2$ (511 keV), so 2.8 reduces to $\varepsilon_1' = \varepsilon'$, substituting in 2.9 gives $\varepsilon_1 = \gamma\varepsilon'\eta_1'$. The values for ε'_{max} and ε'_{min} in 2.10 then give

$$\eta_1'(min) = \frac{\varepsilon_1}{\gamma^2\varepsilon(1-\cos\phi)}$$

and $\eta_1'(max) = \frac{2\varepsilon_1}{\varepsilon}$ respectively.

Therefore 2.16 becomes:

$$\frac{dN_{\gamma,\varepsilon}}{dt\ d\varepsilon_1} = \frac{\pi r_o^{\,2} c}{\gamma^3(1-\cos\phi)}\ \frac{n(\varepsilon)d\varepsilon}{\varepsilon^2}\ \iint \frac{\varepsilon'}{\eta_1'}\,(2-\eta_1'+\eta_1'^{\,2})\,\delta\left(\frac{\varepsilon_1}{\gamma\eta_1'}-\varepsilon'\right) \cdot S\left(\eta_1';\ \frac{\varepsilon_1}{\gamma^2\varepsilon(1-\cos\phi)},\ \frac{2\varepsilon_1}{\varepsilon}\right) d\varepsilon'\ d\eta_1' \qquad 2.17$$

The integration over ε' is trivial with the delta function, while the limits on η_1' become

$$\text{upper limit on } (1-\cos\theta_1') = \min\left(2, \frac{2\varepsilon_1}{\varepsilon}\right) = 2$$

$$\text{lower limit} = \max\left(0, \frac{\varepsilon_1}{\gamma^2\varepsilon(1-\cos\phi)}\right)$$

The integration then becomes

$$\frac{dN_{\gamma,\varepsilon}}{dt\ d\varepsilon_1} = \frac{\pi r_o^2 c\ n(\varepsilon)d\varepsilon}{\gamma^4\varepsilon^2(1-\cos\phi)}\left\{2\varepsilon_1 \quad \ell n\left[\frac{\varepsilon_1}{2\gamma^2\varepsilon(1-\cos\phi)}\right] + \varepsilon_1 + 2\gamma^2\varepsilon(1-\cos\phi) - \frac{\varepsilon_1^2}{\gamma^2\varepsilon(1-\cos\phi)}\right\} \qquad 2.18$$

In order to evaluate the total scattering rate, it is necessary to specify a specific form of the electron energy spectrum. We assume a power law in electron energy with index p and high and low energy cutoffs γ_m and γ_o. That is

$$dN_e = k_e\gamma^{-P}\ d\gamma \qquad \gamma_o < \gamma < \gamma_m$$
$$= 0 \qquad \gamma_o > \gamma;\ \gamma > \gamma_m$$

this corresponds to a radiation spectrum which is also a power law with index $\frac{P-1}{2}$.

The validity of the Thomson limit provides a limit on the allowed range of γ. The restriction $\varepsilon_1 \leqslant \varepsilon_{1_{max}}$, and 2.7, 2.8 and 2.9 lead to

$$\gamma_{min} = \left(\frac{\varepsilon_1}{2\varepsilon(1-\cos\phi)}\right)^{\frac{1}{2}}$$

so we get finally,

$$\gamma_{min} = \max\left[\gamma_o, \left\{\frac{\varepsilon_1}{2\varepsilon(1-\cos\phi)}\right\}^{\frac{1}{2}}\right] \qquad 2.19$$

the total scattering rate is given by:

$$\frac{dN_{TOT}}{dtd\varepsilon_1} = \iint_{(\varepsilon,\gamma)} N_e(\gamma)\,d\gamma\ \frac{dN_{\gamma,\varepsilon}}{dtd\varepsilon_1} \qquad 2.20$$

which becomes

$$\frac{dN_{TOT}}{dtd\varepsilon_1} = \frac{k_e \pi r_o^{\,2} c}{(1-\cos\phi)} \iint n(\varepsilon)\,d\varepsilon \left\{ \frac{2\varepsilon_1}{\gamma^{4+P}\varepsilon^2}\ \ell n\ \frac{\varepsilon_1}{2\gamma^2\varepsilon(1-\cos\phi)} + \frac{\varepsilon_1}{\gamma^{4+P}\varepsilon^2} + \frac{2(1-\cos\phi)}{\gamma^{2+P}\varepsilon} - \frac{\varepsilon_1^{\,2}}{\gamma^{6+P}\varepsilon^3(1-\cos\phi)} \right\} d\gamma \qquad 2.21$$

The first of the γ integrations is conveniently carried out by substituting

$$Z = \frac{\varepsilon_1}{2\gamma^2\varepsilon(1-\cos\phi)}$$

which reduces it to the form $\int uvdz$, with $u = Z^{(P+1)/2}$, $v = \ell nZ$. This term finally becomes

$$\frac{4\varepsilon_1}{(p+3)^2\varepsilon^2}\,\gamma^{-(P+3)} - \frac{2\varepsilon_1}{(p+3)\varepsilon^2}\,\gamma^{-(P+3)}\ \ell n\ \frac{\varepsilon_1}{2\varepsilon\gamma^2(1-\cos\phi)},$$

while the other terms are straightforward.

We now evaluate this integral at a "typical" value of γ. It is necessary in doing this to assume that we are well away from the upper cutoff electron energy, and are also sufficiently far from the low energy cutoff. Specifically, we use the value of γ such that

$$\gamma_o < \gamma = \left\{ \frac{\varepsilon_1}{2\varepsilon(1-\cos\phi)} \right\}^{\frac{1}{2}} << \gamma_m\ . \qquad 2.22$$

When this value is substituted into the integrated form of equation 2.21, we get:

$$\frac{dN_{TOT}}{dt d\varepsilon_1} = \pi r_o^2 c\, k_e\, 2^{\frac{P+5}{2}} (1-\cos\phi)^{\frac{P+1}{2}} \frac{P^2+4P+11}{(p+1)(p+3)^2(p+5)} \varepsilon_1^{-\frac{P+1}{2}} \cdot$$

$$\int \varepsilon^{\frac{P-1}{2}} n(\varepsilon) d\varepsilon \qquad 2.23$$

This is simply $2^{-\frac{P+1}{2}} (1-\cos\phi)^{\frac{P+1}{2}}$ times the result for the isotropic case (BG equation 2.64), and reduces to it for $1-\cos\phi = 2$.

The electron index P is related to the photon index α, for incoherent electron synchrotron radiation where $F_\nu \propto \nu^{-\alpha}$, by $P = 1 + 2\alpha$. The observed range of α of

$$-0.5 \leqslant a \leqslant 2$$

gives a range of P of 0 to 5. The value of the correction term then ranges from

$$\frac{1}{2}(1-\cos\phi) \text{ to } \frac{1}{8}(1-\cos\phi)^3.$$

Through a less rigorous derivation, Woltjer (1966) derived the factor $(1-\cos\phi)^2$. JOSI quote the result (using $1 + \alpha \equiv \frac{P+1}{2}$), using a different derivation.

2.2 ANALYSIS OF THE CONTINUUM SPECTRUM

2.2.1 General Principles

An application of the theory of synchrotron radiation, together with the constraints provided by the inverse Compton mechanism, allows a determination of the magnetic field and visible angular size of a source. If a distance is available (from a redshift, assumed cosmological) the linear dimensions may be

calculated. If information on the timescale of variation is available, simple causality arguments also provide a lower limit to source size from this timescale. With this size, the source volume, and therefore the energy densities in magnetic fields, relativistic particles and electromagnetic radiation may be computed. Constraints on source geometry (isotropy and homogeneity), as well as a limit on internal relativistic effects, may also be derived.

This analysis is primarily based on equation 2.23. The details of the analysis are described by Jones, O'Dell and Stein (1974a ≡ JOSI; 1974b ≡ JOSII) and Burbidge, Jones and O'Dell (1974, ≡ BJO).

As an illustration of the application of equation 2.23 to the determination of source parameters, a synchrotron - inverse Compton model of the source PKS 0537-441 is constructed below. As noted in section 2.1.3 however, the ability to construct a self-consistent model of this type is not conclusive evidence that the derived physical parameters are meaningful. The range in the adjustable parameters, together with the observational uncertainties, make a variety of models possible. The three contradictory models of Centaurus A mentioned in section 2.1.3 illustrate this.

2.2.2 Observational Data for PKS 0537-441

2.2.2.1 Available information

The quasar PKS 0537-441 was identified by Peterson and Bolton (1972) with a $17^{m}.5$ object, variable

at radio and optical frequencies. A redshift of $z = 0.894$ was derived from 2 lines (Peterson et al, 1976), although the spectrum has often been reported as featureless (Eggen, 1973; Wall, 1974; Peterson et al, 1976). A.E. Wright (private communication) notes that because the lines are weak this redshift is provisional.

Optical photometry showing the object to be highly variable was reported by Eggen (1973), while Liller (1974) found similar behaviour from 430 Harvard archival plates. More recent optical photometry is by Adam (1978) and in this thesis. An Uhuru upper limit of 10^{-6} Jy at 10^{18} Hz is given by Ulmer and Murray (1976), derived from 8 observations in early 1971. Gubbay et al, (1977) report VLBI data at 2.3 GHz, while other radio observations, collected from the literature, are gathered in Table 2.1. The radio spectrum is illustrated in Figure 2.2, and bears some similarity to that of OQ172 (Gearhart et al, 1974). The maximum near 2 GHz is similar to that of PKS 1934-63 (Kellermann, 1966).

Radio variability has been established at 5 GHz (Peterson et al, 1976), 2.3 GHz (Nicholson, 1973; Gubbay et al, 1977) and 0.408 GHz (W.B. McAdam and A.J. Turtle, private communication).

In view of the source's variability, it is fortunate that such a large number of observations were obtained during the 1972 optical activity, including the VLBI data. This allows us to analyse the spectrum as described below.

TABLE 2.1

Frequency (GHz)	Flux (Jy)	Date	Reference
0.080	4±0.6	1972-1973 (5 observations)	1,2
0.085	4		3
0.160	3.3	1972-1973 (3 observations)	2
0.408	variable (25%)		4
1.410	2.70		3
1.420	3.0 (1.6±0.6% poln, p.a. $159^{o} \pm 15^{o}$)		
		1969.9-1970.7	5
2.3	4.98±0.13	1972.06 (3 components)	6
	5.04±0.13	1972.12 (2 components)	
	5.12±0.13	1972.55 (2 components)	
	4.00±0.11	1972.97 (2 components)	
	4.30±0.20	1973.52 (1 component)	
2.7	3.84	1971.7	3,7,8,9,10
2.72	3.5 (0.2 ± 0.2% linear polarisation)		
		1969.1,1969.7,1970.1, or 1970.7	5
5.0	3.80 (0.4±0.3% poln)	1971.2	5
	3.80	1971.8	3,9
	3.96	1971.8	7,8,10
8.87	8.69±0.46	1972.10	11
10^{9}	$< 10^{-6}$	1971.0-1971.25	12

References for Table 1:

1- Slee and Higgins, 1975; 2- Slee, 1977; 3- Bolton, 1977; 4- W.B. McAdam (private communication); 5- Gardner et al, 1975; 6- Gubbay et al, 1977; 7- Savage, 1976; 8- Peterson and Bolton, 1972; 9- Bolton and Shimmins, 1973; 10- Peterson, et al, 1976; 11- Shimmins and Wall, 1973; 12- Ulmer and Murray, 1976.

TABLE 2.1: Observational data for PKS 0537-441

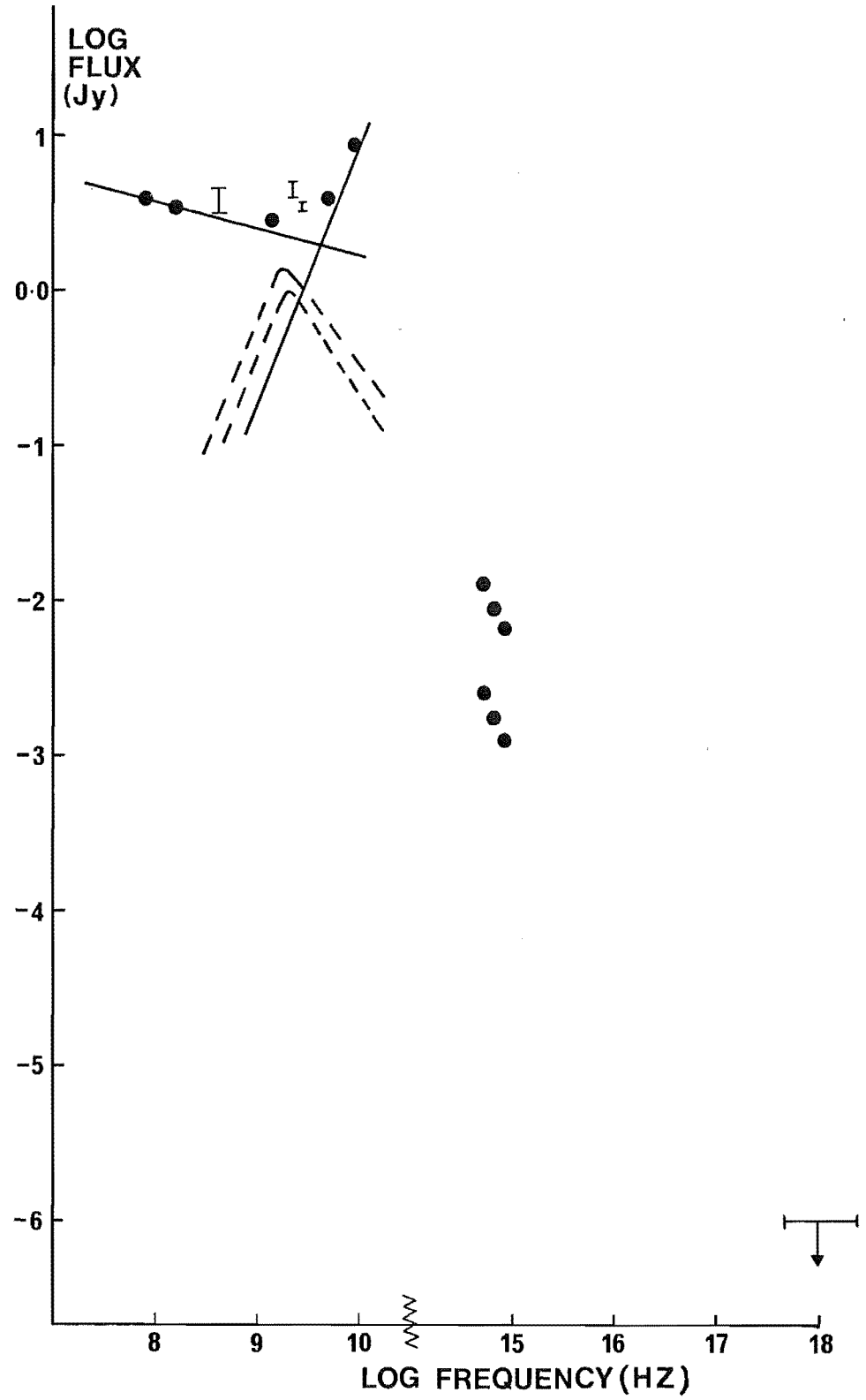

FIGURE 2.2 Published spectral data for PKS 0537-441 (solid points) and the two-component model used in the text. Note the break in the frequency scale.

2.2.2.2. Analysis into components

Eggen's V band photometry is presented in Figure 2.3 on a linear (intensity) scale, as is a possible decomposition into 2 flares. The most striking feature of Eggen's data is the change in U-B colour index after JD2441308. The mean U-B before this date is -0.52 (σ = 0.02), while after this it is -0.60(σ = 0.02). The mean B-V shows no change, and is, for all points, 0.46(σ = 0.02). This suggests a change in optical spectral index at this time, and is consistent with the double flare behaviour shown in the figure. The rates of flux increase and decrease are the same for the 2 flares, the first of which peaks near JD 2441310 with a flux of 11 mJy (m_V = 13.9), and the second at JD 2441420 with a flux of 14 mJy. These peak values are typical of minor flares in Liller's (1974) historical light curve.

Correcting these values for reddening following Kinman (1976), gives a corrected spectral index for the two components of

$$\alpha_{(B-V)_o} = 1.36 \; ; \; \alpha_{(U-B)_o} = 1.65 \text{ (component 1)}$$

$$\alpha_{(B-V)_o} = 1.36 \; ; \; \alpha_{(U-B)_o} = 1.28 \text{ (component 2)}$$

using Kinman's notation. We now approximate these (curved) spectra by single power laws of index 1.5 and 1.3 respectively.

The concurrent VLBI data suggest the presence of at least two compact ($\theta \leqslant 10^{-3}$ arc s.) components at 2.3 GHz, with a third unresolved at 1972.06, but not detected at

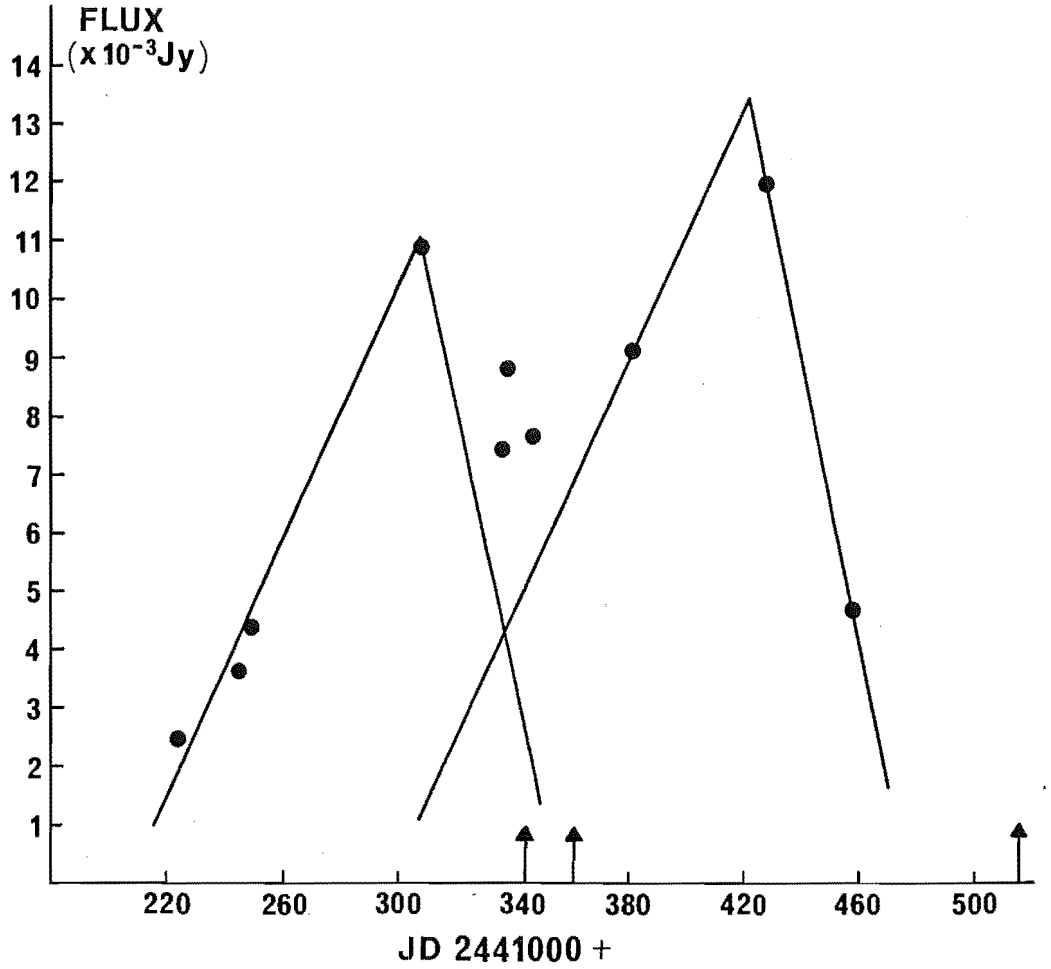

FIGURE 2.3 Decomposition of the optical photometry of PKS 0537-441 into two components. The arrows indicate the epochs of the 2.3 GHz VLBI observations.

1972.12. This may be explained by a decrease in resolved flux from this component to $\leqslant 0.5$ Jy, or an increase in size to greater than $\sim 10^{-3}$ arc s.

The radio spectrum shown in Figure 2.2 has been deconvolved into components assuming:

a) the halo component is adequately defined by the data at 80 MHz, and extends to at least 10 GHz (but see below). This component has a power law spectrum with index -0.3. However this value is not well defined over this narrow frequency interval.

b) The 5 GHz and 8.87 GHz data (with halo contribution subtracted) represent the self absorbed section of a component which becomes optically thin at high radio frequencies. This then has spectral index $\alpha = -2.5$ in the 5-10 GHz region. Provided this is a self absorbed component, or the sum of several such components, the turn-over frequency does not significantly affect the conclusions below.

c) The optical radiation is inverse Compton scattered from these radio components, one of which therefore has spectral index about 1.5, and the other about 1.3. While these spectra are much steeper than the $\alpha \approx 0.5$ usually adopted for variable sources, the fact that a consistent model can be derived illustrates the flexibility of models of this type.

The 2 compact components are then required to peak in the range 2.0 - 2.5 GHz, with maximum fluxes (epoch 1972.1) of ~ 1 Jy. The model parameters derived below are not sensitive to the exact values assumed.

If the halo component turns over below 2 GHz, then one of the 2.3 GHz compact components could be the extension of the self-absorbed higher frequency component. If so, the parameters derived below refer to the other compact component, which must become optically thin near 2.3 GHz. A possible scenario in this case is for the component which became resolved between 1972.06 and 1972.12 to be associated with the first optical flare; the second compact component, which peaks near 2.3 GHz, and was resolved by 1973.52 to be associated with the second optical flare; and the component which remained unresolved to be associated with the higher frequency source.

2.2.3 Derivation of the Source Parameters

The necessary observational parameters are: α, the optically thin synchrotron spectral index; ν_n, the frequency at which the source becomes optically thin; F_{ν_n}, the flux at frequency ν_n; $F^s_{\nu_s}$, the synchrotron flux at the optically thin frequency ν_s; $F^c_{\nu_c}$, the inverse Compton scattered flux at frequency ν_c; and E^{sc}_{ν}, the ratio between the power law extension of the synchrotron flux, and the inverse Compton scattered flux from the synchrotron emitting source.

BJO provide a general expression for the ratio E_ν^{sc} (their equation 12). This relation may be expressed in a more convenient form by substituting in the expression for the Lorentz factor of an electron radiating at the self-absorption frequency. By then choosing the values of the relevant parameters for the case of homogeneous, isotropic, quasi-static electron synchrotron radiation, with the turnover due to self-absorption, and converting the units of brightness temperature to degrees Kelvin, we get:

$$E_\nu^{sc} = \frac{F^c_{\nu_c}}{F^s_{\nu_s}} \left(\frac{\nu_c}{\nu_s}\right)^\alpha$$

$$= \frac{16\pi}{3} \frac{e^{sc}_{\alpha o}}{i^{2+2\alpha}_{\alpha o}} \ell n\ \Lambda\ \frac{r_e \nu_n}{c} (1+z)^{4+2\alpha} \left(\frac{kT_n}{m_e c^2}\right)^{3+2\alpha} \qquad 2.24$$

In this relation, $e^{sc}_{\alpha o}$ and $i_{\alpha o}$ are weak functions of spectral index and are defined and tabulated in JOSI, T_n is the source brightness temperature at frequency ν_n and Λ is defined in JOS I. Over the range of the first order Compton spectrum, $\Lambda = \frac{\nu_\ell}{\nu_k}$, where ν_ℓ and ν_k are the high- and low-frequency cut offs in the synchrotron component. The other parameters have their usual meaning.

This equation is quoted by Margon et al, (1976) but this paper contains a misprint in the definition of Λ. It is also often mentioned that the dimensionless functions of spectral index $e^{sc}_{\alpha o}$ and $i_{\alpha o}$ are of order unity. This however is misleading, as $i_{\alpha o}(1.5) = 0.114$. The factor $i^{-2(1+\alpha)}_{\alpha o}$ then has the value 5.19×10^4, which is far from order unity.

For PKS 0537-441, we may determine the flux at the Compton scattered frequency ν_c by using

$$F^c_{\nu c}\ (\mathrm{Jy}) = 3.85 \times 10^3 \times 10^{-0.4 m_v} \qquad 2.25$$

where m_v is the V-band magnitude. The necessary values for this source to be substituted into equation 2.24 are then:

$F^s_{\nu_s} = 1$ Jy $\qquad F^c_{\nu_c} = 1.4 \times 10^{-3}$ Jy

$\nu_s = 2.10^9$ Hz $\qquad \nu_c = 6 \times 10^{14}$ Hz

$\nu_\ell = 10^{10}$ Hz $\qquad \nu_k = 2.10^8$ Hz

$1+z = 1.894 \qquad \alpha = 1.4$

The following values for the source brightness temperature T_n are then derived:

$T_n = 4.1 \times 10^{11}\ ^oK \quad (\alpha = 1.3)$

$= 7.9 \times 10^{11}\ ^oK \quad (\alpha = 1.4)$

$= 3.4 \times 10^{11}\ ^oK \quad (\alpha = 1.5)$.

These are consistent with the value $T = \frac{10^{12}\ ^oK}{1+z}$ at which inverse Compton scattering becomes significant. These values of T_n imply $E^{sc}_\nu \sim 10^7$.

With these values it is straightforward to calculate the source visible angular size, using equation 4 in JOS II. Because the compact component is not directly detected however, it is necessary to derive synchrotron fluxes at optically thick and optically thin frequencies by assuming $\alpha = 1.4$ for

for $\nu >> \nu_n$, and $\alpha = -2.5$ for $\nu << \nu_n$. This leads to

$$\theta_{\pi/2} = 0.871 \text{ ms}$$

$$\theta_5 = 0.227 \text{ ms}$$

where one ms $\equiv 10^{-3}$ arc s, both values assume isotropy, $\theta_{\pi/2}$ assumes homogeneity, while θ_5 represents a source in which the photons and electrons are constrained to move within 5^{o} of each other's direction of motion. The VLBI measured angular size was θ = 1 ms, in good agreement with these values. These results are only weakly dependent on the value of the spectral index. For α = 1.3, the angular sizes are

$$\theta_{\pi/2} = 0.778 \text{ ms}$$

$$\theta_5 = 0.319 \text{ ms} .$$

Using the parameters listed above, the magnetic field can be calculated (JOSII equation 7), to give

$$B_{\pi/2} = 10.3 \text{ mG}$$

$$B_5 = 1.2 \text{ mG} .$$

It is also possible to derive the magnetic field strength corresponding to equipartition of magnetic and relativistic electron energy densities (JOSII, equation 8). This calculation requires the minimum electron energy in the source's flow frame of reference (γ^k), and the source's luminosity distance.

The first of these values may be found by inverting equation 2.8 of Moffet (1975) to give

$$\gamma^k = \left(\frac{4\pi m_e \; c \; \nu_k}{3e \; B}\right)^{\frac{1}{2}} \qquad 2.26$$

$$= 218 \text{ here.}$$

Similarly, the value of γ corresponding to ν_ℓ is

$$\gamma^\ell = 1.54 \times 10^3$$

The luminosity distance is cosmological-model dependent, within a factor ~2 for an object of redshift $z = 1$ (McVittie, 1974). The derived values are however only weakly dependent on this value. For this calculation the values $q_o = 1$, $^c/H_o = 6$ Gpc are used (Sandage, 1972). This gives a definition of luminosity distance as

$$D_\ell = 6Z \text{ Gpc}$$

$$= 5.36 \text{ Gpc for PKS0537-441.}$$

The equipartition magnetic field strengths are then

$$B^{eq}_{\pi/2} = 45 \text{ Gauss}$$

and

$$B^{eq}_{5} = 32 \text{ Gauss}$$

The disparity between these values and the actual source values indicates that the dynamics of the source are particle dominated.

The radiation energy density and magnetic energy density are independent of source distance, and may be readily calculated (BJO, equations 6 and 7) to give:

$$u_{m\pi/2} = 6 \times 10^{-8} \text{ ergs cm}^{-3}$$

$$u_{m5} = 8 \times 10^{-5} \text{ ergs cm}^{-2}$$

and

$$u_r = 7 \times 10^{-6} \text{ ergs cm}^{-3} \quad \text{(no angular dependence).}$$

These estimates are however very sensitive to uncertainties

in the other parameters, especially so for the magnetic energy density, and they should be considered very poorly determined.

The electron number density and the energy density of the electrons may also be calculated (BJO, equations 4 and 5). This calculation requires the source angular size to be converted to linear measure. This is also somewhat cosmological model dependent. The relation is approximately, suppressing relativistic and anisotropy corrections,

$$R = \frac{\theta_s D_\ell}{(1+z)^2} \quad .$$

This is more conveniently written as

$$R = 4.85 \frac{\theta_s D_\ell}{(1+z)^2} \quad \text{pc} \qquad 2.27$$

where now the units of θ_s are ms, and of D_ℓ are Gpc. Source anisotropy will scale this relation as $\frac{1}{\sin\theta}$, with θ the photon - electron interaction angle described above. The source transverse size is therefore:

$$R_{\pi/2} = 6.31 \text{ pc} = 1.94 \times 10^{19} \text{ cm}$$

$$R_5 = 1.64 \text{ pc} = 5.06 \times 10^{18} \text{ cm}$$

this then gives the following values for the electron number density - n_e, and the energy density in relativistic electrons - u_e:

$$n_{e\,\pi/2} = 425 \quad \text{cm}^{-3}$$

$$n_{e5} = 1{,}630 \text{ cm}^{-3}$$

$$u_{e\pi/2} = 0.12 \text{ ergs cm}^{-3}$$

$$u_{e5} = 0.59 \text{ ergs cm}^{-3}$$

These values are again very uncertain. We may then determine the total energy in the source U_{TOT}, to be:

$$U_{TOT\pi/2} = 3.52 \times 10^{57} \text{ ergs} \approx 2 \times 10^{3} M_{\odot}c^{2}$$

$$U_{TOT\ 5} = 3.19 \times 10^{56} \text{ ergs} \approx 2 \times 10^{2} M_{\odot}c^{2}$$

These values, while very uncertain, are typical of the results for equally active sources considered by BJO.

It is also possible to predict the X-ray flux due to second-order inverse Compton scattering. The first order spectrum extends to the frequency

$$\nu_{*}^{1} = \gamma_{n}^{2} \nu_{n} \left(\frac{\nu_{\ell}}{\nu_{n}}\right)^{2} (1-\cos\theta) \qquad 2.28$$

which gives

$$\nu_{*\ \pi/2}^{1} = 6.7 \times 10^{16} \text{ Hz}$$

$$\nu_{*\ 5}^{1} = 2.5 \times 10^{14} \text{ Hz}$$

the maximum occurs at

$$\nu_{*} \approx \gamma_{n}^{2} \nu_{n} \approx 10^{15} \text{ Hz}$$

The second order spectrum therefore peaks at

$$\nu_{**} \approx \gamma_{n}^{2} \nu_{*} \approx 10^{21} \text{ Hz}$$

with a flux

$$\left(\frac{\nu_{*}}{\nu_{**}}\right)^{\alpha} F_{\nu_{c}}^{c} \cdot E_{\nu}^{sc} \sim 10^{-2} \text{ Jy}$$

It should be noted that the definition of $\Lambda = \frac{\nu_{\ell}}{\nu_{n}}$

is no longer valid at these frequencies. The correct definition of E_ν^{sc}, which is very dependent on the frequency range considered, is given by Mushotzky (1976).

The inverse Compton flux at the Uhuru frequency of $\sim 10^{18}$ Hz would be $\sim 10^{-9}$ Jy, well below the Uhuru limit. Scatterings higher than second order are suppressed by the Klein-Nishina cutoff in cross-section.

Another constraint on the source can be found from the timescale for variation at 2.3 GHz. JOSII define a variability parameter i_v by

$$i_v = \frac{\theta_s D_\ell}{t_v (1+z) c} \qquad 2.29$$

where

$$t_v = \left| \frac{d \ \ell_n \ F_\nu}{d \ t} \right|^{-1} = \bar{F}_\nu \left| \frac{\Delta t}{\Delta \bar{F}_\nu} \right| \quad . \qquad 2.30$$

t_v is derived directly from observation, while i_v can be used to determine the extent of relativistic effects in the source. Any value of $i_v \geqslant 3$ indicates relativistic expansion, so that the source size derived from the causality relation can be consistent with the measured (VLBI) or deduced (see above) angular size, converted to linear measure assuming a cosmological distance. For $\beta_o = {}^{v_o}/_{c}$, and γ_o the relevant Lorentz factor

$$i_v \approx 3 \gamma_o \beta_o \quad . \qquad 2.31$$

For PKS 0537-441 the timescale t_v for variation at 2.3 GHz (from the data in Table 2.1) is

$$t_v \approx \bar{F}_v \left| \frac{0.42}{1.12} \right| \quad \text{years}$$

$$\approx 0.5 \text{ yr.}$$

This number is uncertain by ~100% due to the uncertainty in the mean flux from the variable component. Rewriting equation 2.29 in convenient units gives

$$i_v = 15.873 \frac{\theta(\text{ms}) \quad D_\ell(\text{Gpc})}{t_v(\text{yr}) \quad (1+z)} \qquad 2.32$$

which here gives

$$i_v = 78 \qquad (t_v = 0.5 \text{ yr})$$

$$= 26 \qquad (t_v = 1.5 \text{ yr})$$

which implies relativistic expansion with $\gamma_o \sim 10\text{-}20$, for an isotropic source. This is similar to the Lorentz factors quoted by BJO for CTA102 and 3C 454.3, which are equally active variables.

Because the Lorentz factor is not negligible, the parameters listed above must be corrected for the effects of time dilation. The relevant factors of γ_o for each parameter are tabulated in BJO (their table 4). The corrected parameters, assuming $\gamma_o = 15$, are listed in Table 2.2

It should be noted that the values of some of these parameters are very uncertain. In particular the ratio $E_{em} = {}^{u_e}/_{u_m}$ is proportional to (visible angular size)$^{-17}$, and is very poorly determined.

Consistent models for sources of this type can also be derived for relativistic blast wave models. Derivation of a consistent set of physical parameters from this

TABLE 2.2

$F^{s}_{\nu_s}$	Synchrotron Flux	1.0 Jy
ν_n	Self Absorption Frequency	2 GHz
α	Spectral Index	1.4
$F^{c}_{\nu_c}$	Inverse Compton Flux	1.4 mJy
ν_c	Inverse Compton Frequency	6.10^{14} Hz
E^{sc}_{ν}	Self-Compton Synchrotron Ratio	$\sim 10^{7}$
D_{ℓ}	Luminosity Distance	5.36 Gpc
T_n	Brightness Temperature	$\sim 5.10^{11}$ ^{o}K
$\theta_{\pi/2}$	Angular Size (isotropic)	0.78 marc s
θ_5	(anisotropic)	0.32 marc s
$R_{\pi/2}$	Physical Size	95 pc
R_5		25 pc
$B_{\pi/2}$	Derived Magnetic Field	0.15 Gauss
B_5		0.02 Gauss
$B^{eq}_{\pi/2}$	Equipartition Magnetic Field	670 Gauss
B^{eq}_5		480 Gauss
$u_{m\pi/2}$	Magnetic Energy Density	$1.4.10^{-5}$ ergs cm^{-3}
u_{m5}		0.02 ergs cm^{-3}
u_r	Radiation Energy Density	10^{-10} ergs cm^{-3}
$u_{e\pi/2}$	Electron Energy Density	10^{-8} ergs cm^{-3}
u_{e5}		5.10^{-8} ergs cm^{-3}
$n_{e\pi/2}$	Electron Number Density	6.10^{-4} cm^{-3}
n_{e5}		2.10^{-3} cm^{-3}
$E_{em\pi/2}$	Ratio u_e/u_m	7.10^{-4}
E_{em5}		3.10^{-6}
$E_{re\pi/2}$	Ratio u_r/u_e	10^{-2}
E_{re5}		2.10^{-3}
$U_{\pi/2}$	Total Energy Content	$1.4.10^{57}$ ergs
U_5		$2.2.10^{60}$ ergs

model merely indicates that such a model is possible. It does not exclude rival models. In general however, other models require numerical modelling, and are not amenable to a simple analytic treatment such as that above.

CHAPTER 3

THE CANTERBURY QUASAR MONITORING PROGRAMME

3.1 INTRODUCTION

Systematic optical monitoring of a sample of quasars to determine frequency, amplitude, and rates of variation has been carried out at Palomar (Peach, 1969), Herstmonceux (Penston and Cannon, 1970), Yale (Lü, 1972), Texas (Uomoto et al, 1976), Florida (Scott et al, 1976) and Asiago (Barbieri et al, 1977). Of these the Florida programme is the most systematic and substantial, and only it and the Asiago programme are continuing. In addition to these, many light curves have been derived for the brighter sources from Harvard Patrol plates (Angione, 1973; Liller and Liller, 1975; Heckman, 1976).

More recently, Usher (1978) and Usher and Mitchell (1978) have studied the variability of a sample of optically selected quasars using Schmidt plates of the Sandage-Luyten survey fields. Several radio-quiet sources are also included in the Florida programme (Edwards and Smith, 1977).

However, very few southern quasars have been studied. A compilation of 86 known variables in mid-1974 (Grandi and Tifft, 1974) listed only four south of $\delta = -20^{\circ}$. Similarly, the catalogue of quasars with measured redshifts compiled by Burbidge et al (1977) lists 73 known variables, of which only 7 are south of $\delta = -20^{\circ}$.

Because of this a systematic programme to monitor the optical behaviour of a sample of southern quasars

was initiated at Mount John University Observatory in late 1974. The aims of this programme were:

1) To provide reliable photometry of highly active sources with sufficient time resolution to detail their behaviour;

2) To monitor a sample of known quasars to determine rates, amplitudes and frequency of variation in an effort to constrain the available models;

3) To test possible correlations of optical activity with other source parameters.

A sample of radio-quiet quasars was added to the programme in early 1978 to allow the additional parameters of high redshift and low radio flux to be considered.

3.2 SELECTION OF SOURCES

An initial sample of approximately 100 quasars was selected from the Parkes radio source identifications. The selected sources had the following properties:

a) declination south of $\delta = -20^{\circ}$;

b) estimated magnitude brighter than 18; and

c) evidence of a compact high frequency component.

This third requirement was considered only when some rejection of sources satisfying the first two requirements was necessary, due to an unsatisfactory distribution in right ascension.

In addition six sources of the BL Lac type were included, although only three of these satisfied the requirements above. A seventh such source (PKS 0548-322) was later added, when its identification was available.

These sources are listed below (Table 3.1).

TABLE 3.1

PKS 0003-06	PKS 0537-441	PKS 1510-089
PKS 0048-097	PKS 0548-322	PKS 1514-242
PKS 0521-365		

Table 3.1 Known BL Lac-type sources included in the Canterbury Programme.

As of December 1978, a total of 139 objects has been observed usefully at least once. These are listed in Table 3.2. Of these sources, 11 have only upper limits available from the present observations, 7 are resolved galaxies (including 3 of the BL-Lac objects), and 4 are now known to be misidentified galactic stars. 85 of the 139 have measured redshifts, while a further 9 are known to have featureless spectra. 31 are not yet detected as radio sources.

In total 1,262 useful observations of the 139 objects have been obtained. Of these plates, 44 were obtained by Mr. Rod Austin and 159 by Mr. Mike Clark. The remainder, as well as all test and calibration plates were obtained by the author during a total of 409 scheduled nights at Mt. John Observatory.

3.3 OBSERVING PRIORITIES

An extensive study of the Mt. John Observatory's 61cm Optical Craftsman reflector was carried out by McKay (1972). He showed that this telescope (which has since been rebuilt)

TABLE 3.2

Object	# of plates	Notes	Object	# of plates	Notes
0000-398	1	A	0548-322	30	D,V
0002-422	1	A	0551-366	3	A
0003-06	6	B	0609-609	1	
0005-239	6		0622-441	17	
0007-353	1	A	0720-52	1	
0029-414	4		0743-67	31	D
0046-315	8		0829+047	4	
0048-097	24		0858-27	3	C
0049-393	1	A	0903-57	17	C,D
0118-272	3		0925-203	24	
0130-403	2	A	0959-443	2	
0135-247	13	D	1004-217	4	
0138-381	1	A	1010-427	13	C
0149-397	1	A	1020-103	1	
0149-474	1	A	1050-184	6	
0150-334	4		1053-282	17	C,D
0154-512	1	A	1101-264	8	A
0202-76	18	D,V	1101-32	16	D,V
0223-71	1		1104-44	13	
0230-790	2		1116-46	13	
0234-301	1	B	1117-248	16	D
0242-410	2	A	1206-238	5	
0302-623	2	B	1207-399	16	
0321-337	1	A	1233-24	16	D
0324-407	3	A	1240-294	10	
0329-385	2	A	1243-412	3	B
0331-654	3		1244-255	20	D,V
0334-359	2	A	1256-229	4	
0355-483	16		1300-243	9	A
0427-435	11		1311-270	4	
0439-433	5		1327-21	17	D
0453-423	3	A	1328-264	6	
0506-61	12		1349-439/1	21	D,V
0521-36	31	D,V	/2	21	A,D,V
0524-433	2	B	1355-41	23	D,V
0537-441	65	D,V	1420-27	11	

TABLE 3.2 (continued)

Object	# of plates	Notes
1422-29	14	D
1424-419	27	D,V
1448-232	7	
1451-375	15	
1510-089	43	
1514-24	66	D,V
1540-73	1	
1814-519	14	
1834-436	12	
1912-549	3	
1921-29	25	
1922-62	8	B
1933-400	18	D,V
1934-63	7	
1950-613	4	C
1953-325	6	
1954-388	30	D,V
2000-329	2	B
2020-370	15	D
2039-51	3	A
2040-374	4	A
2049-368	12	
2050-188A	2	
2052-47	24	D,V
2054-377	3	B
2055-440	3	A
2058-297	4	
2058-425	15	D,V
2112-407	4	A
2115-30	16	D,V
2116-358	4	A
2125-153.1	1	
2128-124	20	D
2138-377	11	
2144-362	4	
2155-152	1	
2204-540	9	
2219-394	3	A
2222-396	3	A
2223-051	1	B
2225-404	3	A
2226-41	10	
2227-399	5	
2240-26	8	
2245-328	2	
2251-178	4	A
2254+075	1	
2255-282	8	
2258-619	1	
2300-683	9	
2306-312	3	
2309-416	4	
2310-322	7	
2312-31	7	
2314-409	3	
2315-404	4	B
2321-375	3	
2326-477	7	
2329-384	2	
2331-241	1	
2340-567	5	
2350-338	2	A
2352-342	5	
2352-455	3	B
2353-683	8	A
2355-364	1	A
2357-348	1	A

TABLE 3.2 (continued)

Notes: A = non radio source; B = upper limits only from available plates; C = misidentified galactic star; D = data reduced and a light curve available; V = objects in group D which are definite variables

Table 3.2 Those objects which have been usefully observed at Mount John University Observatory as at December, 1978.

---

was unsuitable for direct photography to faint limiting magnitudes. The quasar monitoring programme was therefore carried out by image intensifier photography at the f/16 Cassegrain focus of this telescope. To allow observations of the maximum number of sources, all observations were unfiltered. A major defect in the telescope mirror mounting system produced large, unpredictable jumps in the optical axis, which led to the rejection of approximately 50% of all plates taken with this telescope. In addition, many of the remaining plates are of lower than average quality.

This situation was remedied in November, 1975, when a 61cm Boller and Chivens reflector became available. All observations after this date were made at the f/13.5 Cassegrain focus of this telescope.

The observing priorities were as follows:

1) 2-3 plates per month, if possible, of the known highly active sources (7 objects);

2) regular (once per month, weather permitting) observations of those quasars showing evidence of a compact, high frequency radio component (50 objects);

3) observations as time permits of sources without evidence for a compact radio component (57 sources);

4) from early 1978, observation of non radio source quasars, which were assigned to priority group 2) (27 objects).

All plates are visually examined at the end of each night, and objects showing variations are observed as in group 1) during the activity.

3.4 THE CANTERBURY PROGRAMME IMAGE TUBE

3.4.1 General Description

All observations were obtained with one of the 61cm reflectors described above, and a single-stage electrostatically-focussed image intensifier. This is a Varo type 8605, with a 40mm S20R photocathode, a 35mm P20 phosphor screen output, and fibre optic faceplates. Descriptions of the operation of such tubes are given by, for example, Coleman and Boksenberg (1976).

3.4.2 Spectral Sensitivity

The spectral sensitivity of this image-tube was measured by Dr. John Nicholas of the Physics and Engineering Laboratory, D.S.I.R., Lower Hutt. His results are shown in Figure 3.1a, while his report is reproduced in full in Appendix 1.

3.4.3 Sensitivity Variations

All image intensifiers show some non-uniformity of response over the photocathode, usually without azimuthal symmetry (Gudehus, 1970; Cromwell and Dyvig, 1973). There are two methods of calibrating this variation. The first involves a microdensitometer scan of a plate of the uniformly-illuminated photocathode. The second relies on observations of photometric standard stars in different parts of the photocathode.

3.4.3.1 Uniform Illumination Profile

Several plates of the twilight sky and the interior of the telescope dome were obtained, and scanned with the Joyce-Loebl microdensitometer. A typical scan is shown in Figure 3.1b. The overall sensitivity decline with radius is evident, as is the smaller scale fluctuation, due primarily to shear discontinuities and clumping of the fibre optics. The apparent increase in sensitivity near the edge of the field is due to a geometrical scale change which compresses the outer regions of the photocathode into a significantly smaller radius on the phosphor screen.

Because of the steep change in photocathode sensitivity farther than 10mm from the tube centre, no images recorded outside this radius were considered acceptable for photometry.

3.4.3.2 Standard Star Calibration

The second method utilises the position-dependent changes in apparent magnitude of a star of known magnitude to calibrate the sensitivity variations. Because

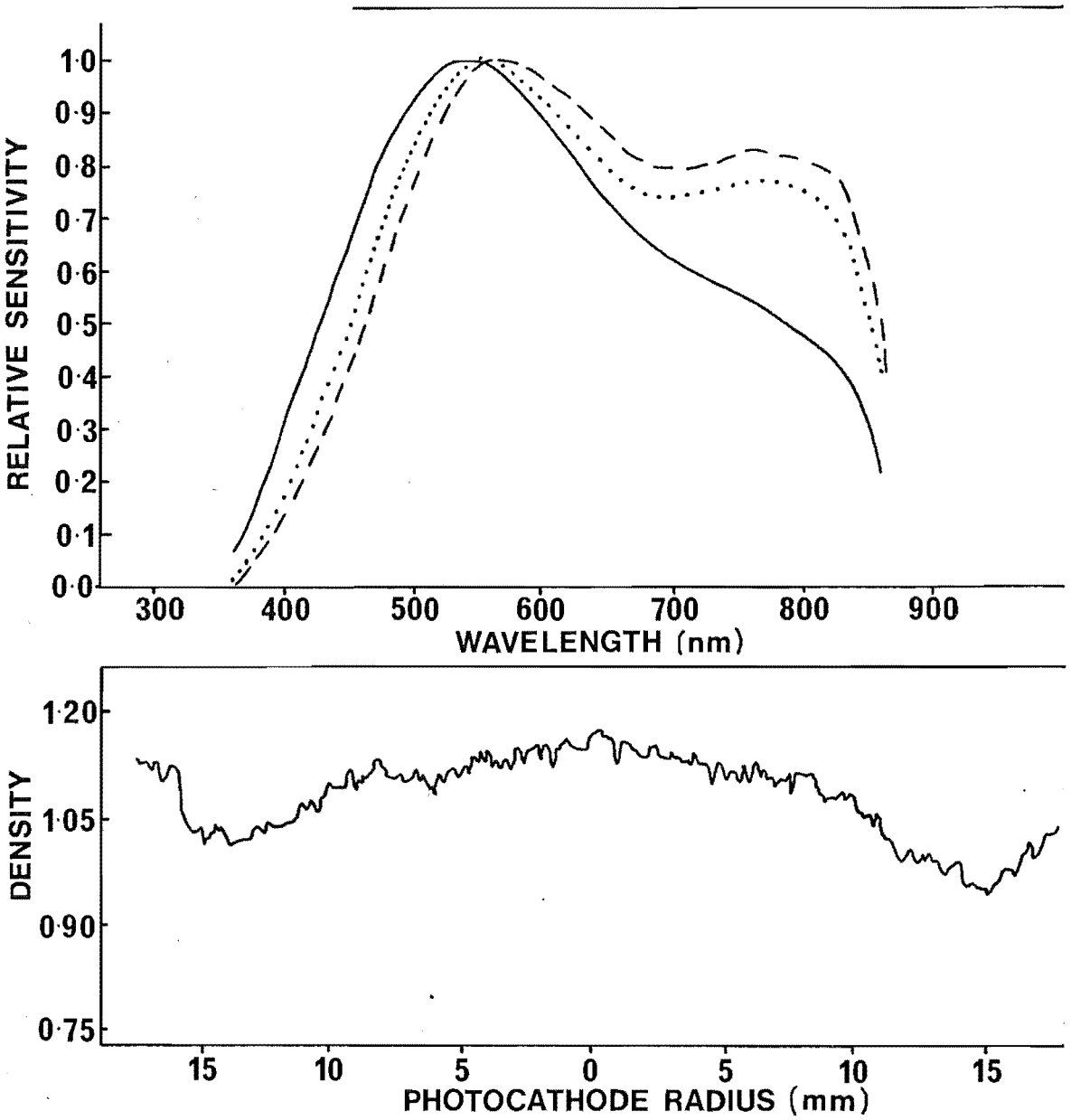

FIGURE 3.1 a) Spectral response of the Varo image tube at centre (solid line) and two edge (broken line) positions. Each curve is independently normalised to unity at 560nm. (Measurements by Dr. J.V. Nicholas - see text).

b) Microdensitometer tracing of a IIaD plate of the uniformity illuminated photocathode.

accurate magnitudes are necessary, observations must be in a standard photometric system. As an approximation to the standard V band, a combination of Corning 3-70 and 4-94 glass filters was used. The transmission of this combination, measured with the Cary Recording Spectrophotometer of the Physics Department, Canterbury University, is compared to the Johnson V band in Figure 3.2.

With this filter, 2 plates of the cluster NGC 2477 (Hartwick et al, 1972) were obtained, and 211 stars were iris photometered. This was done by Mr. Vince Ford of Mt. Stromlo Observatory. An iris reading-magnitude calibration was drawn for all points, and the deviation of each point from the mean relation was measured, assuming no error in the iris readings. The standard deviation of the 211 magnitude values defined by the iris readings was $0^{m}.11$. There was no significant dependence of magnitude residual on stellar magnitude, B-V colour, or sky fog reading adjacent to the star image.

The cathode was then divided into eight azimuthally equal sections, and the dependence of magnitude error on radius in each section was tested. There was no significant difference between the segments within a radial distance of 12mm on the phosphor. Outside this radius, fewer stars were available, but the scatter was observed to increase significantly. There is therefore no significant azimuthal asymmetry within this radius, in agreement with the results from section 3.4.3.1. When all stars are considered as a function of radius alone, the results presented in Figure 3.3 are obtained. A

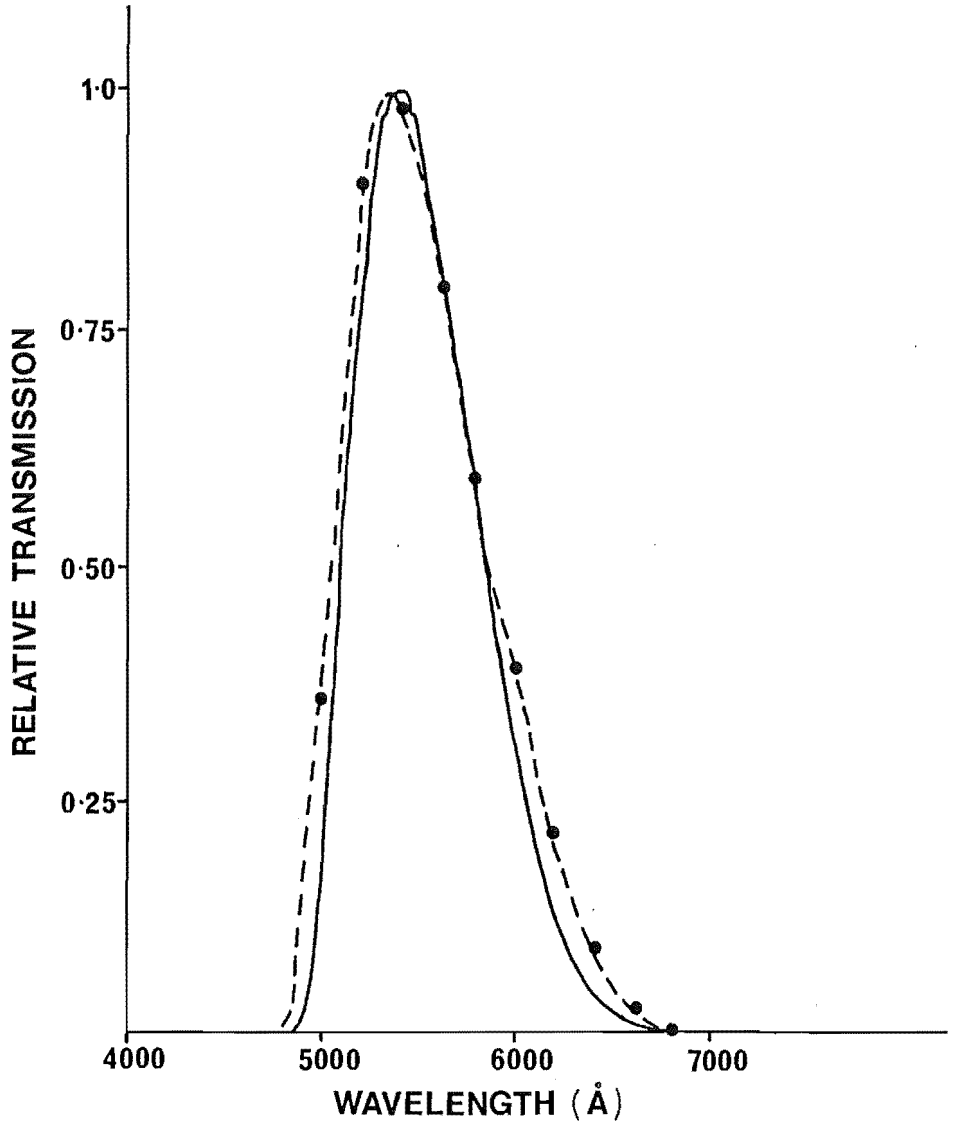

FIGURE 3.2 Spectral response of the composite Corning glass filter (solid line) and the Johnson V system (broken line).

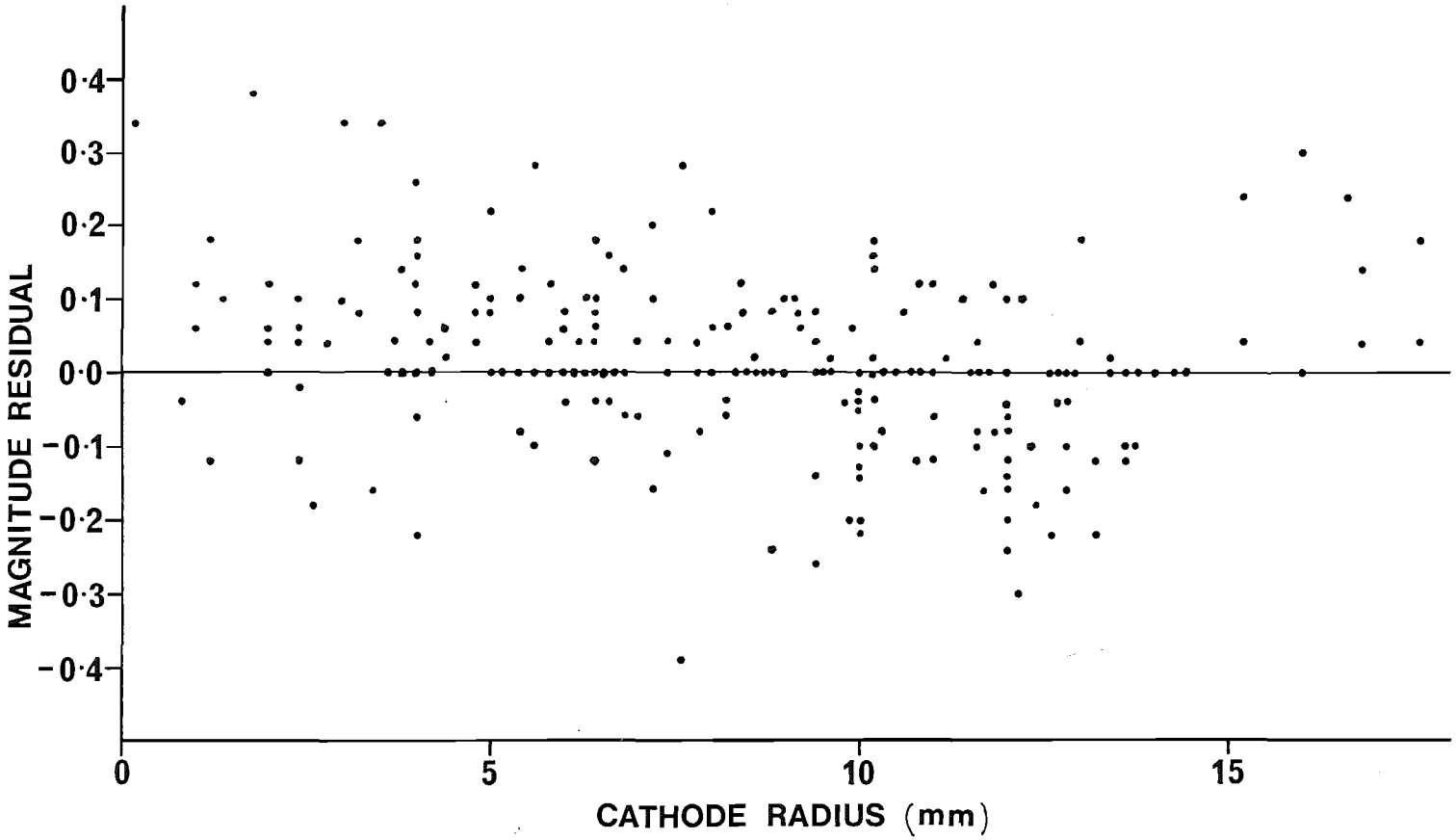

FIGURE 3.3 Radial dependence of photometric accuracy from observations of the photometric sequence in NGC 2477.

sensitivity gradient of $0^m.06$ over the inner 12mm radius (~5 arcmin radius) exists.

Because almost all observations of a given quasar field have the images positioned consistently to within at most 5mm of their mean positions, this variation will not affect the apparent magnitude of a given image, other than by a zero point term, by more than $0^m.02$, therefore, no correction for this sensitivity gradient has been applied.

3.4.3.3 Image Tube Background

Image intensification devices suffer from three sources of background light:

a) physically small ($\lesssim$ 0.1mm) high intensity spots. These may be readily distinguished from stellar images by their very high densities. They always occur at the same place on the phosphor, and are probably due to defective fibre optics. They disappear with tube use, and have not been detectable since the first few months of tube operation.

b) Large (2-3mm) low density flares. These are due to random ion events in the tube, and occur irregularly. Their rate of occurrence is however undetectably small after the first few minutes of tube use each night.

c) Dark current. This generates a low intensity background similar to sky fog. The tube used in this project is exceptionally low in background, both internally generated and light induced.

No detectable dark emission can be identified on a plate exposed for one hour to the phosphor with no light incident on the photocathode. Similarly, no detectable fogging can be discerned on the unexposed section of a plate of the phosphor with part of the photocathode masked off. The unmasked section was exposed to a density of 1.5D by uniform illumination. Therefore, if light induced background is present, it must occur on the same part of the exposed plate as the image itself. Tube background is not a significant factor at the light levels and exposure times in use in this programme.

3.5 OBSERVING PROCEDURE

Recording of the output image from the phosphor screen is achieved by placing a photographic plate in direct contact with the phosphor faceplate. Uniform contact is achieved by releasing a spring-loaded pressure plate, which holds the photographic plate firmly in position during exposure. An image tube camera incorporating a filter holder, shutter, and spring-loaded plate holder was designed and built for this project by Mr. Graham Kershaw of the Physics Department.

Operational procedure is as follows:

1) The image-tube faceplates are carefully washed with alcohol, and brushed with a camel-hair air brush.
2) The +6.75 VDC power supply is connected to the image tube. This is done at least 30 minutes before the first exposure to allow time for tube stabilisation.

3) The telescope is focussed by visual examination of a suitable star (6^m - 9^m) with a 10X lens. Focus is checked hourly through the night.

4) The telescope is set to the object's precessed position and the field centring is checked by comparison of the field seen through the guide telescope with a suitable finding chart. These charts were prepared by the author to the approximate scale of the guide telescope from the original negatives of the Mount John University Observatory Photographic Sky Survey (Doughty, Shane and Wood, 1972). These plates were kindly made available by Dr. Noel Doughty.

5) A suitable guide star is chosen, and centred in the guiding eyepiece by means of the X-Y offset system. A high power eyepiece is exchanged for the wide field eyepiece during exposure.

6) The photographic plate, which has been hypersensitised and cut to size as described below, is loaded into the plateholder, mounted onto the camera, and released against the faceplate.

7) Shutter operation is performed manually, and the exposure is timed with a standard darkroom timer. Initially, exposures were 30 minutes with IaE or IaO emulsion. With hypersensitised IIaD, exposures reach the sky limit in 10 minutes. The limiting magnitude under ideal conditions is then comparable to the limit of the POSS E prints.

8) After exposure, all plates have a previously unexposed area exposed for 10 minutes through a VG9 filter on a spot sensitometer. This sensitometer is identical to the Kitt Peak model described by Schoening (1976). The VG9 filter approximates the spectral output of the P20 phosphor.

9) At the end of each night all plates are tank developed in D19 at 20°C for 4 minutes with continuous agitation. Fixing and washing are as usual.

10) The next day the plates are catalogued, and compared to a print of an earlier plate of that field. In this way rapid variations may be detected and confirmed on the next fine night.

This visual examination led to the discovery and reporting of a 2^m flare with a rise and fall time both under 3 weeks in the quasar PKS 1954-388 (Gilmore, 1978a). This allowed a spectroscopic search using the Anglo-Australian Telescope (AAT) for possible line profile changes as a consequence of photoionisation effects (A.E. Wright, private communication). Another result was the discovery of supernova 1978a in MCG-4-32-23 (Gilmore, 1978b, 1978c). This galaxy is in the field of PKS 1327-21, and the supernova was discovered as a $17^m.5$ object approximately 25 arc s from the nucleus. The discovery plate was taken on 1978 May 8th, and a confirmatory plate the following night.

Later observations at the AAT (Elliott et al, 1978) showed it to be of Type V and of magnitude 20.0 on 1978

May 25th. Rather surprisingly therefore, it was still visible on a Mount John plate taken on 1978 June 12th.

3.6 PLATE HYPERSENSITISATION

Initially, observations were on Kodak spectroscopic plates, type IaE (usually) or IaO (rarely). IIaD plates have a higher resolution, and are a good match to the P20 phosphor (Millikan, 1972). Therefore they were adopted when hypersensitising facilities became available.

An excellent review of hypersensitising techniques relevant to all types of astronomical emulsions, with references to the original literature, has recently become available (West and Houdier, 1978). The details will not therefore be repeated here.

The two forms of hypersensitising most suited to IIaD plates are baking in a nitrogen atmosphere and soaking in a hydrogen atmosphere. (A third treatment, baking in forming gas, has recently been suggested, but has not been tested at Mount John (Scott et al, 1977)). These two treatments are chemically independent, and are additive (Scott and Smith, 1976). A series of tests was carried out to determine the most suitable combination of these treatments for present purposes.

3.6.1 Experimental Procedure

The plates used in these tests were three 4 inch x 5 inch IIaD's from batch HD1L6. One of the plates was baked for 12 hours at 65^{o}C in dry nitrogen, one was baked for 4 hours, and the third was not baked. The oven was especially designed in the Physics Department workshop to ensure a

uniform temperature throughout, and a uniform flow of preheated gas over the emulsion's surface. A 0.5 litres per minute flow of dry nitrogen is used to ensure efficient removal of outgassed impurities from the emulsion.

Each plate was then cut into four sections, and one section of each plate was soaked in hydrogen for 9 hours, 4 hours and 1 hour respectively. The remaining sections were untreated. Hydrogen treatment consisted of vacuum pumping the container, filling to one atmosphere pressure with hydrogen, vacuum evacuation again, and refilling with hydrogen to one atmosphere pressure. Plates were left to soak at 20^{o}C until further evacuation and flushing with dry nitrogen at the end of the soaking time. The plates are stored in dry nitrogen until use.

After treatment, all plates were exposed for 10 minutes through a VG9 filter on the spot sensitometer described above. This choice of filter and exposure time matches the exposure to the P20 phosphor during quasar observations. All test plates were developed together for 4 minutes in D19 at 20^{o}C.

Each plate was measured with a Joyce-Loebl micro-densitometer. Densities were calibrated by comparison with scans of a calibrated step wedge. The characteristic curve of each plate was drawn, and the exposure required to produce a density of 0.6 above fog was read off. The choice of this density is not critical as the curves are approximately linear and parallel above 0.4D. The inverse of this exposure was used as a measure of the "speed" of the emulsion.

3.6.2 Experimental Results

The results obtained are presented in Table 3.3, while some typical characteristic curves are shown in Figure 3.4. Total speed gains of up to 2.85 times, with fog increases up to 0.34D are indicated, in agreement with results by other workers (Miller, 1975). These gains would of course have been much greater had the chosen reference density been more appropriate to threshold detection. Hypersensitising produces a much greater effect near the toe of the characteristic curve, which is the region of importance for faint object photometry.

TABLE 3.3

Nitrogen (Hours at 65°C)	Hydrogen (Hours at 20°C)	Fog	Speed	Speed Gain
0	0	0.07	3.51	1.00
0	1	.07	3.70	1.05
0	4	.12	4.55	1.30
0	9	.12	6.25	1.78
4	0	.17	5.41	1.54
4	1	.17	5.71	1.63
4	4	.17	7.41	2.11
4	9	.18	8.20	2.34
12	0	.32	6.45	1.84
12	1	.34	6.90	1.97
12	4	.38	7.41	2.11
12	9	.41	10.00	2.85

Table 3.3 Results of the hypersensitising tests on Kodak spectroscopic plates, Type IIaD.

Because of the unavoidable increase in fog levels with long baking times, the hypersensitising technique considered most suitable for Mount John requirements is the following. Four hours baking in dry nitrogen at 65°C with a flow rate of 0.5 litres per minute, followed by 9 hours soaking in pure hydrogen at 20°C and one atmosphere pressure, and storage in dry nitrogen until use. Storage up to 12 hours is at 20°C, while for longer periods it is at 0°C. These results have been discussed elsewhere (Gilmore, 1978d).

3.7 PLATE CUTTING

At the beginning of each night, the 4" x 5" plates are cut into quarters. The correct procedure for this, which should be followed closely, is described by Miller (1969). A replica of the plate cutting device described in that reference was constructed in the Physics Department workshop from drawings supply by Mr. Miller. With care, plate wastage through breakage can be eliminated, as can the danger of damage to the image tube faceplate from glass chips.

3.8 PLATE MEASUREMENT

3.8.1 Choice of Comparison stars

Between 10 and 14 comparison stars were chosen for each plate to satisfy the following requirements:

1) To span the range of quasar variation, with as uniform a distribution in magnitude as possible;
2) To be as near as possible to the quasar on the plate;
3) In no case to be more than 10mm from the plate centre on more than ¼ of the plates;

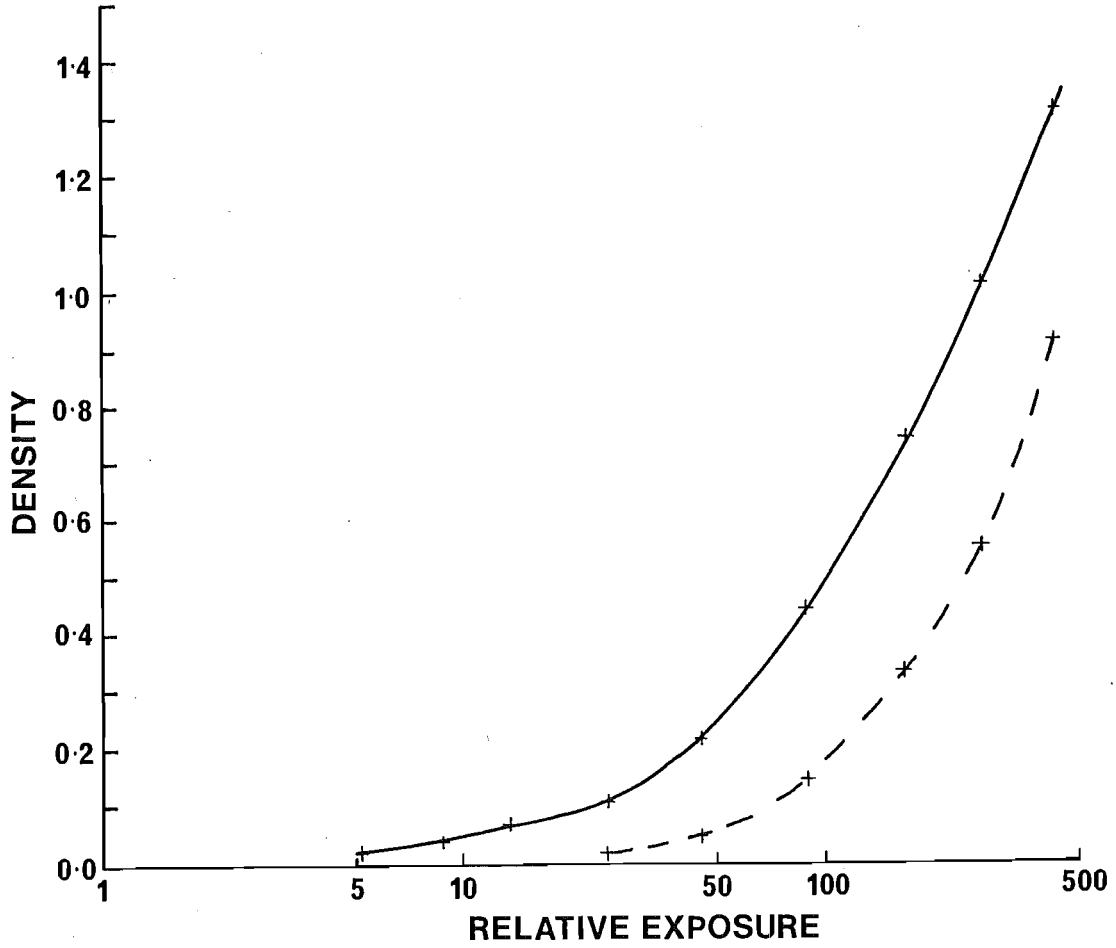

FIGURE 3.4 Characteristic curves for IIaD emulsion. Untreated (dashed line) and H_2-soaked plus N_2-baked as described in the text (solid line).

4) To be free from confusion with nearby images

In two cases (PKS 1514-242; PKS 2128-124) a comparison sequence was available near the quasar. In these cases the sequence stars were used as comparisons, subject to the above constraints. The results for these two fields are discussed in section 4.6.2.

3.8.2 Microdensitometry

The only microdensitometer available at Canterbury is a Joyce-Loebl Mk IIIc scanning microdensitometer, designed primarily for spectrum measurement. This densitometer is a dual beam device which compares the density on the photographic plate with that of a wedge with a linear density gradient. The position of the wedge is recorded graphically. The adjustable parameters relevant to its use for stellar image measurement are the dimensions of the measuring aperture, and the density gradient of the comparison wedge. The latter is limited in that the total density range must exceed the range of interest on the plate, while being sufficiently gradual to allow reliable magnitude discrimination.

An important consideration in the choice of projected aperture dimensions was noted by Cayrel (1953). Because the mean photographic density of two regions is not the arithmetic mean of their densities, a systematic error will be introduced by scanning an image with a slit large enough to encompass a wide range of densities. This effect has also been discussed by Wooster (1964) and Wlérick et al (1971). This effect is not an important consideration in this case, as any such systematic effects will be removed either in the data reduction process

(section 4.3) or in the later magnitude calibration (section 4.6).

After considerable experimentation, the most suitable aperture setting was found to be a square of projected size 300μ x 300μ on the plate for plates taken with the f/7 astrograph, and a square of size 130μ x 130μ on the plate for image tube plates. These settings ensure that all except the brightest stars to be measured are contained completely within the aperture, which therefore mimics fixed-iris type photometry. Because the brightest stars overlap the aperture, the densitometer response-magnitude relation flattens for these objects. The most suitable measure of densitometer response is then the maximum deflection of the density wedge above the mean value for the adjacent sky reading.

Because the illumination of the aperture is centrally peaked, considerable care is necessary in image centring. In practice, it is necessary to maximise the wedge deflection with the object in the aperture by use of the X-Y offsets, before scanning the image. This, combined with difficulties of image identification due to the small viewing screen (about 1 arc m. is visible) make accurate use of this machine very slow.

With this procedure, the series of 20 blue exposures of HD 199757 taken to calibrate the data reduction procedure (see section 4.4.4 for details) were measured and reduced. The mean accuracy of magnitude determination for this variable star was $\bar{\sigma} = 0^{m}.070$.

3.8.3 Iris Photometry

To remove the limitations of the microdensitometer, the Sartorius iris photometer of Mt. Stromlo and Siding Spring Observatory, Australian National University, was utilised for 3 weeks in November, 1977. All the plates reduced to date (apart from the 2 plates of NGC 2477 mentioned in section 3.2.3) were measured by the author at that time. In total, 519 plates were measured. The quasar and between 10 and 14 comparison stars were measured on each plate. Because of the sky fog variations, due to positional variations in the sensitivity of the photocathode, the sky fog level was measured adjacent to every stellar image.

The iris reading minus adjacent sky readings for the twenty plates of HD 199757 meantioned above, yielded a mean accuracy of magnitude determination for the variable of $\bar{\sigma} = 0\overset{m}{.}038$. The iris photometer is therefore approximately a factor of two more accurate than the Joyce-Loebl microdensitometer, and is considerably easier and faster to operate. As yet it has been possible to finance use of this iris photometer for only the period mentioned above. Therefore only those 519 plates (41% of the number available in December, 1978) have been measured and reduced to date.

CHAPTER 4

DATA REDUCTION

4.1 INTRODUCTION

There are currently three standard techniques for photometry of stellar images recorded on photographic plates. The most widely used consists of fitting a smooth curve through a measure of the integrated stellar image density and the magnitude of several comparison stars. The magnitude of any other object of interest is then read from this curve. This technique is described, for example, by Stock and Williams (1962), Weaver (1962) and Burkhead and Seeds (1971).

The second utilizes the brightness profile of an adjacent, bright field star, and is described by Kormendy (1973) and references therein.

Both these methods, however, require a least one suitable standard star in the field of interest. In some cases this may be an undesirable restriction. Examples include photometry at high galactic latitudes, in spectral bands where standards are sparse, or of high redshift objects, where the standard systems are not always the most appropriate.

This situation is considered in the third technique, which allows detection of stellar (or quasi-stellar) variability from photographic observations in the absence of any standard stars. It was devised by Penston and Cannon (1970) for the Royal Greenwich Observatory quasar patrol programme.

This technique however suffers from several limitations (see below, section 4.2.2). Because of these, a generalised version of this method has been devised, and is described in this chapter.

4.2 OTHER REDUCTION TECHNIQUES

4.2.1 Approximate Methods

Direct indications of object variability can be obtained from blink comparison (cf. for example, Mayer 1976), subtraction photography (cf. for example, Zwicky 1957), and by-eye estimation (Uomoto, Wills and Wills, 1976). None of these techniques, however, is capable of providing photometric information limited in accuracy only by the DQE of the photographic plate.

4.2.2 The R.G.O. Method

This was devised by Penston and Cannon (1970) to reduce the iris photometer results from the R.G.O. quasar patrol plates. By removing the dependence of the iris readings on the properties of one specific plate, this method produces plate-independent, though non-Pogson, measures of a quasar's apparent magnitude.

Mean iris readings are determined for each comparison star from all plates. Two simultaneous equations are then solved to determine both the standard deviation of each plate, and the coefficients of the curve relating the set of iris readings for each plate to the mean iris readings.

The final set of coefficients is used to scale the quasar iris reading to a plate-independent value, and the final standard deviation for each plate is a measure of

the reliability of this value.

Because of analytical difficulties, the weighted mean iris readings for the comparison stars, and the plate standard deviations are evaluated assuming the iris reading versus mean iris reading relation is a straight line. The scaled iris readings for the quasar, however, are evaluated from a quadratic. The reduction method also requires the replacement of missing or highly discrepant data points with the mean value for that star. This may impart spurious apparent accuracy to that mean value, and so reduce the reliability of the standard deviation appropriate to the reduced data.

A more rigorous algorithm has been devised in an attempt to remove these limitations. Tests of this method using simultaneous photoelectric and photographic observations of the short period variable ZZ Microscopii (HD 199757), show that photometric behaviour can be determined to within an accuracy limited only by the DQE of the photographic plate. No photometric information on any object in the field is necessary, other than non-variability of some comparison stars.

4.3 THE MODIFIED REDUCTION METHOD

We have a set of iris photometer readings

$$h_{ij} \quad i = 1, \ldots.s, s+1.$$
$$j = 1, \ldots.p.$$

of s comparison stars and the object of interest on each of p plates. Some of the h_{ij} may be missing. We adopt the null hypothesis that the apparent magnitude of each of

the comparison stars is constant. The h_{ij} will however not be constant for given $i \leqslant s$, because of differing observing conditions among the p plates.

We wish therefore to determine a plate-independent number for each star which is monotonically related to the star's apparent magnitude, and which may be used to calibrate this variation. That is, we wish to find the relation

$$G_i = a_j + b_j h_{ij} + c_j h^2_{ij} + \ldots \qquad 4.1$$
$$(i = 1,\ldots s; j=1,\ldots p.)$$

where G_i are the plate-independent comparison star values, and the a_j, b_j, c_j, etc., are the coefficients which scale the observed iris readings for plate j to these values.

At a first estimate of the G_i we form an unweighted mean iris reading - H_i - for each star from its observed reading on all plates:

$$H_i = \frac{1}{p} \sum_{j=1}^{p} h_{ij} \qquad (i = 1,\ldots s) \qquad 4.2$$

We are also able to estimate, by eye, the quality of each plate. This is used to form a first estimate of the plate standard deviation for the least squares routine described below.

At this stage in the RGO method, p quadratic equations of the form

$$H_i = a_j + b_j h_{ij} + c_j h^2_{ij} \quad (j = 1, \ldots p) \qquad 4.3$$

are fit by least squares to minimise

$$\sum_{j=1}^{p} (\epsilon_{ij})^2 = \sum_{j=1}^{p} \{H_i - a_j - b_j h_{ij} - c_j h^2_{ij}\}^2 \qquad 4.4$$

for each i. This sum of squared residuals is then used to derive the standard deviation of the residuals about the H_i, and this in turn is used to derive the standard deviation appropriate to the iris readings. It is this last step which requires the assumption of a nearly-linear characteristic curve (more specifically that $c_j h_{ij} << b_j$). If this restriction does not hold, the standard deviation applied to the scaled iris reading for the quasar from this plate will be in error, and any statistical test for variability will be similarly unreliable.

To avoid this, we fit equations similar to 4.3, but of arbitrary polynomial order, using a generalised least squares algorithm which allows for uncertainties in both dependent and independent variables. This algorithm was originally developed by Deming (1931), and was generalised by Brown (1955). A recent, less rigorous description is given by Brandt (1970).

The algorithm generates the polynomial coefficients and their uncertainties, a set of smoothed iris readings and their uncertainties, and a set of smoothed mean iris readings, and their uncertainties, for each plate. Denoting these latter two by H'_{ij} and s_H respectively, we can then form an updated mean iris reading $-H_i^{(1)}$ for each star by:

$$H_i^{(1)} = \frac{1}{p} \frac{\sum_{j=1}^{p} \frac{H'_{ij}}{s_H^2}}{\sum_{j=1}^{p} \frac{1}{s_H^2}} \qquad 4.5$$

The uncertainty of the smoothed iris readings is then used as a better estimate of the uncertainty of the original iris readings. Using this weighting, the original iris readings are refitted to the updated means $H_i^{(1)}$. This produces a new set of smoothed values which is used to form a new weighted mean - $H_i^{(2)}$ - and to further update the uncertainty of the original iris readings. This iteration is continued until consecutive estimates of the weighted mean converge.

If the mean for a particular star does not converge, the original iris readings are examined for discrepant points. To do this the value of iris reading which corresponds to the current values of the mean is found and denoted c_{ij}. A measure - f_j - of the plate standard deviation is then formed from:

$$f_j = \left\{ \frac{\sum_{i=1}^{s} (h_{ij} - c_{ij})^2}{s - K_j - NR} \right\}^{\frac{1}{2}} \qquad 4.6$$

where K_j is the number of missing iris readings on plate j, and NR is the degree of the polynomial used in the curve fitting. The denominator corrects for the reduction in the number of degrees of freedom caused by the curve fitting.

Any iris readings for the non-convergent star which are more than 3 standard deviations from the value c_{ij} are set to zero (Chauvenet's criterion). This is physically justified in that a non-normal error distribution is caused by photographic plate defects, which impose a small number of highly discrepant points on the normal distribution. These points are usually

visually detected during plate measurement, but if missed are rejected here. The various criteria for rejection of discrepant points are referred to in Harter (1976) and references therein (and cf. Kinman et al, 1968).

This form of reduction has the added advantage that points discarded or missing need not be interpolated. The number of degrees of freedom for the relevant plate is simply reduced by one, and reduction proceeds normally.

When the mean values for all stars have converged, we have a final set of coefficients which scale the original iris readings of both the comparison stars and the suspected variable to plate-independent values.

We also have two estimates of the standard deviation of the iris readings on each plate. The first is the "internal" estimate from the least squares fitting of the iris readings to the final curve. The second is the f_j formed from equation 4.6, using the final curve coefficients and weighted mean to evaluate c_{ij}. These are consistent provided a suitable choice of initial plate standard deviation, and the degree of the polynomial is made.

Finally, the null hypothesis of comparison star and suspect object constant intensity can be tested by χ^2.

4.4 TESTS OF THE METHOD

4.4.1 The Least Squares Algorithm

The least squares algorithm was tested both by reproducing the test data listed in Brandt (1970), which

was successfully recovered, and using several sets of artifically generated data.

The Mount John quasar monitoring programme is being carried out using a 61cm reflector and an unfiltered Varo single-stage electrostatic image intensifier with an S20R photocathode. To approximate the numerical range of image densities expected, a plate of M80 was taken with the same equipment and reduced against V magnitudes using the sequence of Harris and Racine (1974). The reduction was carried out using the first technique described in the introduction, henceforth referred to as the standard method. The plate was scanned with the Joyce-Loebl MkIIIc scanning microdensitometer of the University of Canterbury, with a square aperture of side 3 arcseconds. The derived relation between densitometer deflection - d_i - and magnitude over the range V = 12.0 to V = 18.0 was:

$$m_V = 18.0 - 0.12\ d_i + 2.1 \times 10^{-3} d_i^2 - 1.5 \times 10^{-5} d_i^3. \qquad 4.7$$

Fifteen points were then chosen separately from both uniform and random distributions between 0 and 1, and scaled to span the range of the densitometer deflections. Corresponding magnitudes were determined from equation 4.7. Random numbers from a distribution with zero mean, and standard deviations appropriate to magnitude uncertainties of $0^m.1$, $0^m.3$, and $0^m.5$ and the corresponding densitometer uncertainties were then added to these values. This produced 24 sets of noisy data randomly

scattered about a known curve, which were input to the least squares routine. A typical solution is shown in Figure 4.1 and the results are summarised in Table 4.1.

TABLE 4.1

True Coefficients	: 18.0	-0.12	2.1×10^{-3}	-1.5×10^{-5}
Recovered Means	: 18.1	-0.12	2.1×10^{-3}	-1.4×10^{-5}
Standard Deviation	: 0.1	0.01	2×10^{-4}	1×10^{-6}

Table 4.1 Results of 24 tests of a generalised least squares algorithm in the reduction technique.

4.4.2 Using Standard Stars

Using this curve fitting routine, the full reduction method was then tested. Eleven twenty minute exposures of a standard magnitude sequence in Aquila ($\alpha = 18^h\ 59^m.3$, $\delta = +04^\circ\ 50'$ (1950.0), Purgathofer 1969) were obtained on the nights of August 3rd, 1976, (3 plates), and August 20th, 1976, (8 plates). Kodak 1aO with Wr 2B filter and Mount John Observatory 10" f/7 astrograph were used to approximate the standard B band. The plates were measured on the Joyce-Loebl microdensitometer with a 200μ square aperture.

This data was used to test the reliability of the modified reduction techniques as a function of:

a) number of plates reduced,

b) number of comparison stars per plate, and

c) degree of polynomial in equation 4.1.

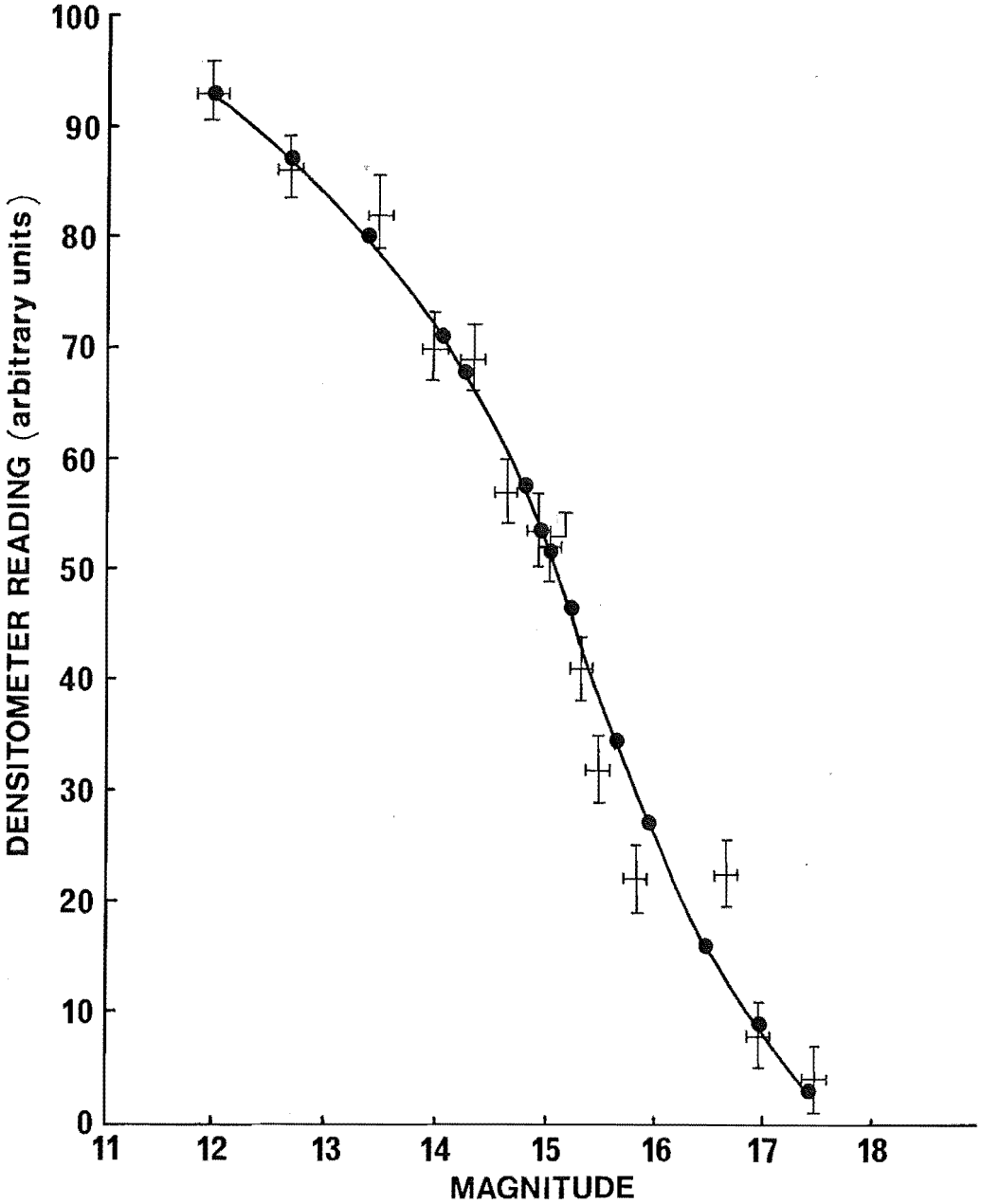

FIGURE 4.1 A typical solution generated by the least squares algorithm. The error bars represent $\pm\sigma$, and mark the input points. The solid points and the smooth curve are the results from the algorithm.

To do this, a set of densitometer deflections, for a given combination of the 3 variables above, was reduced to plate-independent values using the technique of section 4.3. The coefficients of the curve relating initial values to scaled values were then used to scale the densitometer deflections for ten stars not used in the curve fitting to plate-independent values. This ensures no loss of the number of degrees of freedom of the test data. Both scaled and unscaled values for these same ten stars were then reduced against magnitude using the standard reduction technique. The mean scatter of the derived magnitudes about the photoelectric values then will indicate any increased scatter due to scaling technique.

The large scatter in both sets is caused by the small number of comparison stars used over a large magnitude range, and the unsuitability of the Joyce-Loebl for measuring stellar images. It is not a measure of the reliability of the standard reduction method employed.

The stars used in the accuracy test were (Purgathofer's numbering):

3,6,11,14,16,18,19,26,27,29

with magnitudes from B = 9.56 to B = 14.26. Those used in the full reduction programme were:

1,2,4,5,7,8,10,12,13,15,20,22,23,25,28,30

with magnitudes from B = 8.68 to B = 14.35. No colour-dependence of the residuals was found and a third order polynomial was used in the standard reduction method.

4.4.2.1 Polynomial Degree Required

To determine the most suitable polynomial degree for equation 4.1 in section 4.3, polynomials of degree 1 to 4 were tested, as described above. Data from eleven plates each with ten comparison stars were used. The results are shown in Table 4.2 and Figure 4.2a. The slight increase in scatter with increasing polynomial order is due to the small number of comparison stars over a large magnitude range. While the choice of polynomial appears unimportant, experience with image tube plates suggests that a second order polynomial is most suitable. This was therefore chosen for all future reductions.

TABLE 4.2

Polynomal Degree	Mean Residual
1	$0^m.10$
2	$0^m.11$
3	$0^m.11$
4	$0^m.13$
unscaled data	$0^m.11$

Table 4.2 Determination of the polynomial degree relating microdensitometer deflection and mean deflection (equation 4.1). Each mean is formed from 110 points.

4.4.2.2 Number of Comparison Stars

To determine the required number of comparison stars, eleven plates were reduced using a second order polynomial and each of 8,10 and 16 comparison stars. Accuracy was tested using the ten stars as above and the results are shown in Table 4.3 and Figure 4.2b. Again, the slight increase in scatter with number of comparison stars is due to the large magnitude range covered.

TABLE 4.3

Number of Comparison Stars	Mean Mangitude Residual
8	$0^m.12$
10	$0^m.11$
16	$0^m.13$
Unscaled data (10 stars)	$0^m.11$

Table 4.3 Determination of the required number of comparison stars per plate.

4.4.2.3 Number of Plates Required

Using ten comparison stars per plate, and a second order polynomial, the dependence of accuracy on number of plates was tested in the same way as above. Results are presented in Table 4.4 and Figure 4.2c.

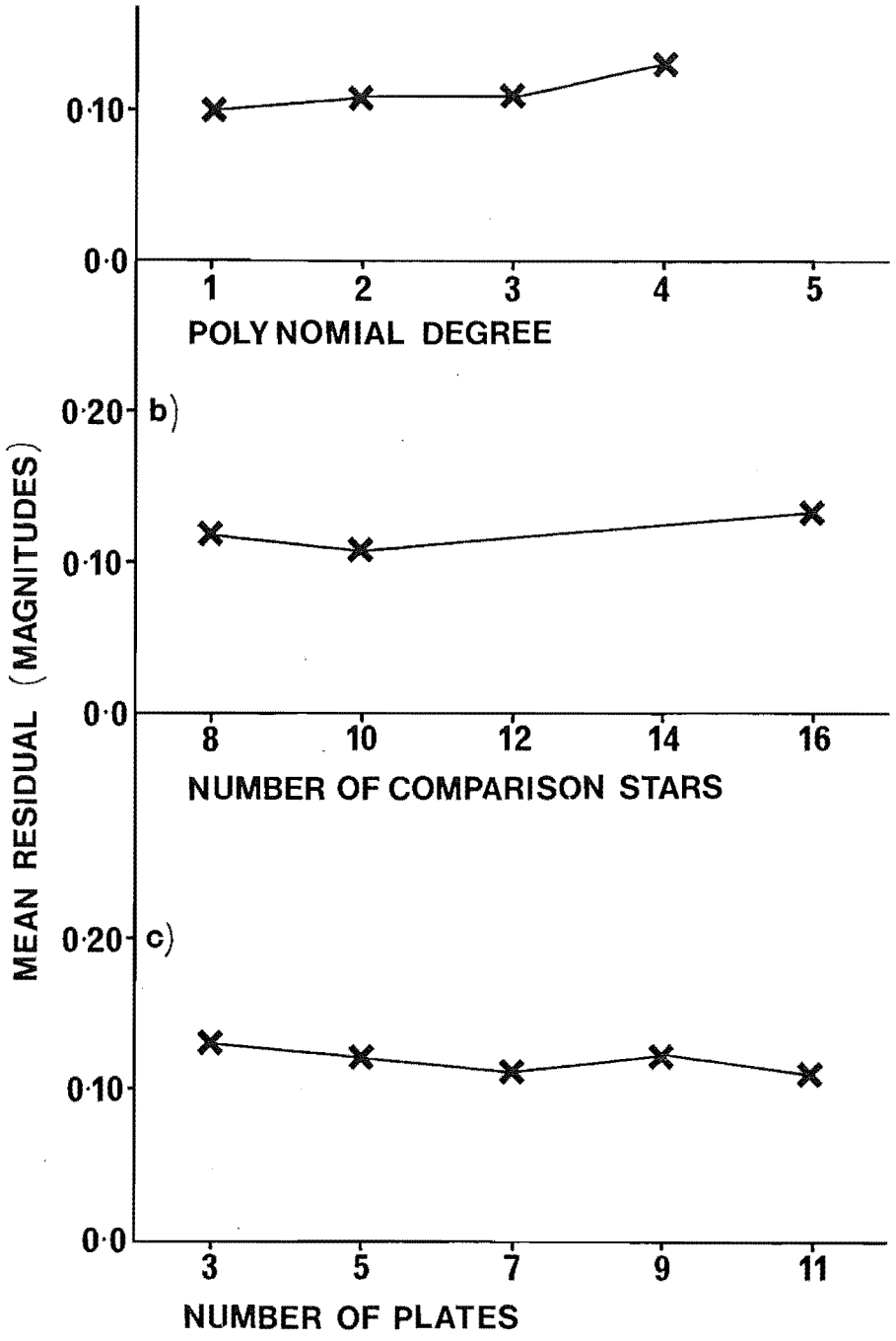

FIGURE 4.2 Dependence of the accuracy of the data reduction method described in the text on the important adjustable parameters. Each point is the mean of 110 individual results.

TABLE 4.4

Number of plates	Mean Magnitude Residual
3	$0^m.13$
5	$0^m.12$
7	$0^m.11$
9	$0^m.12$
11	$0^m.11$
Unscaled data (10 plates)	$0^m.11$

Table 4.4 Determination of the dependence of prediction accuracy on the number of plates of each object.

4.4.3 Tests Using 3C 273

Five 30 minute laO + Wr2B exposures of the field containing the quasar 3C 273 were obtained with the Mount John Observatory 10 inch f/7 astrograph on each of April 4th and April 6th, 1976. The quasar and nine comparison stars from the sequence of Penston et al. (1971) were measured with the Joyce-Loebl microdensitometer. These densitometer deflections were used to generate scaled plate-independent deflections for the quasar using the technique of section 4.3 with a second-order polynomial. Both unscaled and scaled deflections for the comparison stars and quasar were reduced against magnitudes using the standard (i.e. assuming magnitudes are available) technique in the same way as in section 4.4.2. Both unscaled and scaled densitometer deflections are shown in figure 4.3 as are the magnitudes derived from these, while the results are

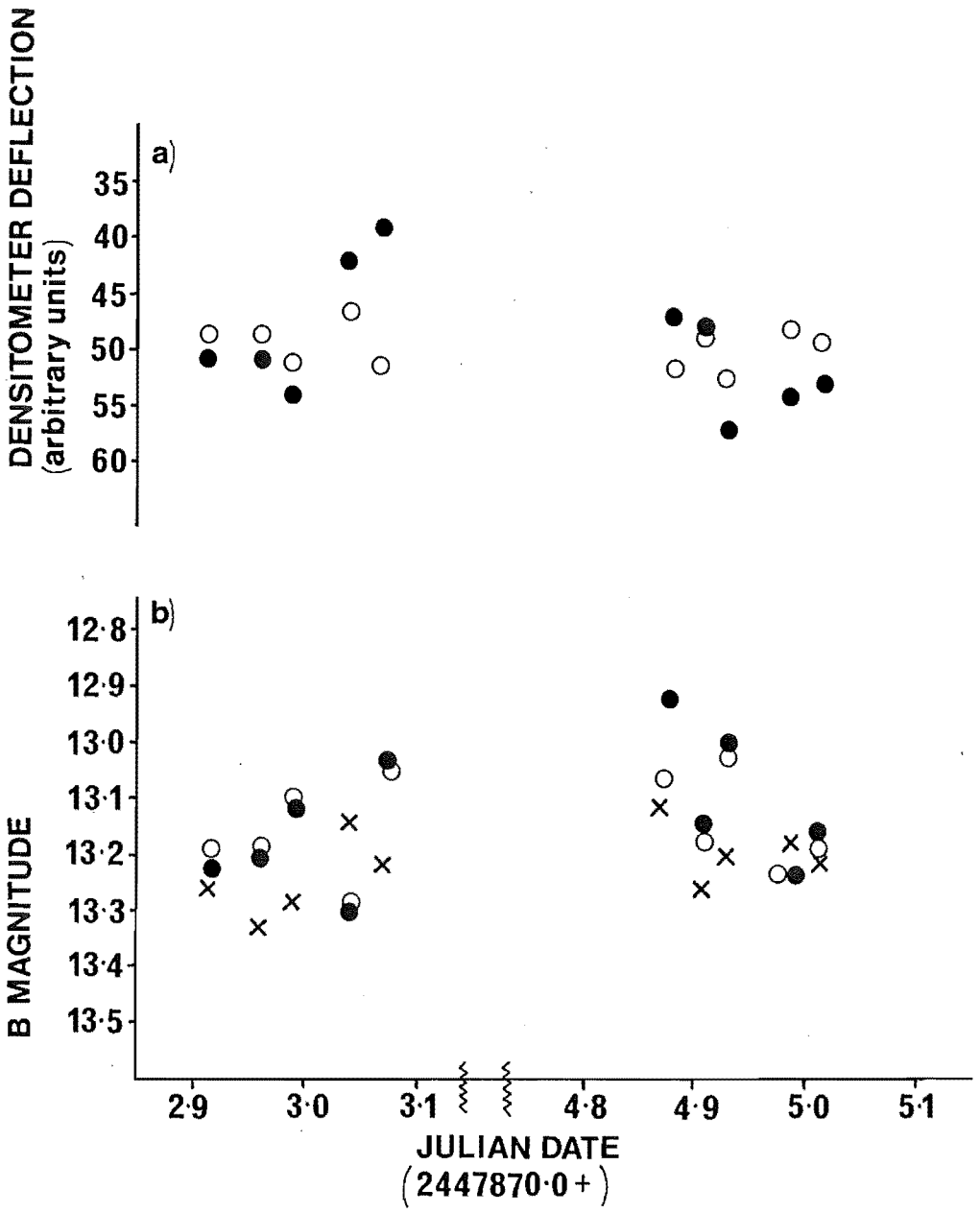

FIGURE 4.3 a) Observed (solid points) and scaled (hollow points) densitometer deflections for the quasar 3C273.

b) The magnitudes derived from these values (same symbols). The magnitudes from the unscaled values for comparison star D are shown for comparison (crosses).

summarised in Table 4.5.

The diagrams clearly show the success of the reduction technique for reduction to plate-independent values. No increase in random scatter is apparent for the magnitudes derived from the scaled values. In fact the standard deviation of the magnitudes derived from the unscaled densitometer deflections is $0^{m}.12$, while that from the scaled values (which do not require magnitudes for the field stars) is $0^{m}.09$. The standard deviation of the ten magnitudes produced from the unscaled data for comparison star D was $0^{m}.07$. The greater value for the quasar may be due to low-level rapid variations.

TABLE 4.5

			B magnitude:	
Julian Date 2440000.+	Densitometer Deflection	Scaled Deflection	Unscaled Deflection	Scaled Deflection
2872.911	51	48.4	13.22	13.19
2872.957	51	48.7	13.20	13.19
2872.988	54	51.0	13.11	13.10
2873.038	42	46.4	13.20	13.29
2873.067	39	51.4	13.04	13.04
2874.885	47	41.4	12.92	13.06
2874.912	48	49.0	13.16	13.17
2874.933	57	52.4	13.00	13.02
2874.992	54	48.0	13.23	13.23
2875.019	53	49.3	13.17	13.18
MEAN	49.6	49.6	13.14	13.15
STD DEVN	5.7	1.9	0.12	0.09

Table 4.5 Results derived from the modified reduction technique applied to the quasar 3C273.

4.4.4 Tests using HD199757

As a final test, twenty plates of the short period variable star ZZ Microscopii (HD199757; Churms and Evans, 1961) were obtained on the night of June 23rd, 1977, (U.T.). Exposures were 60 seconds each 5 minutes on unfiltered 103aO with the Mount John Observatory 10-inch f/7 astrograph. Simultaneous B-band photoelectric observations were obtained by M. Clark with one of the 61cm reflectors at Mount John. The variable and twelve comparison stars were measured with both the Joyce-Loebl microdensitometer and the Sartorius iris photometer of Mt. Stromlo Observatory of the Australian National University, Canberra. Both sets of data were reduced with the technique of section 4.3, using a second order polynomial, and the results are shown in figure 4.4. The improvement in accuracy in the iris photometer data is apparent (cf. section 3.8).

Using the iris photometer data, the reliability of the final weighted mean for each star was tested. The first estimate of this mean, formed in equation 4.2 by averaging the input data was adjusted by adding random numbers with zero mean and standard deviation corresponding to 5% of the total numerical range of the means. Convergence proceeded as before, though more slowly. No significant change occurred in the scaled iris readings for the variable, nor in its χ^2 statistic. This, with 19 degrees of freedom, changed from 369 to 366.

Finally, the comparison star with mean magnitude nearest the mean for the variable was reduced in the same way as the variable. No spurious indication of

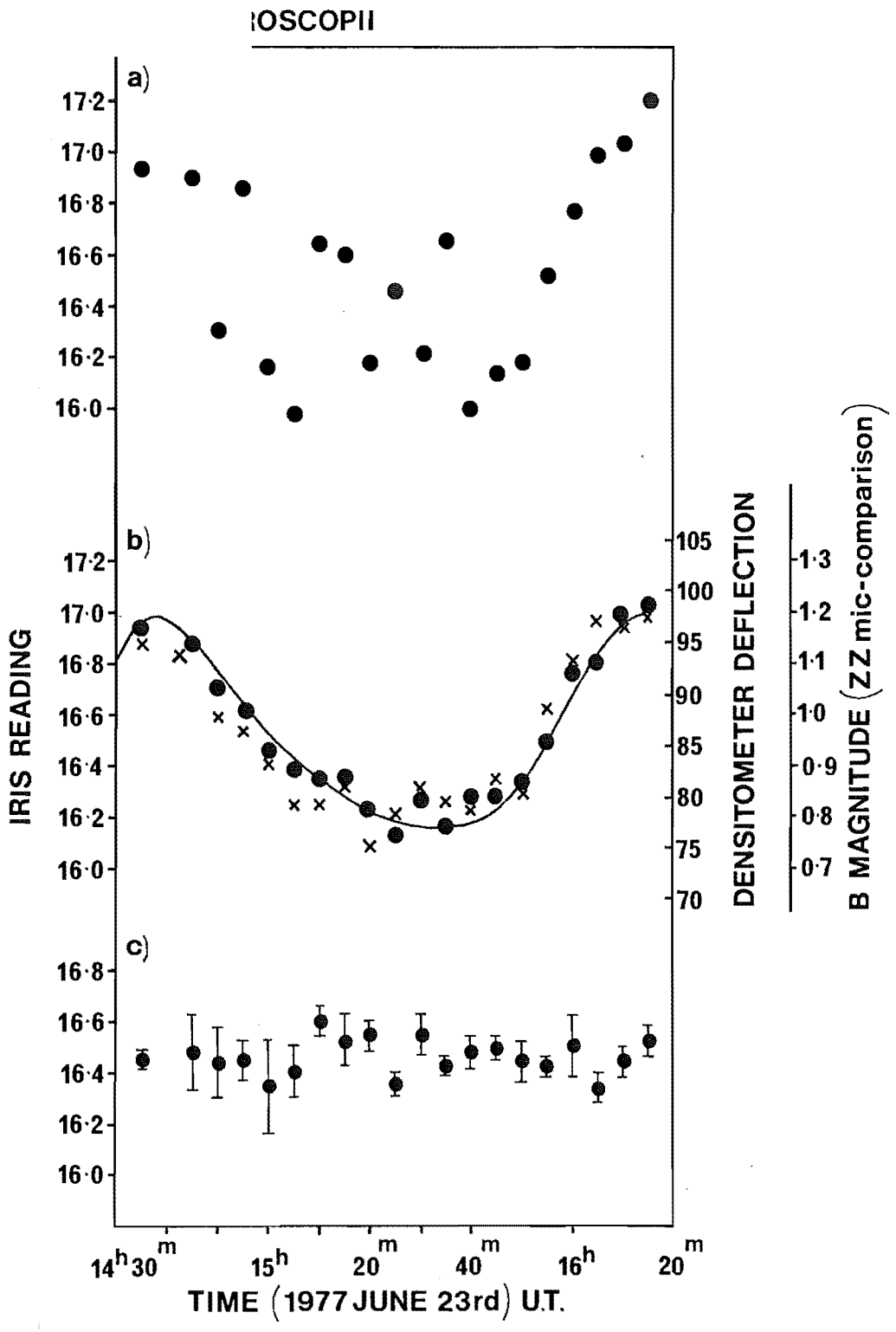

FIGURE 4.4 a) Unscaled iris photometer measures for HD 199757.

b) Scaled microdensitometer deflections (crosses) and iris photometer readings (solid points) for HD 199757. The solid line represents the simultaneous photoelectric photometry.

c) The light curve of a comparison star reduced as a suspected variable.

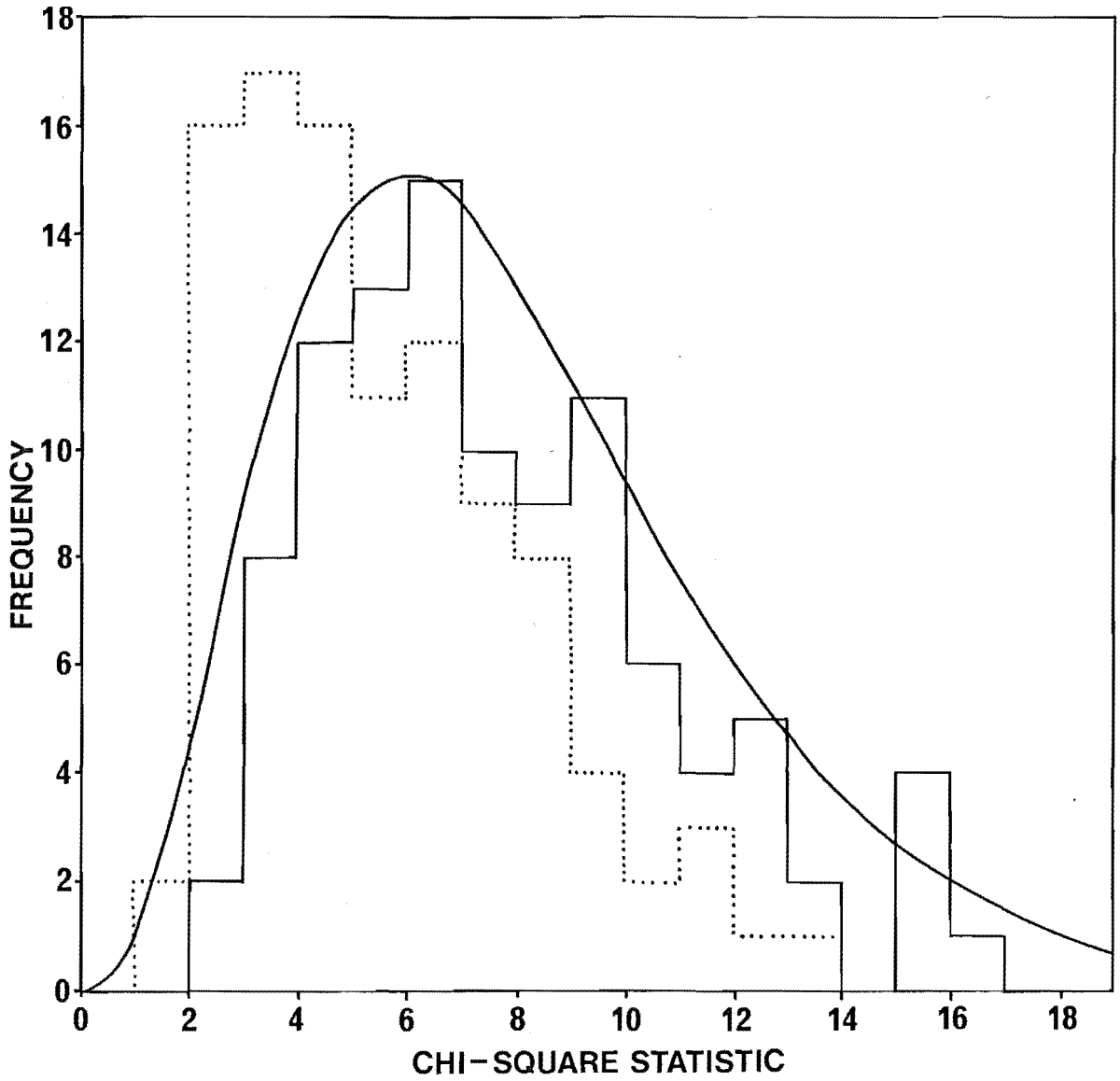

FIGURE 4.5 The distribution of χ^2 values for all comparison stars with 7, 8 or 9 degrees of freedom (solid lines) and the same values scaled as described in the text (dotted lines). The smooth curve is the expected χ^2 distribution.

variability was produced. The light curve of this star is shown in Figure 4.4.

4.5 TEST FOR VARIABILITY.

Once data reduction is complete, the final set of scaled iris readings and their uncertainties can be used to test for variability. The null hypothesis of constant intensity of comparison stars and quasars is most conveniently tested by χ^2.

Penston and Cannon (1970) derive a correction factor (NF-2)/NF for χ^2, where NF is the number of degrees of freedom of the observation. Values of χ^2 for all comparison stars with NF = 7,8 or 9, both with and without the correction factor, are shown in Figure 4.5. A χ^2 curve with NF = 8 is shown for comparison. Because of the adequacy of agreement between the uncorrected values and the expected χ^2 distribution, all χ^2 values were evaluated without the (NF - 2)/NF factor.

4.6 CALIBRATION OF SCALED IRIS READINGS.

The scaled iris readings for the quasar can be related to a Pogson scale in two ways. Firstly, by comparison with other (Pogson-scale) observations of the same object at the same time in a similar photometric system. Secondly, by calibrating the scaled iris readings for the comparison stars onto a Pogson scale.

4.6.1 Calibration using other observations

Overlapping observations of 11 of the objects monitored in the Mount John Programme were fortuitously

obtained by Dr. G. Adam at E.S.O. in 1976 September and 1977 January (Adam, 1978), while further observations are scheduled for 1978 February/March (G. Adam, private communication). Of these objects (Table 4.6), five have light curves reduced from the Mount John data, and allow an approximate zero point determination of those observations by equating V magnitude and scaled iris reading. These results are indicated on the relevant diagrams. This procedure is necessarily approximate because the image intensifier spectral response does not exactly match the standard V band.

As yet no variable objects have been concurrently observed over a sufficiently wide magnitude range to allow direct magnitude calibration of the iris readings scale.

TABLE 4.6

Sources with light curves available	Sources for which data reduction is not yet complete.	
0202-76	0355-483	0622-441
0537-441	0439-433	0925-203
0743-67	0506-61	1207-399
1101-325		
1117-248		

Table 4.6 Quasars observed both at E.S.O. and at Mount John.

Four objects which are included in the Florida monitoring programme (McGimsey et al, 1975; Scott et al, 1976) are also being observed at Mount John. Of these,

two (0048-097 and 2128-12) are non-variable from the Florida data, while two (1510-089 and 1514-24) are variable. The usefulness of these results for calibration purposes is somewhat limited, however, as all the Florida observations are in the Johnson B or the (similar) photographic spectral systems. In addition, for the two variable sources, there is no overlap in time with the Mount John data for the results published to date.

4.6.2 Calibration using comparison sequences.

Calibration may be achieved by comparison with a similarly exposed, developed and reduced plate of an accurate photometric sequence. This method is necessarily approximate, especially so in this case because the scale on which the comparison stars lie is a composite which depends on the characteristic curves of all plates of that field. This will not closely correspond to a single determination, partly because of random batch-to-batch variations in emulsion properties, but primarily because up to three different emulsions (IaO, IaE and IIaD) have been used for the observations.

The approximately V band observations of NGC2477 described in Chapter 3 are, however, suitable as an indication. For those plates, one iris reading is equivalent to $0^m.52$ at $m_v=14$, and $0^m.63$ at $m_v=17$.

Reliable comparison star sequences are available in the field of only two of the objects monitored. These are PKS 1514-242 (A.G. Smith, private communication) and PKS 2128-124 (Angione, 1971). The sequence near

PKS 1514-242 was established by photographic transfer, and is in the B photometric system, which is not closely matched by the Mount John image tube. A least squares fit of a straight line to the relation between magnitude (m_B) and scaled iris reading (I_s) for the comparison stars yields (Figure 4.6a):

$$m_B = - 0.37\ I_s + 18.72\ ; \quad r = 0.93.$$

Over the magnitude range considered, $14^m.2 - 16^m.2$, this provides the calibration

$$1.0\ I_s = 0^m.38.$$

For the sequence near PKS 2128-124, UBV data is available for 6 stars. (UBV data for 7 stars is tabulated by Angione (1971), but only 6 are identified on the finding chart). The relations for B and V magnitudes (Figure 4.6b) are:

$$m_V = - 0.41\ I_s + 18.51\ ; \quad r = 0.99$$
$$m_B = - 0.38\ I_s + 18.83\ ; \quad r = 0.98.$$

the resulting calibration in the interval $13.71 \leqslant m_B \leqslant 16.33$ is then:

$$1.0\ I_s = 0^m.41 \qquad (m_V)$$
$$1.0\ I_s = 0^m.38 \qquad (m_B).$$

The mean error of the 62 Mount John observations of these two sources is $0.31\ I_s$, which corresponds to $0^m.12$. This is to be compared to the values of $0^m.04$ for HD 199757, and $0^m.07$ for 3C273. The increase in uncertainty is caused partly by the use of the image tube, which was not used for the latter two sources, and partly by increasing apparent magnitude. This

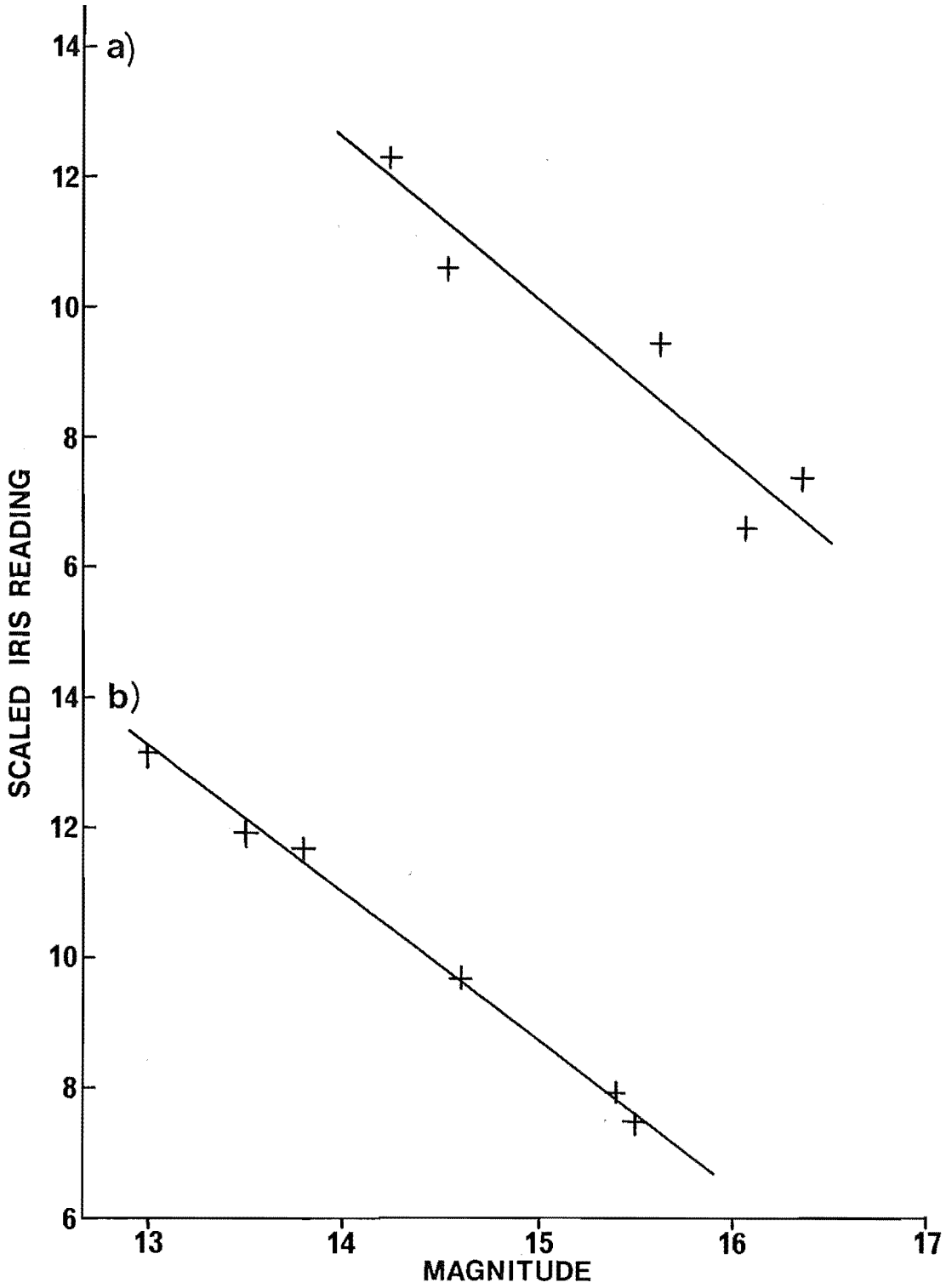

FIGURE 4.6 a) Relation between B magnitude and scaled iris reading for the comparison stars near AP Librae.

b) Same relation with V magnitude for comparison stars near PKS 2128-124.

increased from 9^m for HD 199757 to 13^m for 3C273, to 16^m for the other two sources. By comparison, the results for NGC 2477 (section 3.4.3.2) indicate a mean error with this system of $0^m.11$ at $m_v = 16^m$. This is similar to the accuracy quoted by other users of image tubes for stellar photometry (Cromwell, 1969; de Veny, 1970; Sudehus, 1970).

Using direct photography, the Florida group report a mean error in magnitude determination for 41 non-variable sources of $0^m.14$ (Scott et al, 1976). Many of these sources were however much fainter than 16^m. The mean error of the published Florida photometry for PKS 1514-242 is $0^m.17$, while that for PKS 2128-124 is $0^m.12$. The error of $0^m.12$ with image tube photometry of 16^m objects with the Mt. John 61cm reflector therefore compares favourably with results by other workers.

4.6.3 Establishment of Calibration Sequences

4.6.3.1 Methods available.

Where no information on the comparison stars is available in the literature, it is possible to set up a differential magnitude scale in several ways.

The most widely used is photographic transfer from a nearby sequence (Weaver, 1962). This however requires observations in a standard photometric system, and is not appropriate here.

An objective grating is suitable in many cases (Harding et al, 1971), but suffers for use in the red in that the secondary images are noticeably elongated.

Accurate photometry is therefore difficult.

A method employing the secondary image of a plano-convex lens has been described by Harris and Racine (1974). The magnitude step in this method is necessarily large ($\geqslant 4^m$), which makes it more suitable for extending bright sequences than internally calibrating a small magnitude interval.

A more suitable device is the combination of a polaroid filter and a doubly-refracting calcite prism (Brück et al, 1969; Piirola, 1973, 1975; Robertson, 1974). Because of the difficulty of obtaining suitable quality calcite prisms, however, the filter below was utilised.

A calibration technique utilising a ½-filter was described by Weaver (1962). In this method, one-half of a clear plate is coated with a partially opaque neutral material. This is then mounted in the telescope beam before the focal plane. With this filter, three exposures are obtained of a given field. The first with the filter in position, the second with it rotated through 180°, and the third with it removed and the telescope refocussed. Those images recorded through the attenuating section of the filter are then less bright by a known amount than the images of the same stars in an identical exposure through the other part of the filter. This amount is the filter step, and is calibrated independently.

The plates should be taken under stable sky conditions, and if possible, symmetrically about meridian transit. The relation between the iris readings for all stars on the unfiltered plate and the same stars on the unexposed

part of the ½-filter plate is then found. This is used to determine the iris readings the stars under the filter would have if the filter were absent. The actual readings for those stars will differ from these predictions by an amount which corresponds to the magnitude of the filter step. A relation between magnitude and iris reading is then available. A similar procedure is followed for the second ½-filter plate, and the results are averaged. This does not however provide a zero point for the magnitude scale.

A neutral density half-filter was constructed by the author by vacuum deposition of nichrome on flat plate glass. The spectral transmission of the filter and glass were measured with the Cary 14 recording spectrophotometer of the Physics Department, University of Canterbury. A considerable improvement in the spectral neutrality of both glass and filter was achieved by overcoating with MgF_2. This also improves the handling qualities of the filter. The optimum coating was determined by trial and error. The uniformity of the filter coating was also tested by scanning the filter with the Joyce-Loebl microdensitometer. The spectral transmission and uniformity of the final filter are illustrated in Figure 4.8 and Figure 4.9 respectively.

Spectral transmission is flat to within a few percent over the range of significant response of the image tube. The filter step corresponds to $0^m.39 \pm 0^m.03$ between clear and overcoated sections of the filter.

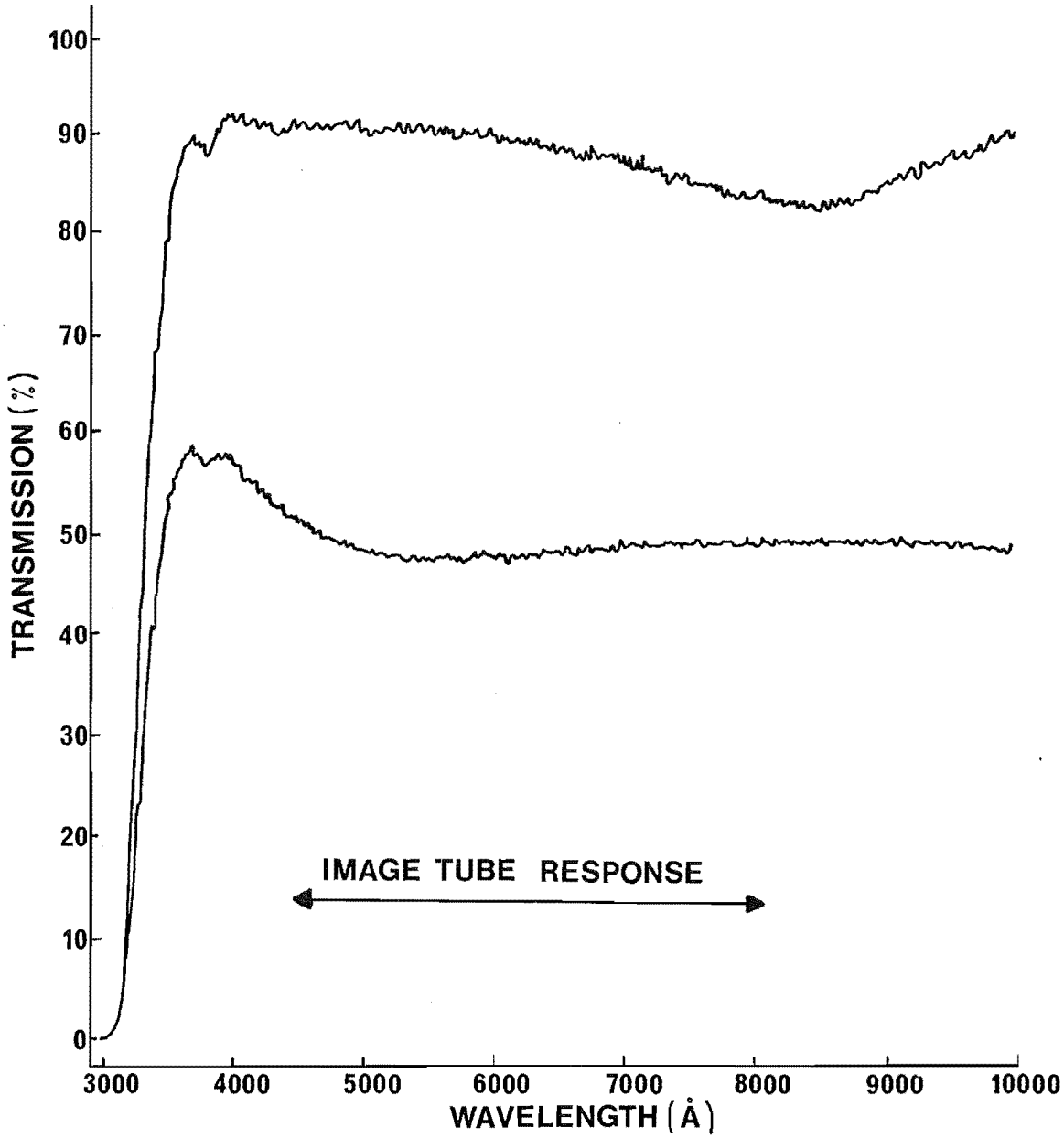

FIGURE 4.7 Spectral response of the half-filter described in the text: clear glass (top curve) and coated glass (bottom curve). The region of significant image tube sensitivity is indicated.

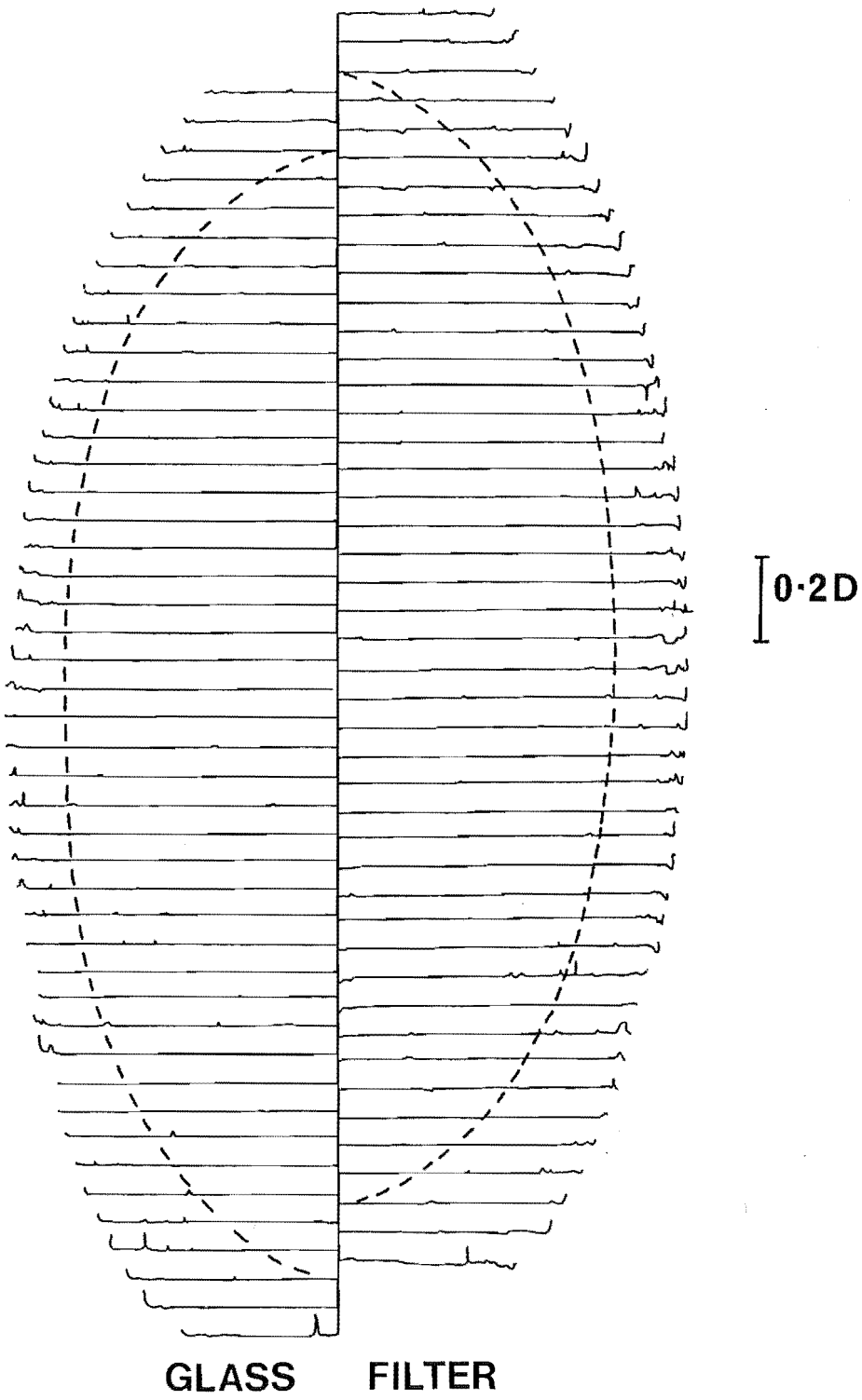

FIGURE 4.8 Densitometer scans of the ½ - filter. The dotted area is that illuminated. Successive scans have offset zeroes, and density increases upwards. The uniformity of the coating is apparent.

4.6.3.2 Observations

To date, ½-filter plates have been measured for only 3 objects (0521-365, 0537-441, and 1514-242). In each case only the comparison stars used in the data reduction were measured. This resulted in an insufficient number of points to reliably determine the magnitude scale. There is however no need to restrict the measured stars to the set of comparison stars. Remeasurement of these plates will lead to comparison star differential magnitudes limited in accuracy only by random photometric limitations.

The mean value determined for these three fields from the ½-filter plates is 1.0 iris units = $0^{m}.5$, this result is however uncertain. It should be noted that this calibration must be carried out for each object independently, and should be repeated as more plates are reduced. This is necessary because the relation between magnitude and mean iris reading for the comparison stars will depend on the characteristic curve of every plate of that field, and so may alter from field to field, and for a single field as more plates are added.

4.6.4 Establishment of Standard Magnitudes

In principle it is possible to derive standard magnitudes for a quasar from broad band observations, such as those presented in this thesis. This process requires that no significant variations in the spectral index of the quasar occur during the time of interest. This is the case for sources such as PKS 0537-441, which did not change its spectral index detectably

during a 1^m variation over 120 days (Eggen, 1973).

The spectral response of the detector must be known accurately, as must the spectral type of at least one comparison star. The star's energy distribution can be numerically integrated over the bandpass of both the image tube and the standard photometric system. These values can then be equated to the observed iris reading and known magnitude of the star, to define the zero points of the two integrations.

The quasar power-law energy distribution is also integrated numerically over both the standard system and the image tube spectral responses. The quasar's scaled iris reading is equated to the value of the numerical integration, and the relative zero point determined above allows the value of the integration in the standard system to be converted to a magnitude. This assumes that no strong spectral features (such as emission lines) are present.

4.7 PHOTOMETRY OF RESOLVED OBJECTS.

Iris photometry of objects which are spatially resolved is complicated by the difference in image structure between an extended galaxy and the point-source comparison stars. Atmosphere turbulence has a different effect on the image profile of the galaxy than on the profile of a point-source. Similarly, variations in the effective measuring aperture will occur due to changes in the fog level of the plate. In particular, the combined fog level plus galaxy magnitude may raise

extended regions of the image above the plate threshold detection limit on some occasions, and not on others. The derived magnitudes for the (stellar) nucleus of an active galaxy will therefore contain a dependence on both the seeing during the exposure, and the plate fog level.

A simple comparison of galactic and stellar images without consideration of these effects, especially on plates exposed with a fast optical system, can lead to substantial errors. For example, Hoffmeister (1964) estimated AU Leonis at magnitude 15 on the Palomar Observatory Sky Survey print, while consideration of its extended nature led Bond, Green and Huchra (1974) to estimate magnitude 17, from the same print.

Similarly, Cannon, Penston and Brett (1971) note that normal galaxies show spurious variations of up to $0^{m}.5$ due to variable seeing, even in a consistent series of exposures with an f/10 refractor. To remedy this, they took exposures of extended objects slightly out of focus for the Hertsmonceux quasar monitoring programme. They also advise caution on analysing their Seyfert galaxy results.

More quantitative techniques have been discussed by Netzer (1974) and Green, Huchra and Bond (1977). Netzer derived a relation between the galaxy magnitude derived from the iris measurements, and the plate exposure, defined in terms of the iris reading for two suitable stars. This relation was empirically determined from a set of exposures of a non-variable galaxy. The iris readings for the two comparison stars on any later plate can then be

used to read off the appropriate correction to the galaxy magnitude derived from that plate. The extent of this correction was minimised by Netzer by restricting all his observations to short exposures. With this technique he was able to achieve a standard deviation $\sigma = 0^m.07$, a substantial improvement over the $\sigma \approx 0^m.20$ achieved by Cannon et al (1971).

A more extensive analysis was performed by Green et al, (1977). They derived a linear relation between the observer's estimate of the seeing during exposure and the magnitude derived from iris photometry of a non-variable galaxy of similar angular size to that under study. This relation was then used to correct the derived magnitude of the galaxy of interest for the effects of seeing. These corrected values were found to be independent of sky fog level. The correction to a particular magnitude was as great as $0^m.9$, while the scatter in the corrected magnitudes was reduced by a factor of 3 below that for the uncorrected values.

Because of the difficulty of obtaining reliable, consistent seeing estimates, a slightly modified version of this procedure was employed in this study. A star near the galaxy of interest was scanned on each plate with the Joyce-Loebl microdensitometer. The ratio of the height to the width at half-height of the density scan of the stellar image was then used as an estimate of the seeing for that plate. The relations between the scaled iris reading of the galaxy (I), the seeing parameter (s), and the sky fog adjacent to the galaxy image (I_s) were then

derived by least squares fitting for the 3 resolved sources with data reduced to date. These are:

PKS 0521-365

PKS 0548-322

PKS 1514-242

the derived relations are then:

PKS 0521-365

$$I = 0.12\ s + 7.28 \qquad r = 0.49$$

$$I = 0.19\ I_s + 5.50 \qquad r = 0.45$$

PKS 0548-322

$$I = 0.08\ s + 5.03 \qquad r = 0.32$$

$$I = 0.14\ I_s + 3.78 \qquad r = 0.51$$

PKS 1514-242

$$I = 0.23\ s + 5.10 \qquad r = 0.70$$

$$I = 0.33\ I_s + 6.64 \qquad r = 0.58.$$

The principal uncertainty in these relations is due to intrinsic variability of the objects. Because the form of this variation is not gaussian about a mean, the formal uncertainty in these relations cannot be readily determined.

Each of the three data sets was corrected for its dependence on the parameter with the greater value of the correlation coefficient. None of the three corrected data sets then showed a significant dependence on the other parameter ($r < 0.26$ in all cases). Correction of the data for PKS 0548-322 for its (marginal) dependence on the seeing parameter, for consistency with the other

two objects, had no significant effect on either the scatter of the data, or the correlation of the corrected data with the sky fog level.

The different dependence of the results for this object and the other two may be attributed to the difference in the appearance of the image of this galaxy. Both PKS 0521-365 and PKS 1514-242 show compact images, with a very steep density gradient outside a radius about twice that of the stellar nucleus on a typical plate. Variations in seeing, which might be expected to vary iris size over this radius will therefore be significant. Because effectively all the galaxy image is above the plate threshold on all exposures, background fog variations will be less important. For PKS 0548-322 however, the image shows a much more gradual density profile over a larger area. The iris diameter will therefore show a greater dependence on sky fog and a lesser dependence on seeing. None of the comparison stars showed any dependence on either of these parameters.

The light curves of these three galaxies, corrected as described above, are discussed in Chapter 5.

CHAPTER 5

RESULTS AND DISCUSSION

5.1 INTRODUCTION

Light curves are presented here for the 24 quasars with plates measured to date. These results have been obtained, measured, reduced, and where necessary corrected for image structure, as described in Chapters 3 and 4. The observations for the 24 sources are tabulated in Appendix II. In addition, data for 2 galactic stars which were misidentified with radio sources, and 2 probably variable comparison stars, are given in the same Appendix.

To allow a discussion of the statistical properties of the full sample of the 132 quasars which have been observed to date, a complete listing of published references to all of these sources has been prepared. It is presented in Appendix III.

5.2 VARIABILITY OF PROGRAMME OBJECTS

5.2.1 Airmass-Dependence of Variability

Spurious apparent magnitude variations can be caused by the large spectral band-width of the image intensifier. Differential extinction between a comparison star's spectrum and a quasar's power-law spectrum can lead to an air mass-dependence of the quasar's scaled iris reading. Observations over a range of air masses might then mimic low-level intrinsic variability. This effect was suspected by Kinman (1969) in the Yale observations of 3C 345 (Hunter and Lü, 1969; see also Hunter and Lü, 1970) and has been investigated by Hackney (1972).

Because of this, observations were restricted to near meridian transit whenever possible. The observed residual from the mean scaled iris reading for all quasar observations reported here is shown as a function of air mass in Figure 5.1 No systematic effect is apparent.

5.2.2 Detection of Variability

All quasars and comparison stars have been tested for variability with a χ^2 test. The resulting probability that the observed χ^2 value is consistent with a non-variable parent population is shown in Figure 5.2. The difference in optical behaviour of quasars and comparison stars is evident. Of the four stars with $P(\chi^2) < 5\%$, two have only one discrepant point, while light curves for the other two are presented in section 5.6. Of the five quasars with $P(\chi^2) > 5\%$, two are known variables from other observational programmes. Neither of the two incorrect radio source identifications indicated variability ($P(\chi^2) =$ 27% and 66% respectively). The light curves for the 24 quasars are presented in section 5.6.

5.2.2.1 Efficiency of Detection

The mean number of observations before variability was detected, in those sources found to be variable, was 4.4, with a range from 2 to 8. The mean number of observations of those 8 sources classified as non-variable is 11.5, with a range from 8 to 14. It is therefore unlikely that these sources have not been detected as variable because of insufficient observations. They

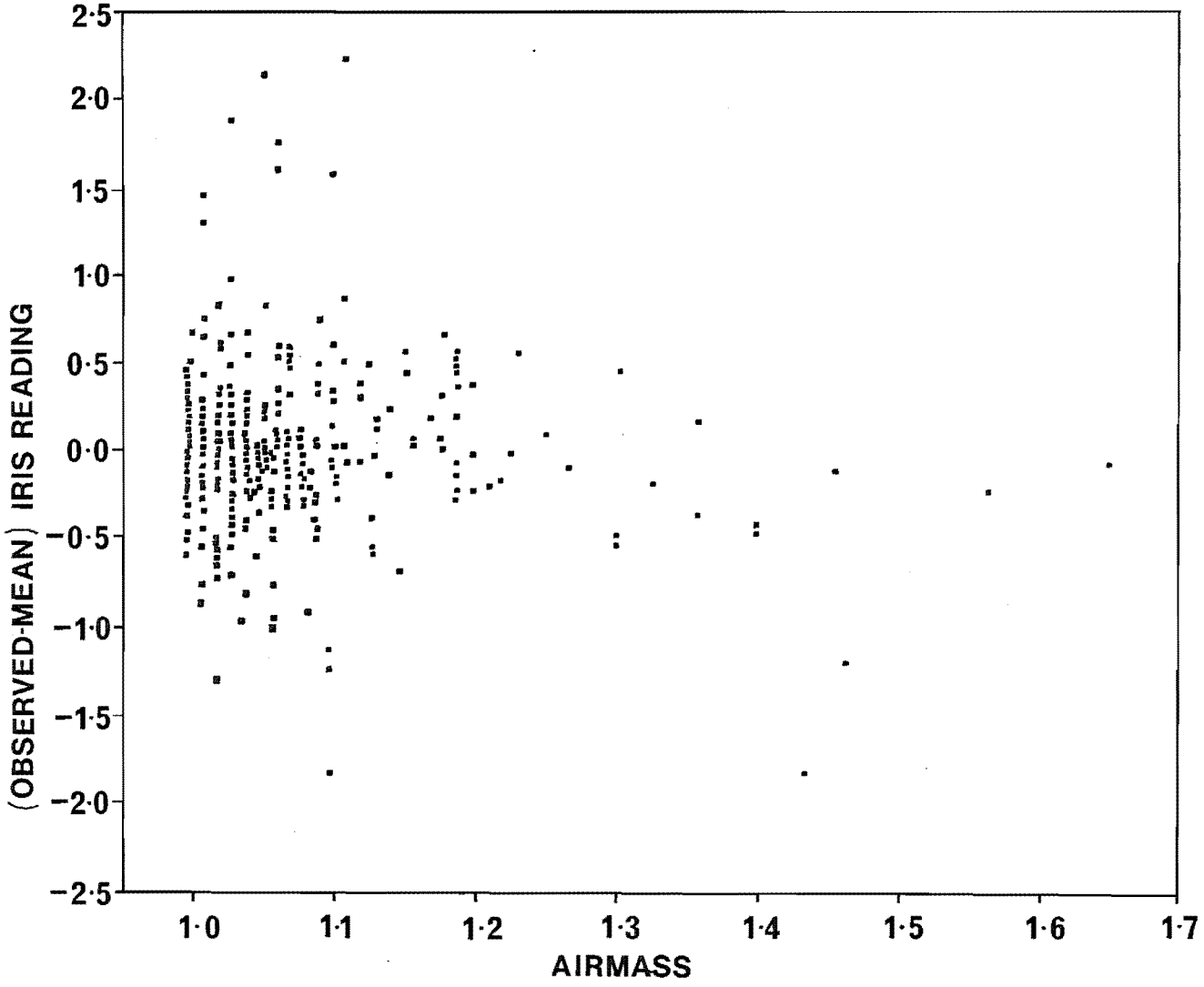

FIGURE 5.1 The residual iris reading from the mean as a function of air mass. There is no evidence for a systematic effect.

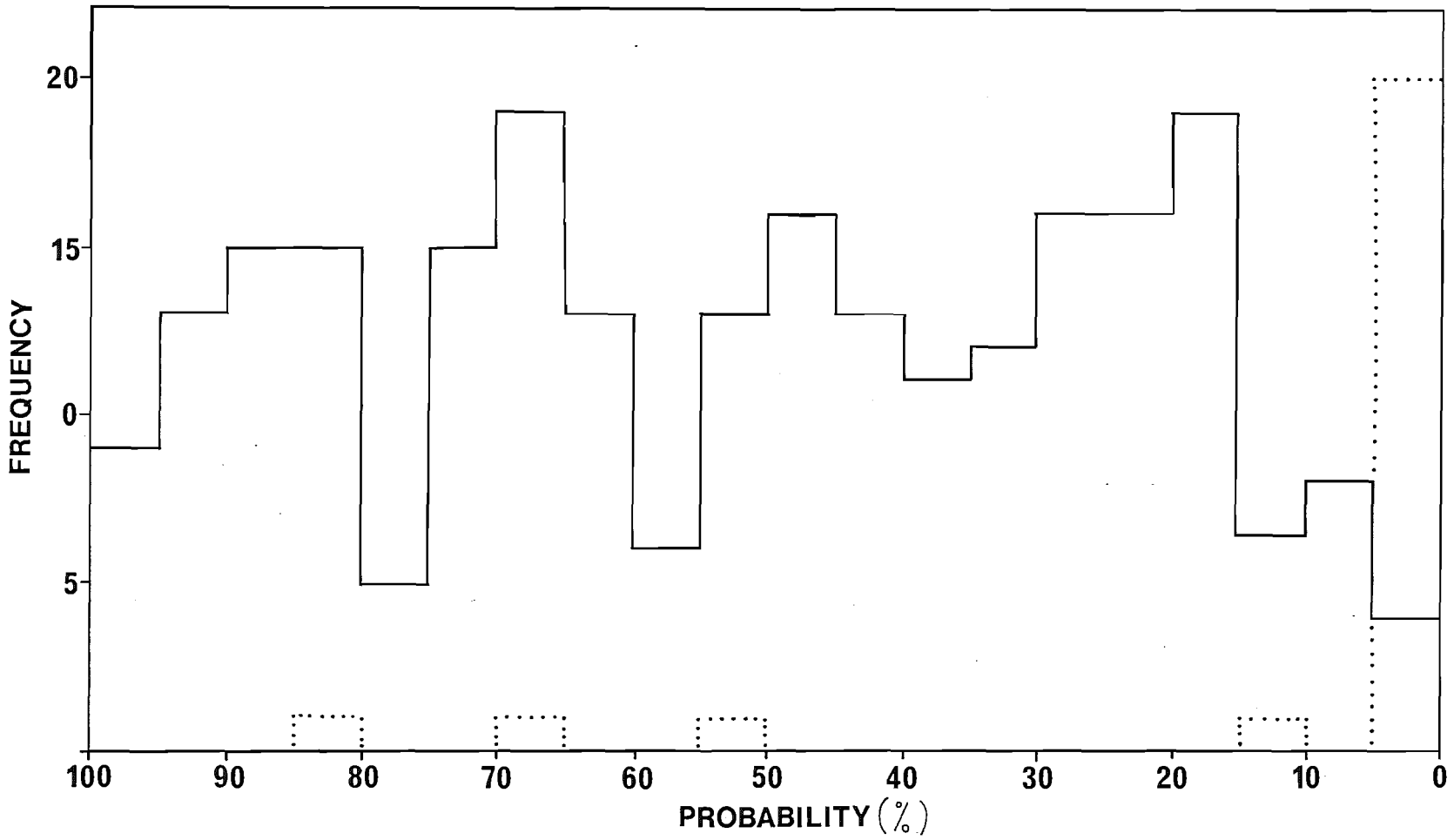

FIGURE 5.2 Probability that the observed χ^2 values are consistent with a non-variable parent population for comparison stars (solid line) and quasars (dotted line).

have been, for the period of observation, less variable than the other sources studied here.

In general, however, the light curves indicate changes which have occurred between observations, rather than a trend in several measurements. (The large flare in PKS 1244-255 is an exception). The light curves are therefore undersampled, and can provide only lower limits on the rates and frequency of variation of these sources. Monitoring of several of the more active sources continually through several nights is planned to help remedy this limitation.

5.2.2.2 Choice of Confidence Limits

A variety of confidence limits for the detection of optical variation exists in the literature. These limits are summarised in Table 5.1.

TABLE 5.1

Adopted Confidence Limit	Reference
95%	Peach (1969)
90%*†	Penston and Cannon (1970)
99.75%	Weistrop (1973)
95%	Scott et al, (1976)
95%	Barbieri et al, (1977)
97%*	Usher (1978)

† Discarding the 10% most discrepant points

* All χ^2 values scaled by 0.8.

TABLE 5.1: Adopted χ^2 significance limits for the detection of optical variability.

For this investigation, single discrepant points have been rejected in considering the light curve, and the 95% confidence limit has been imposed. The rejection of single discrepant points is advisable because of the non-normal error distribution in photographic photometry (cf. Kinman et al, 1968; Richter et al, 1972).

Two other measures of variability are sometimes employed. These are the ratio of the standard deviation of the quasar observations to that of the comparison stars, and the range of observed magnitudes. The first of these was employed by Angione and Smith (1972) and Angione (1973) in their study of 22 quasars from Harvard archival plates. All 22 were found to be variable, in that the ratio was greater than 1.0. Heckman (1976) utilised the range of measured magnitudes for 80 quasars, and considered a range of $1^{m}.5(3\text{-}4\sigma)$ evidence for variability. This latter measure is similar to the radio variability index (cf. e.g. Nicolson, 1978), defined as $(S_{max} - S_{min})/S_{min}$, where S is the flux.

For these observations a more suitable measure, defined as $(I_{max} - I_{min})/\sigma_s$, has been chosen, where I_{max} and I_{min} are the extremes of the scaled iris readings, and σ_s is the mean standard deviation of the comparison stars in that field. The χ^2 significance limit of 95% then corresponds approximately to a range of 4 standard deviations in the iris readings.

The ratio of the standard deviations of the quasar and comparison stars is greater than 1.0 in all except one case (PKS 2128-124, which is a known optical variable). The χ^2 confidence limit for well observed sources corresponds to a ratio ~1.6.

All three measures of variability have been considered, and are tabulated, along with other observational data, in Table 5.2.

5.2.3 Classes of Variation

The observed variations in quasars have been classified into the various combinations of amplitude and rate of variations by Penston and Cannon (1970), Folsom et al, (1971), Angione (1973), and McGimsey et al, (1975). These various classifications may be amalgamated into the following 5 classes:

Class 1: large amplitude ($\geqslant 0^{m}.5$), short timescale ($\leqslant 30^{d}$),

Class 2: large amplitude ($\geqslant 0^{m}.5$), long timescale ($\geqslant 30^{d}$),

Class 3: low amplitude ($\leqslant 0^{m}.5$), short timescale ($\leqslant 30^{d}$),

Class 4: low amplitude ($\leqslant 0^{m}.5$), long timescale ($\geqslant 30^{d}$)

Class 5: no detected variations ($\leqslant 0^{m}.2$).

It is of course possible for a single object to be classified into more than one category. For example, PKS 1954-388 would be grouped in class 2 on the basis of the 1975-1976 data, class 4 on the basis of the 1977 data, and class 1 on the basis of the 1978 data (Gilmore, 1978a). It does not seem profitable either to create new classifications or to classify a single source in several ways. Instead, objects have been classified in terms of their largest amplitude and most rapid activity, as it is this activity which poses the tightest

TABLE 5.2

OBJECT	Red Shift 1	Number of plates	$P(\chi^2)$ 2	Variability class* 3	$(I_{max} - I_{min})/\sigma_s$	$\frac{\sigma(Q)}{\sigma(stars)}$	Known Radio Variable	Known Optical Variable	Radio Spectral Index 4	Radio Structure
0135-247	0.831	8	0.15	5	2.6	2.23	Yes	No	$\alpha_{10700}^{1415} = 0.02$	Compact
0202-76	0.389	13	2.10^{-3}	3	4.5	1.64	No	Yes	$\alpha_{5000}^{408} = 0.93$	Double
0521-365	(CTS) 0.06	26	$<10^{-5}$	1	15.3	3.79	Yes	Yes	$\alpha_{8850}^{80} = 0.55$	Compact
0537-441	(CTS) 0.894	38	$<10^{-5}$	1	21.8	4.11	Yes	Yes	$\alpha_{8870}^{1410} = -0.64$	Compact
0548-322	(CTS) 0.069	17	$<10^{-5}$	1	10.0	3.00	No	No	$\alpha_{5000}^{2700} = 0.48$	?
0743-67	0.40	12	0.02	5	4.3	1.09	No	No	$\alpha_{8870}^{408} = 0.55$	?
1101-325	0.35	10	4.10^{-3}	4	3.3	1.19	No	No	$\alpha_{10600}^{2650} = 0.47$	Compact
1117-248	0.47	14	0.48	5	3.8	1.21	No	No	$\alpha_{5000}^{408} = 0.46$	?
1233-24	0.36	11	0.67	5	3.6	1.05	No	Yes	$\alpha_{5000}^{80} = 0.88$	Extended
1244-255	0.633	11	$<10^{-5}$	1	22.7	6.17	Yes	No	$\alpha_{8085}^{408} = -0.18$	?
1327-21	0.528	10	3.10^{-4}	3	8.9	2.58	No	No	$\alpha_{5009}^{160} = 0.65$	Double
1349-439/R	CTS	11	$<10^{-5}$	3	6.2	1.72	Yes	No	$\alpha_{5000}^{1410} = -0.36$	?
1349-439/O	0.323	11	$<10^{-5}$	2	7.5	2.28	N/A	Yes	N/A	N/A
1355-41	0.313	18	$<10^{-5}$	4	7.2	1.96	Yes	No	$\alpha_{8870}^{80} = 0.78$	Double

cont..

TABLE 5.2 (cont..)

OBJECT	Red Shift [1]	Number of plates	$P(\chi^2)$ [2]	Variability class* [3]	$(I_{max} - I_{min})/\sigma_s$	$\frac{\sigma(Q)}{\sigma(stars)}$	Known Radio Variable	Known Optical Variable	Radio Spectral Index [4]	Radio Structure
1422-29	?	8	0.04	5	4.5	1.79	No	No	$\alpha_{5000}^{80} = 0.84$	Compact
1424-419	?	15	$<10^{-5}$	3	8.8	2.42	Yes	No	$\alpha_{8870}^{5000} = 0.84$	Compact
1514-242	(CTS) 0.05	48	$<10^{-5}$	1	14.1	3.18	Yes	Yes	$\alpha_{8870}^{1410} = 0.10$	Compact
1933-400	CTS	13	3.10^{-3}	5	4.4	1.39	No	No	$\alpha_{8870}^{635} = -0.12$	?
1954-388	0.63	15	$<10^{-5}$	1	11.2	2.60	Yes	No	$\alpha_{8870}^{635} = -0.12$	Compact
2020-370	1.05	12	0.14	5	3.5	1.17	No	No	$\alpha_{5000}^{2700} = 0.23$	?
2052-47	?	19	$<10^{-5}$	1	8.6	2.09	Yes	No	$\alpha_{8870}^{85} = 0.42$	Compact
2058-425	0.221	11	4.10^{-3}	4	4.9	1.65	No	No	$\alpha_{5000}^{1410} = 0.54$	?
2115-30	0.98	12	$<10^{-5}$	1	7.1	2.23	No	No	$\alpha_{8850}^{80} = 0.60$	Double
2128-124	0.50	14	0.81	5	3.4	0.90	Yes	Yes	$\alpha_{8870}^{408} = -0.05$	Compact

Notes: 1. CTS refers to a featureless spectrum
2. Probability that the object is non-variable, from all observations.
3. Variability class, in the object's rest frame, excluding single discrepant points.
4. Spectral index α (from $S(\nu) \propto \nu^{-\alpha}$) between the quoted frequencies (MHz).

TABLE 5.2: Observational data for the 24 sources measured and reduced to date.

constraints on the physical conditions in the source.

The timescale of 30 days is an observational (lunar) convenience, and corresponds to the shortest time between observations for most sources. For those sources with known redshift the timescale in the quasar's rest frame can be considered. Because of the limited range of redshift in the objects considered here, this does not produce a dramatic difference. Only one source changes its classification when considered in its rest frame (PKS 2115-30, from class 2 to class 1). Objects without known redshift cannot of course be corrected.

The variability class derived for each quasar by neglecting single discrepant points, and considering timescales in the quasar's rest frame where possible, is presented in Table 5.2.

5.2.4 Rates of Variation

The relative rates of increase and decrease of luminosity provide a test of several models of quasar activity. For example, the simplest form of the multiple supernova hypothesis (see Chapter 1 for details) requires the rate of decrease of luminosity to be slower than the rate of increase.

These rates may be estimated from the observations presented here simply by dividing the change in iris reading for the quasar between consecutive observations by the time interval between those observations. This method is however unsuitable for observations separated by only a few minutes, as the random uncertainties in the iris

readings together with the short time base generate very large (incorrect) rates of change per day. As estimate of the maximum rate of change generated by statistical uncertainties may be found from $4\sigma_s/10$ days. This is 0.08 iris units/day, and suggests that observed rates of change greater than about this value are real.

The rates of increase and decrease, calculated as described above, and excluding observations separated by less than one day, are shown in Figure 5.3. There is no significant difference between the rates of increase and of decrease of luminosity. This result is in agreement with that of Angione and Smith (1972) and Angione (1973).

This observation is not in agreement with the simple multiple supernova model, or any model which requires an expanding, optically thick cloud in which variation occurs as the source becomes optically thin. It is however consistent with models in which relativistic electrons are injected into a medium which remains optically thin.

5.2.5 Timescales of Variation

Significant variations in quasars are known to occur on timescales of minutes to hours (Angione, 1971). Repeated observations for several hours during periods of activity have been obtained for both PKS 0048-09 and PKS 0537-441 to search for activity on these timescales. As yet however these observations have not been reduced. From the data currently reduced, a total of 9 changes in iris reading which exceed the sum of the uncertainties of the observations have been observed on timescales of

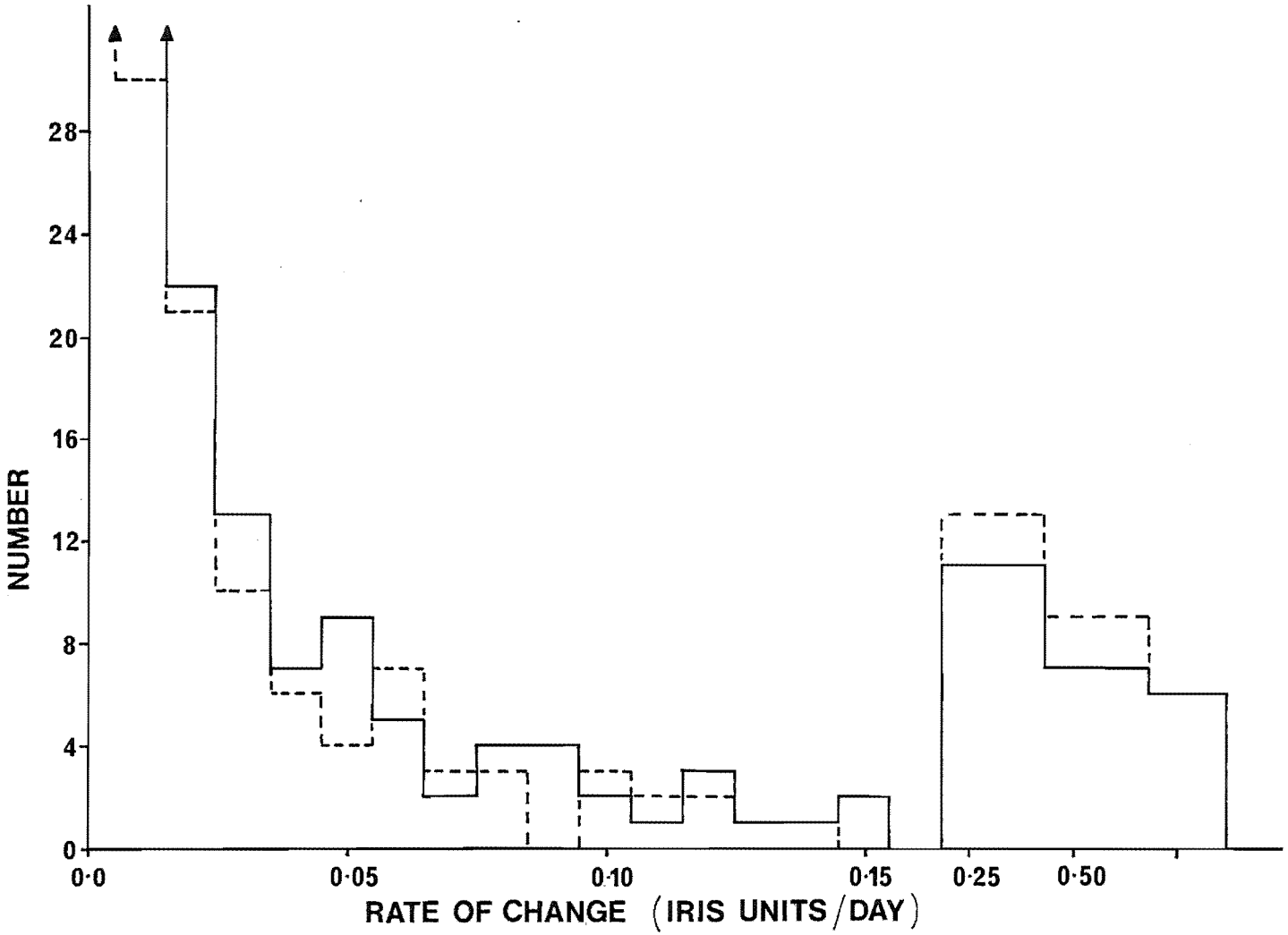

FIGURE 5.3 The observed rate of increase (solid line) and of decrease (broken line) of luminosity of the quasars studied here. Note the change of scale after a rate of 0.16 iris units/day.

less than one day. These have been detected from a total of only 50 pairs of observations of all objects with this time resolution, and suggest that activity on this timescale is a common phenomenon in quasars. The 9 observations are presented in Table 5.3., while further high time resolution observations are scheduled to allow greater study of this behaviour.

TABLE 5.3

Source	Change in Iris Reading	Sum of the uncertainties	Timescale Scale (Days)*
PKS 0537-441	0.63	0.45	0.52
	0.95	0.47	0.52
	0.48	0.32	0.52
PKS 1355-41	0.70	0.46	0.70
	0.69	0.54	0.75
PKS 1514-242†	0.78	0.42	0.98
	0.41	0.32	0.01
	0.37	0.27	0.04
	1.58	0.46	0.95

* Corrected to the rest frame values

† A change of $0^{m}.5$ in 20 min. was reported by Miller et al, (1974).

TABLE 5.3 Evidence for short timescale activity in three quasars.

5.2.6 Number of Variables.

The χ^2 test for variability produces 16 of the 24 sources which are definite variables. Of these, five (PKS 0521-365, PKS 0537-441, PKS 0548-322, PKS 1244-255,

and PKS 1514-242) would be classed as OVV (Penston and Cannon, 1970), while PKS 1954-388 would also be included on the basis of more recent observations. This does not however suggest that 25% of quasars are OVV variables. The sources with observations reduced to date were chosen because they were the best observed sources at the time of measuring. Because sources which show evidence of variability from a visual inspection of the plates are observed intensively to define that variation, an obvious selection effect is involved. A valid statistical analysis of the incidence of variability of each class must await reduction of the full data set so far available.

5.3 CORRELATIONS WITH RADIO PROPERTIES

5.3.1 Radio Variability

Eleven of the 24 sources are known radio variables, including 6 of the 8 class 1 variables, 2 of the 4 class 3 variables, 1 of the 3 class 4 variables, and 2 of the 8 non-variable sources. This indicates a tendency for sources which are optically variable to also be radio variables. This is not however a perfect correlation. For example, PKS 2115-30 is an active optical source (class 1), but is not a known radio variable, in spite of being well studied. In addition, both PKS 0135-247 and PKS 2128-124 are active radio variables, but are not detected here as optical variables. This behaviour is in agreement with Figure 2 of Heckman (1976), which shows no correlation between the range of radio

and optical variations in a sample of 11 sources.

5.3.2 Radio Spectral Index

The tendency of active optical variables to have flat high-frequency radio spectra is well known (cf. Scott et al, 1976). This relation is supported by this study in that 4 of the 8 class 1 variables have spectral indices $\leqslant 0.10$, while only 4 of the remaining 15 sources do.

5.3.3 Radio Structure

The available information on radio structure is presented in Table 5.2. As discovered in other analyses, sources with known compact structure tend to be radio variables. The most interesting feature of this sample is however that all four radio double sources are also optical variables. In particular, PKS 2115-30 is a class 1 variable. This, together with its curved high-frequency radio spectrum makes it a possible candidate for the detection of variable compact structure.

It is therefore a potential test of the model recently proposed by Scheuer and Readhead (1979). In this model, rapid observed variations are a consequence of a close alignment between a relativistically moving jet and the line of sight to the observer. Because the jet is required to power the extended radio structure, it cannot be aligned with both that structure and the observer if the source is a resolved double. Scheuer and Readhead note that the detection of relativistic

expansion effects in such a source would disprove their model. VLBI observations would therefore be of considerable interest.

5.3.4 Radio Luminosity

No relation is apparent between the type of optical variation and either the apparent or the absolute radio luminosity. Any such correlation would of course suffer considerable difficulty in accounting for non-radio source quasars which are optically variable.

There is still some confusion whether the radio-detected and radio-quiet quasars do have similar distributions in optical variability. Edwards and Smith (1977) note no differences in the occurrence of variability between the two types in their sample of 17 sources, while Savage and Osmer (reported in Faulkner and Gaskell, 1978) found a considerable difference. Similarly, Bolton (1978, private communication) finds only ~1% of his optically selected sources to be large amplitude variables, while the fraction is ~10% for radio source quasars (McGimsey et al, 1975).

While it is interesting that Q1349-439, the only non-radio source quasar measured to date, is a class 2 variable, it is hoped that the sample of optically selected sources now included in the programme will allow a reliable study of this situation.

5.3.5 Conclusions

The most important correlations noted above are those

with radio variability and radio luminosity. Because it is possible for active radio variables to show little or no optical activity, it is necessary for a viable quasar model either to separate the origins of the radio and optical activity, or to allow instabilities over only a small part of the energy spectrum of the relativistic particles being produced. This requirement is supported by the range of radio properties inherent in quasars of similar optical properties. None of the available quasar models includes these constraints as significant features.

The obvious conclusion is that the approximate correlations of optical activity with radio spectral index and radio variability indicate that a quasar which contains an optically variable source also has conditions appropriate for a variable radio source, or vice versa. The presence of one such component neither requires nor affects the other component. This is also in agreement with the lack of detailed correlation between radio and optical variations in most objects (Pomphrey et al, 1976).

5.4 CORRELATIONS WITH OPTICAL PROPERTIES.

5.4.1 Line Spectrum

Only PKS 0135-247 is reported to have an absorption feature in its spectrum. No valid test of the hypothesis that objects with absorption features are less variable than other sources (Borra, 1975) can then be made. It is interesting rather than statistically significant that this source is non-variable.

Of the six objects known to have approximately featureless

spectra, only PKS 1933-400 is non-variable. Of the other five, one is a class 3 variable, while the other 4 are all class 1 variables. A tendency for sources with featureless spectra to be highly variable is therefore established for this sample.

5.4.2 Redshift

Wills (1976) notes that the tendency of sources with absorption features to be non-variable is more likely, if real, to be a correlation of non-variability with high redshift. The apparent relation with the presence of absorption features is then a consequence of the well established tendency for high redshift quasars to have absorption features in their spectra. On the other hand, Scott et al, (1976) find no evidence for a redshift dependence in their sample of variable sources.

The objects reduced to date span only the redshift range from 0.05 to 1.05. They do not therefore allow a worthwhile test of the redshift dependence of either amplitude or existence of variability. There is no significant difference in the redshift distribution between the various variability classes.

5.4.3 Absolute Luminosity

Uomoto et al, (1976) found a 2.3 σ correlation between their variability parameter over a 20 year time base, and the absolute luminosity at 2500Å in the quasar rest frame. This suggested that low luminosity objects are intrinsically more variable than brighter objects. A similar effect was suspected by Angione (1973).

Calculation of the absolute luminosities of the objects in this sample at a specific rest-frame wavelength cannot be carried out because no optical spectral index (colour) information is available. As an approximation to the absolute luminosity of the measured sources, the parameter

$$I' = I_{mean} + 5 \log z$$

was calculated. Here I_{mean} is the mean scaled iris reading for the quasar, and z is the redshift. I' is a measure of absolute magnitude on a scale in which a numerical increase indicates increasing luminosity. Because the source spectral index is unknown, it refers to the effective wavelength of the image intensifier for each source, and not to a specified rest-frame or observer's frame wavelength. [The image intensifier effective wavelength (in the observer's frame) will be some what spectral index dependent.]

No correlation of the I' parameter with the variability index $(I_{max} - I_{min})/\sigma_s$ is apparent in this sample. Because of the uncertainties in I' however, this does not constitute definite evidence for a lack of correlation between absolute luminosity and variability.

5.4.4 Conclusions

Other than the well known tendency for objects with featureless optical spectra to be active variables, no correlation between variability and any other optical property has been established. This may well be primarily due to the small sample studied, and the fact that in most cases no information other than redshift is available.

Because of the limited time span and irregular spacing of the observations, no worthwhile analysis of possible periodic behaviour is possible.

5.5 TESTS OF QUASAR MODELS

5.5.1 Variations Due to Eclipses

The possibility that a rapid decrease and recovery in luminosity could be due to an eclipse of the central energy source by a filament was considered by Cannon and Penston (1967). They considered the eclipse of the central source in 3C446 by clouds, possibly those associated with the line emission.

Very rapid increases and decreases closely following each other are evident in several instances in the light curves of PKS 0521-365, PKS 0537-441, PKS 0548-322, and PKS 1514-242. Similar activity is possibly present in PKS 1424-419 and PKS 2052-47. It is of interest that the four variables which definitely show this type of activity all have featureless spectra. No observations are available for the other two sources.

This correlation with continuous spectra is strong evidence against an eclipse model for this type of variation. The eclipse-like phenomena are sufficiently common, and of such short duration, that a large number of high velocity clouds would be necessary. If scattering by electrons or dust is the mechanism of extinction, the scattered luminosity from those clouds not in the line of sight would dominate the observed luminosity, and very rapid variations due to a single

cloud eclipse would not be of large amplitude. If the absorption is by bound-bound or bound-free transitions, significant recombination line emission would be expected, in contradiction to observations. Similarly absorption by dust can be excluded. In this case it would be possible to detect substantial thermal re-emission, and large and variable internal reddening. The position of such a dust cloud is also a tight constraint. For an assumed quasar mass of 10^8 $M_\odot$ and a cloud velocity of 4,000 km s^{-1}, the cloud would be only 30 Schwarzschild radii from the central source. It would therefore be both hot and in an environment where long term stability is unlikely.

The possibility that eclipses are caused by stars spiralling into a massive black hole is consistent in both timescale and velocity with the observations reported here. This possibility can be excluded only by observations which show a rapid increase in luminosity above a relatively stable level. Such an observation would, of course, exclude all eclipse models. If the stellar number density were sufficiently high to allow the very large number of eclipses observed however, considerable gaseous debris and consequent line emission would be expected.

It is therefore unlikely that the observed rapid changes in luminosity are evidence of an eclipse-like phenomenon.

5.5.2 Multiple Supernova Models

The disagreement between the predicted and observed ratio of rates of increase and decrease of luminosity is discussed above (section 5.2.4). This ratio, which is not significantly different from unity, is inconsistent with the simple multiple supernova models.

A second possibility in connection with these models is optical emission by Cerenkov radiation (cf. Chapter 1). In this case the source luminosity L and radius R are related by

$$L = 1.6.10^{73} R^{-2} \text{ ergs } s^{-1}cm^{-2} \quad .$$

This implies that low luminosity sources are intrinsically large. If so, there should be a correlation between low luminosity and slow rates of variation. This is not supported by the observations presented here.

Another difficulty for the multiple supernova model is the large flare observed in PKS 1244-255. This does not bear any resemblance to a supernova outburst.

5.5.3 Spinar and Magnetoid Models

Models in which a coherent, massive, non-collapsed object releases energy by low frequency magneto-dipole emission were discussed in section 1.5. These models predict that the observed rate of decrease of luminosity is slower than the observed rate of increase. This prediction is not consistent with the observational results presented in Figure 5.3.

5.5.4 Black Hole Models

A simple relation between source luminosity L and the minimum timescale for substantial variation, t_{min}, may be derived for a black hole accreting at the Eddington limit (Elliott and Shapiro, 1974; section 1.6). This relation is

$$t_{min} \geqslant 7.8.10^{44} L \text{ (ergs s}^{-1}\text{)} \quad \text{s.}$$

The minimum observable timescale is then (1 + z) times this value. This derivation however ignores relativistic effects in the source. As shown in Chapter 2, these may be substantial.

Elliott and Shapiro calculate the total source luminosity by integrating the observed source spectrum as a single power law between rest frame wavelengths of 2500Å and 1 metre. This is conservative in choice of the high energy cutoff, underestimates the infra-red flux, and assumes a single component source. In spite of the lack of evidence for correlated radio and optical variability in most sources (Pomphrey et al, 1976 and cf. Dent et al, 1979), observations by O'Dell et al, (1978) suggest that this last assumption is valid.

The luminosity and fastest observed rate of change (corrected to the quasar rest frame) are related in Figure 5.4., which is adapted from Figure 1 of Elliott and Shapiro (1974). This includes observations of the 7 sources observed to show significant variation ($\geqslant 0^{m}.3$) on timescales (rest frame) of a few days or less. These times, together with the luminosity, derived following

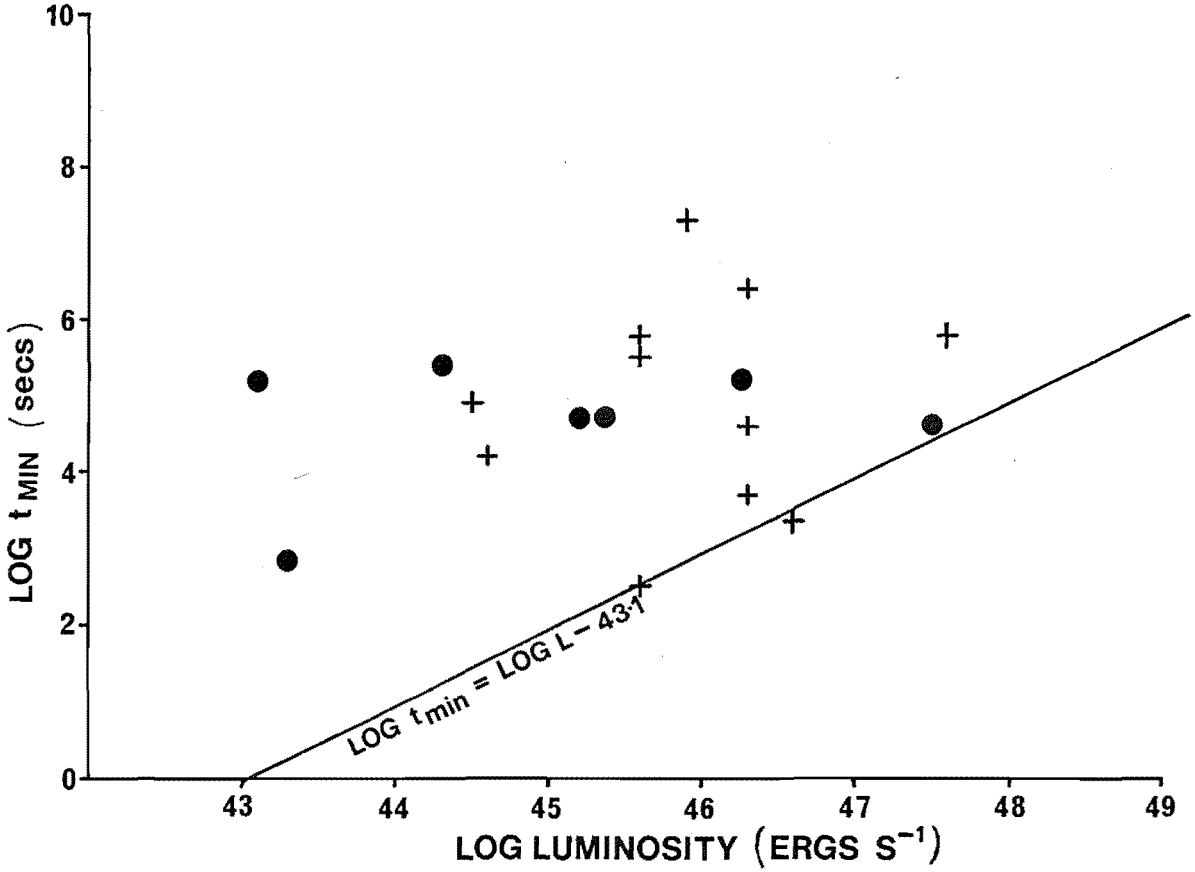

FIGURE 5.4 The relation between fastest observed timescale and luminosity. The crosses are data from Elliott and Shapiro (1974), the solid points from this thesis.

the definition of Elliott and Shapiro, are presented in Table 5.4 for those rapid variables with known redshift.

TABLE 5.4

Source	Log Luminosity (ergs s^{-1})*	Log (Minimum Timescale)**secs.
PKS 0521-365	44.31	5.41
PKS 0537-441	47.50	4.66
PKS 0548-322†	43.11†	5.24
PKS 1244-255	45.33	4.72
PKS 1355-41	45.19	4.82
PKS 1514-242	43.25	2.95
PKS 1954-388	46.26	5.20

* as defined by Elliott and Shapiro (1974)

** rest frame values

† derived from X-ray observations because of insufficient radio data.

TABLE 5.4: Luminosities and fastest timescales for the very rapid variables considered here.

In Figure 5.4., only PKS 0537-441 is close to the limiting line in the figure. This timescale however ignores the internal relativistic expansion in the source, and should be treated with caution.

The fact that no source is significantly below the line in Figure 5.4 is consistent with the model of an accreting massive black hole, but does not of course prove it.

A more complete analysis than that of this chapter must await the reduction of the observation of the remaining sources in the Mt. John sample.

5.6 LIGHT CURVES FOR TWENTY-FOUR QUASARS

This section presents the light curves for the 24 quasars considered in this study (Figure 5.3), and the two probably variable comparison stars (Figure 5.4). The details of the observations are presented in Appendix II.

This section also presents the light curves of the 2 possibly variable comparison stars, and the 2 misidentified galactic stars.

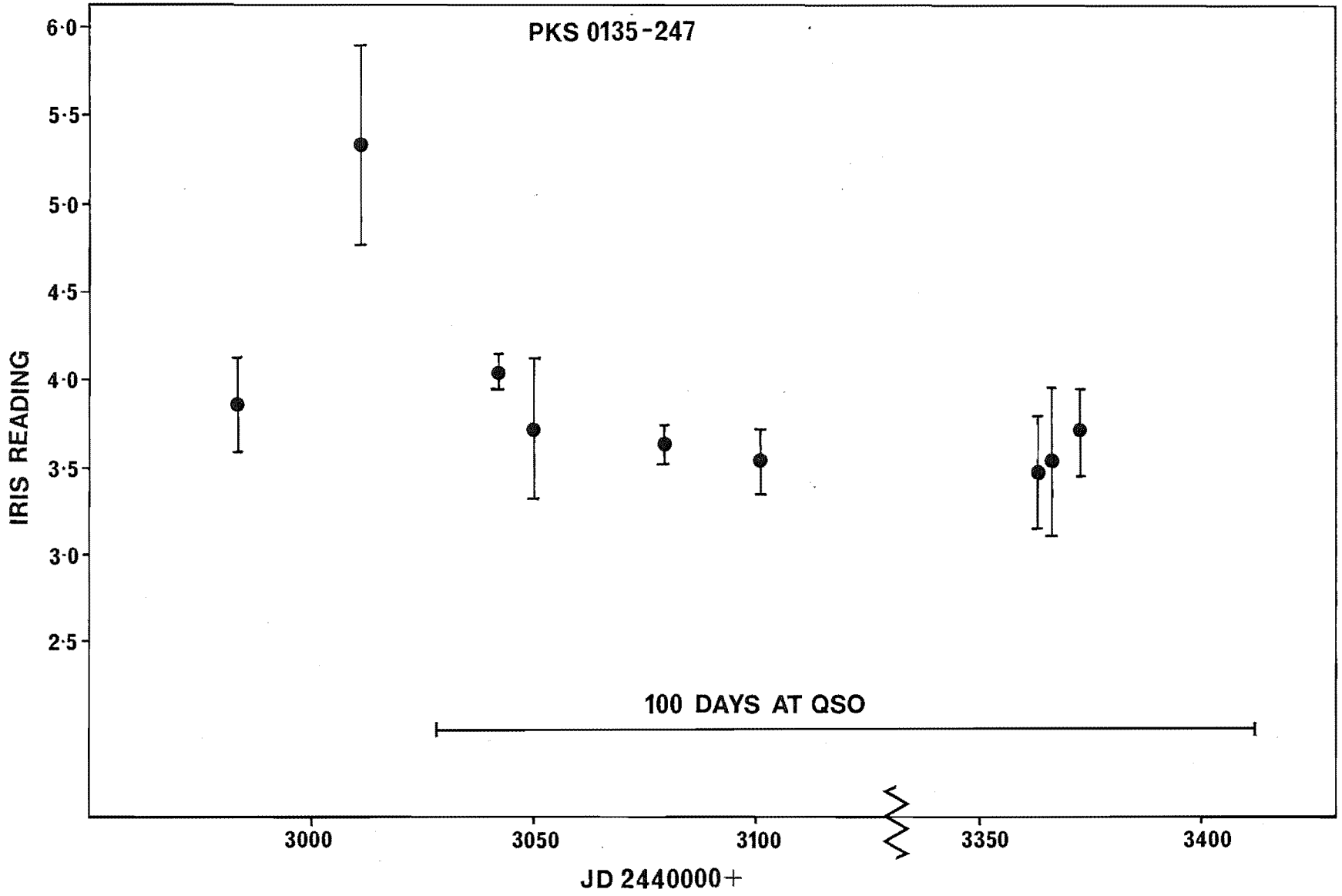
PKS 0135-247
IRIS READING
6·0
5·5
5·0
4·5
4·0
3·5
3·0
2·5
100 DAYS AT QSO
3000
3050
3100
3350
3400
JD 2440000+

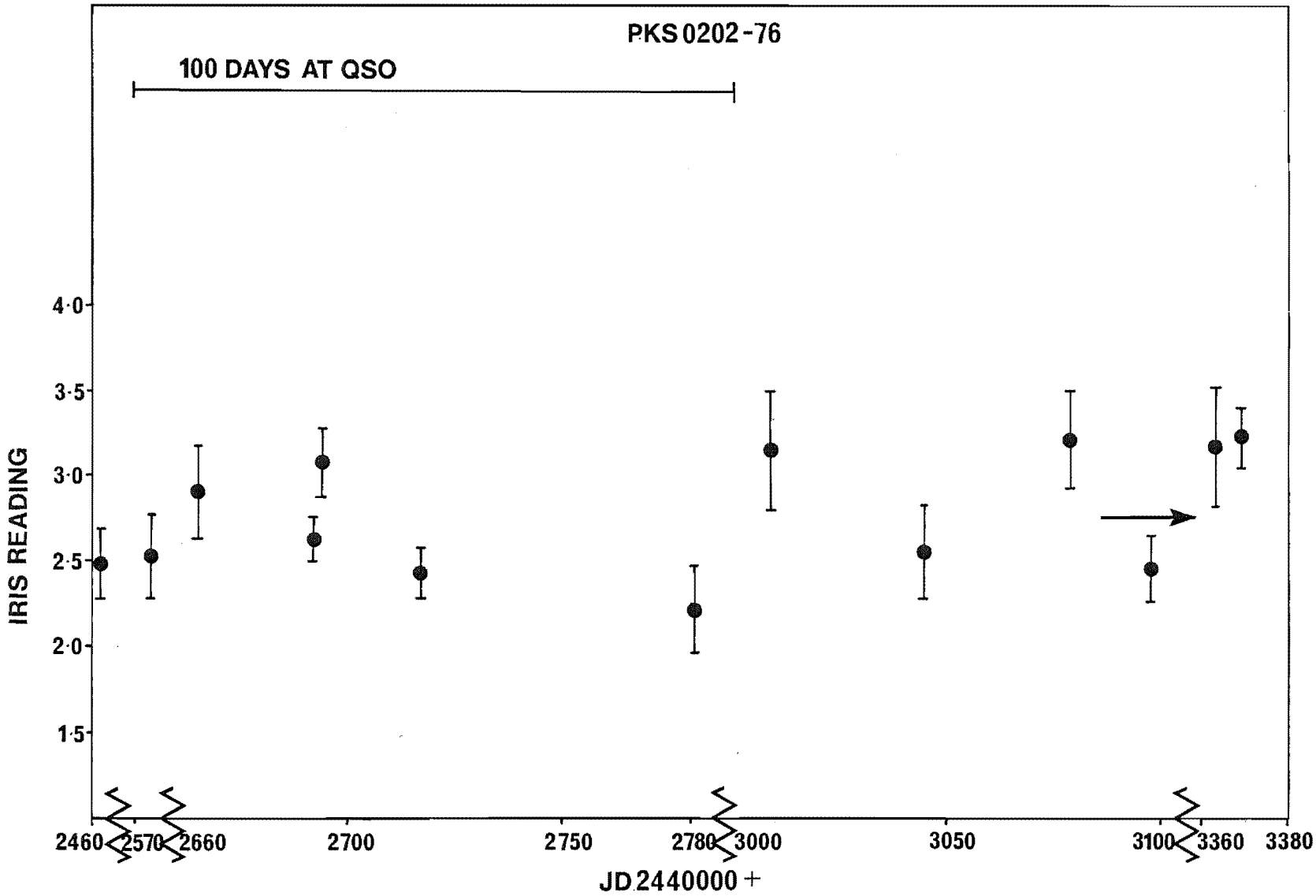
PKS 0202-76
100 DAYS AT QSO
IRIS READING
4·0
3·5
3·0
2·5
2·0
1·5
2460
2570
2660
2700
2750
2780
3000
3050
3100
3360
3380
JD 2440000 +

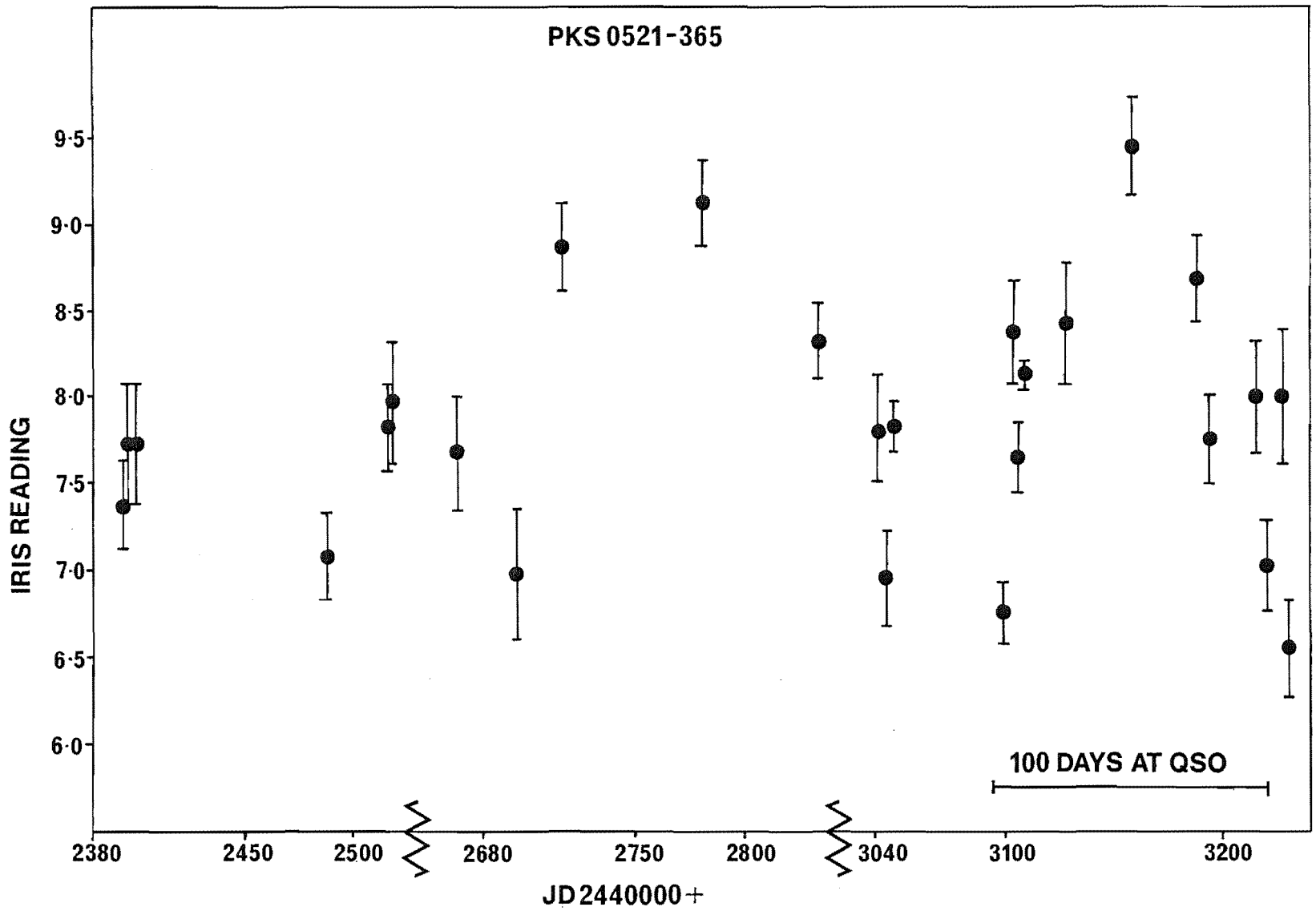
PKS 0521-365
IRIS READING
9·5
9·0
8·5
8·0
7·5
7·0
6·5
6·0
100 DAYS AT QSO
2380
2450
2500
2680
2750
2800
3040
3100
3200
JD 2440000+

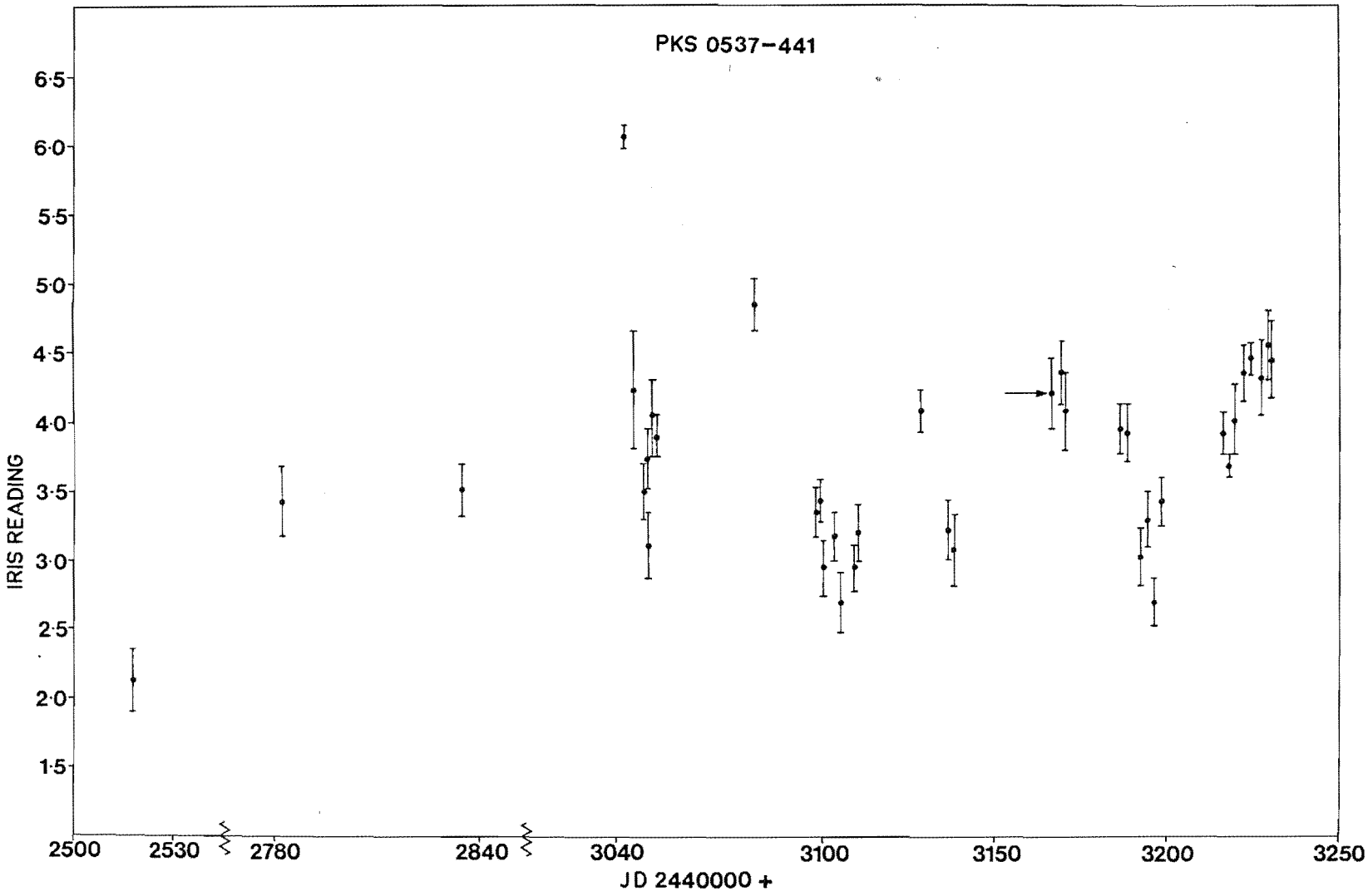
PKS 0537−441
IRIS READING
6·5
6·0
5·5
5·0
4·5
4·0
3·5
3·0
2·5
2·0
1·5
2500
2530
2780
2840
3040
3100
3150
3200
3250
JD 2440000 +

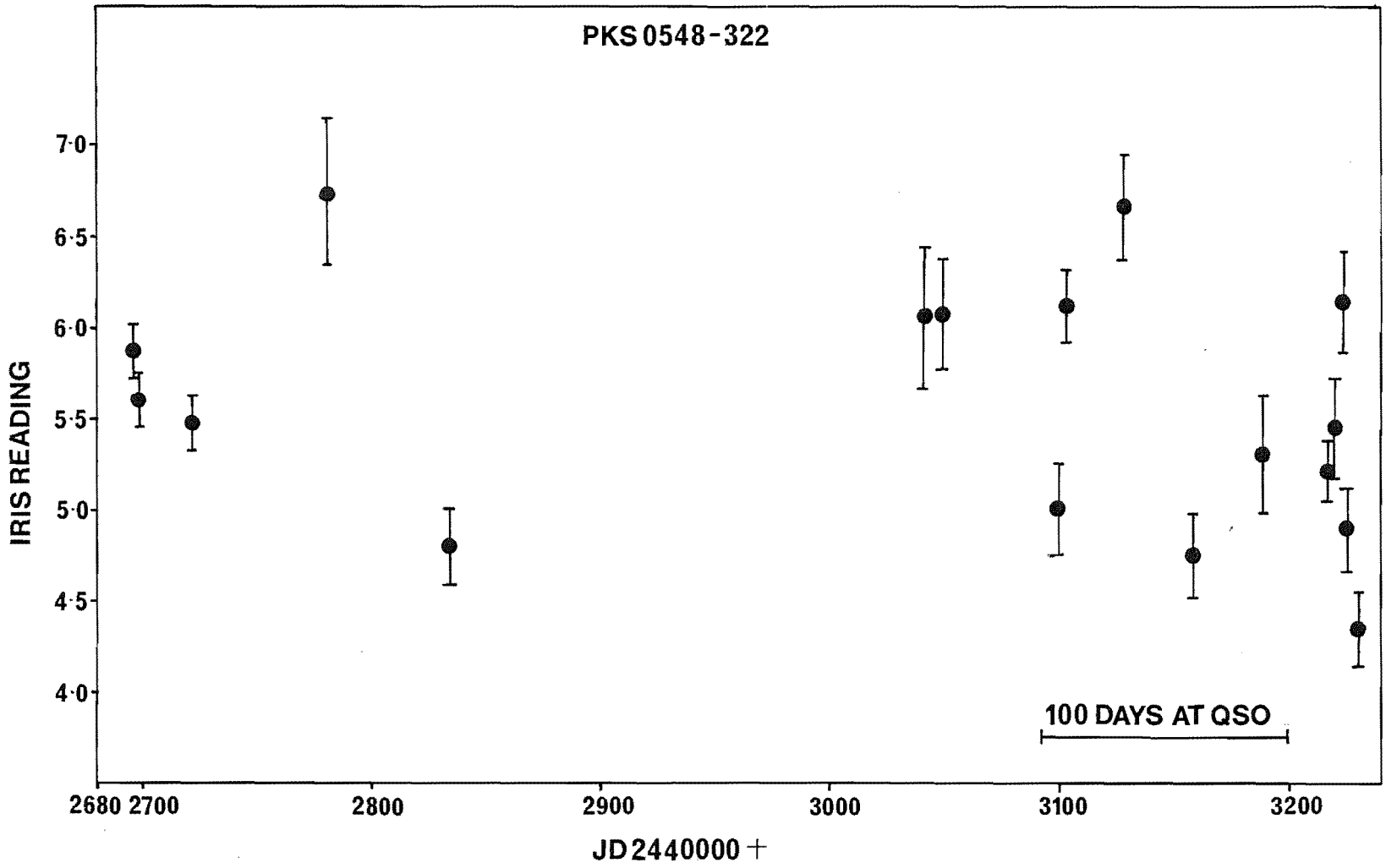
PKS 0548-322
IRIS READING
7·0
6·5
6·0
5·5
5·0
4·5
4·0
100 DAYS AT QSO
2680 2700
2800
2900
3000
3100
3200
JD 2440000 +

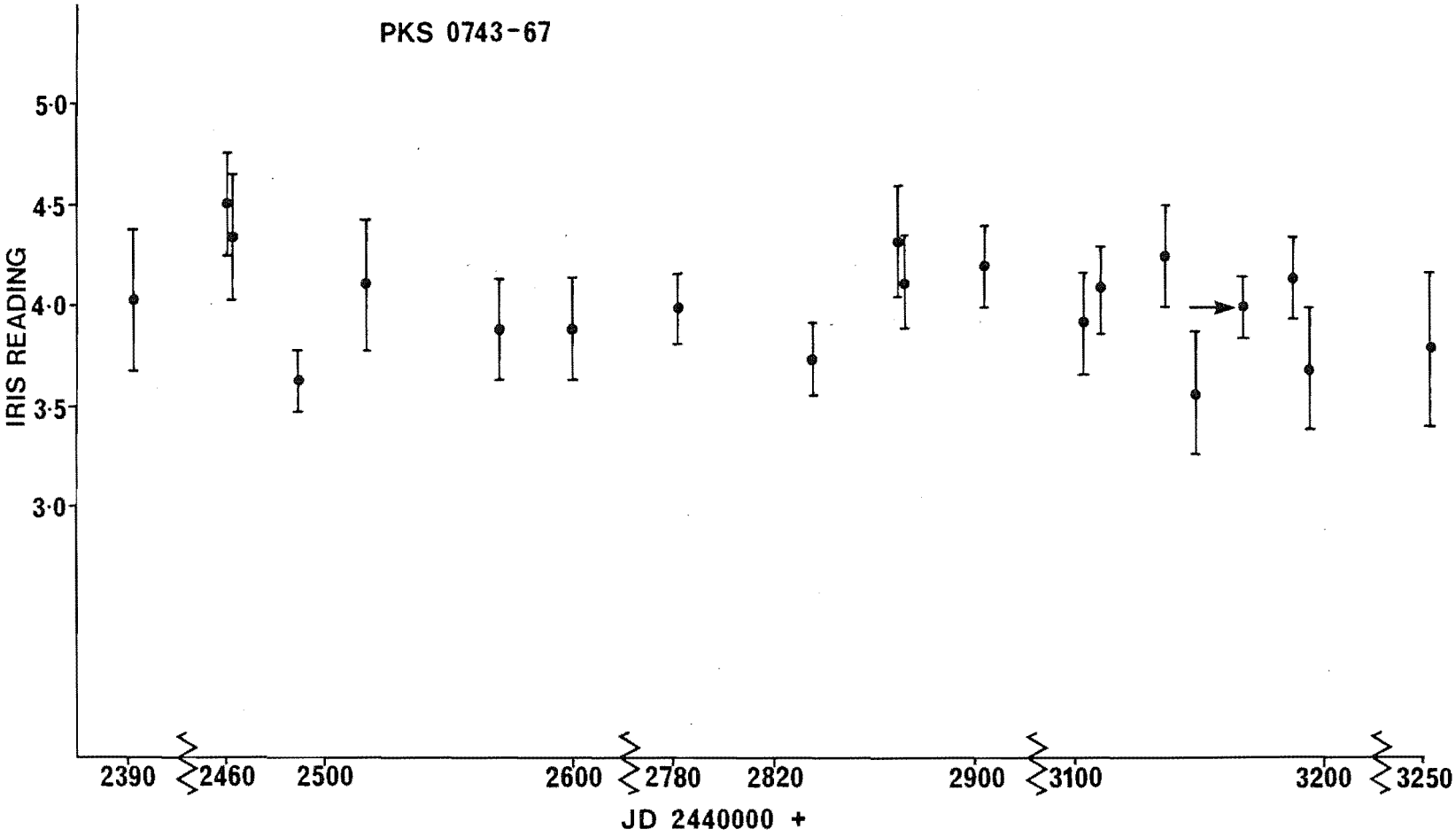
PKS 0743-67
IRIS READING
5·0
4·5
4·0
3·5
3·0
2390
2460
2500
2600
2780
2820
2900
3100
3200
3250
JD 2440000 +

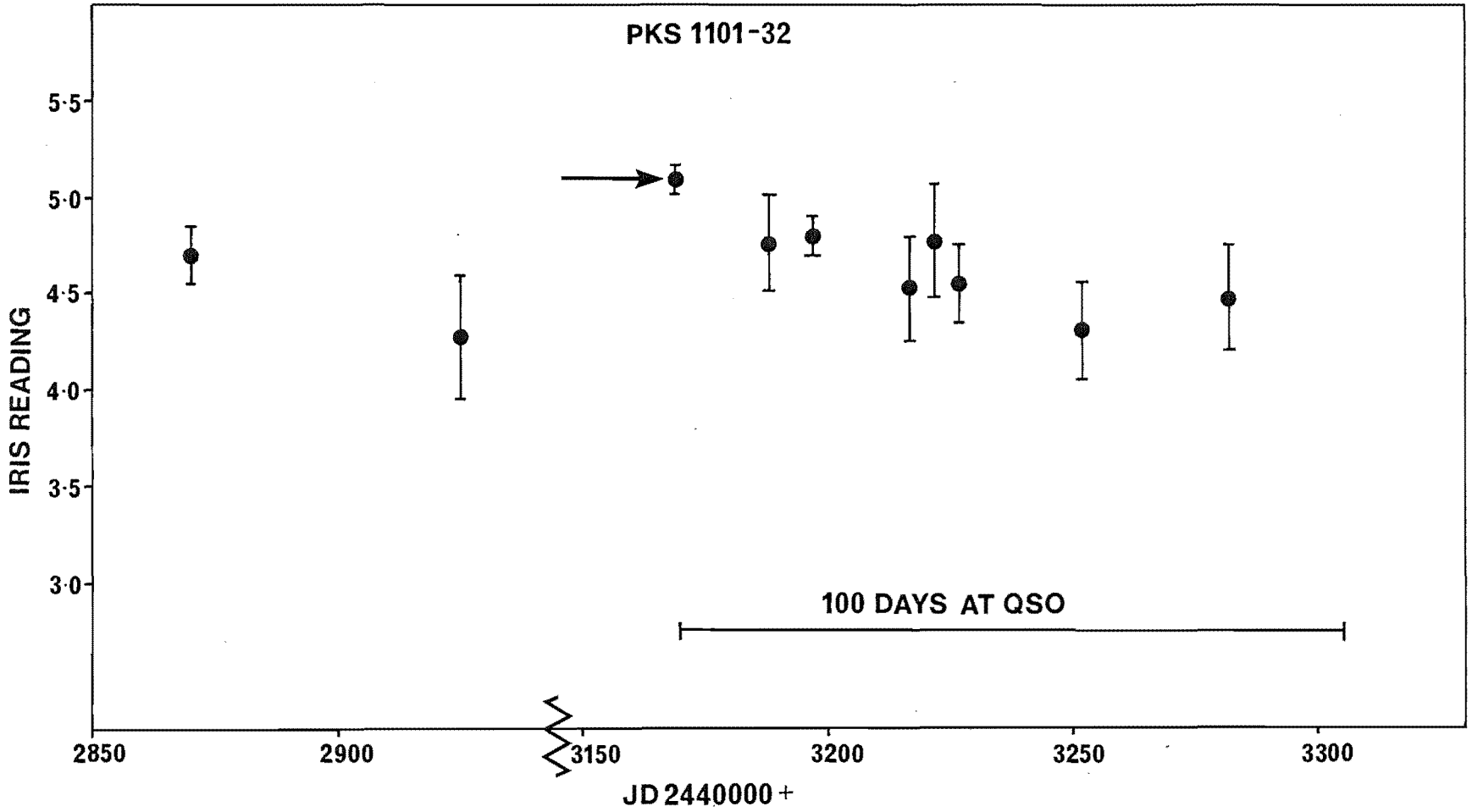
PKS 1101-32
IRIS READING
5·5
5·0
4·5
4·0
3·5
3·0
100 DAYS AT QSO
2850
2900
3150
3200
3250
3300
JD 2440000 +

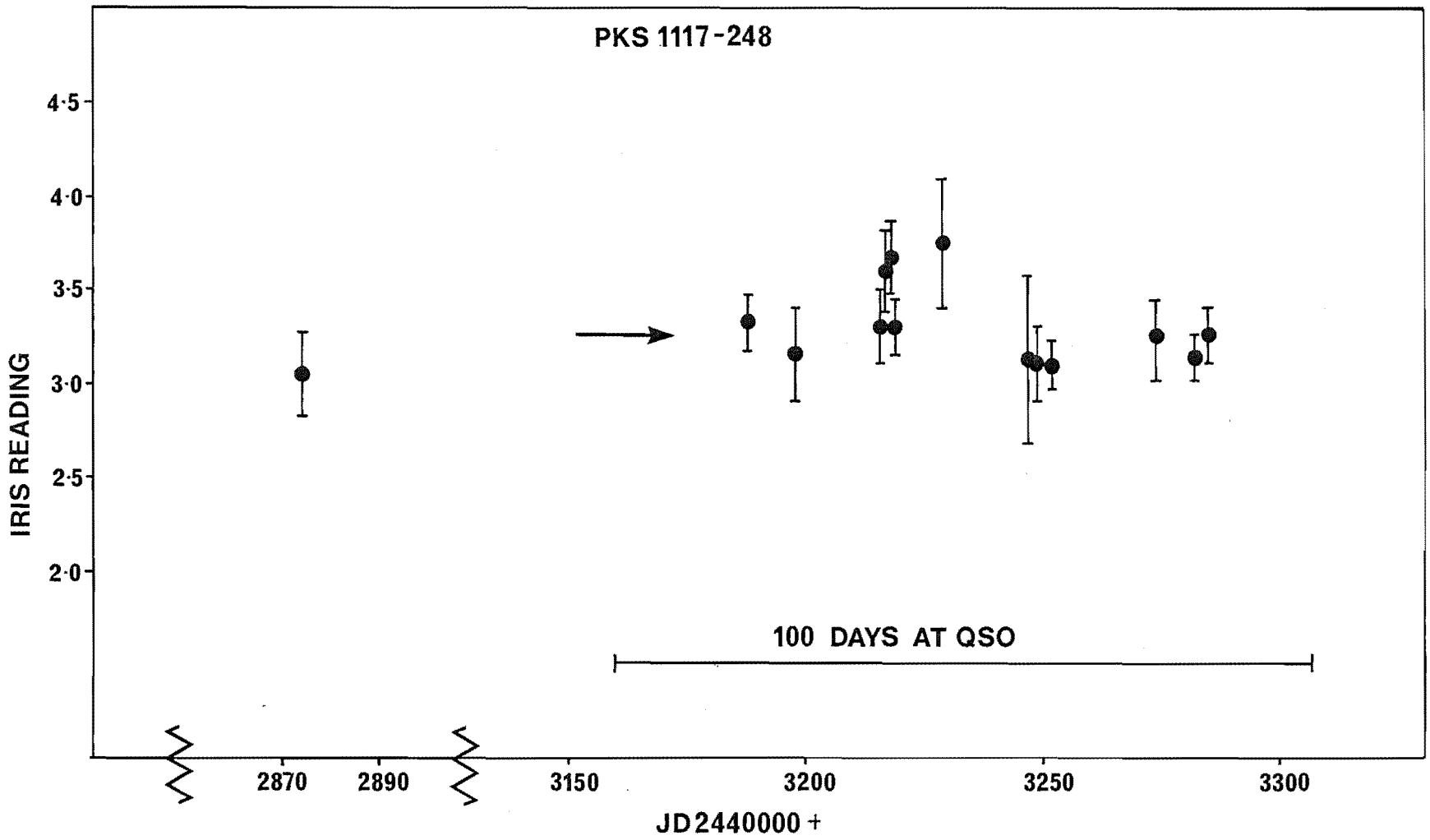
PKS 1117-248
IRIS READING
4·5
4·0
3·5
3·0
2·5
2·0
100 DAYS AT QSO
2870
2890
3150
3200
3250
3300
JD2440000 +

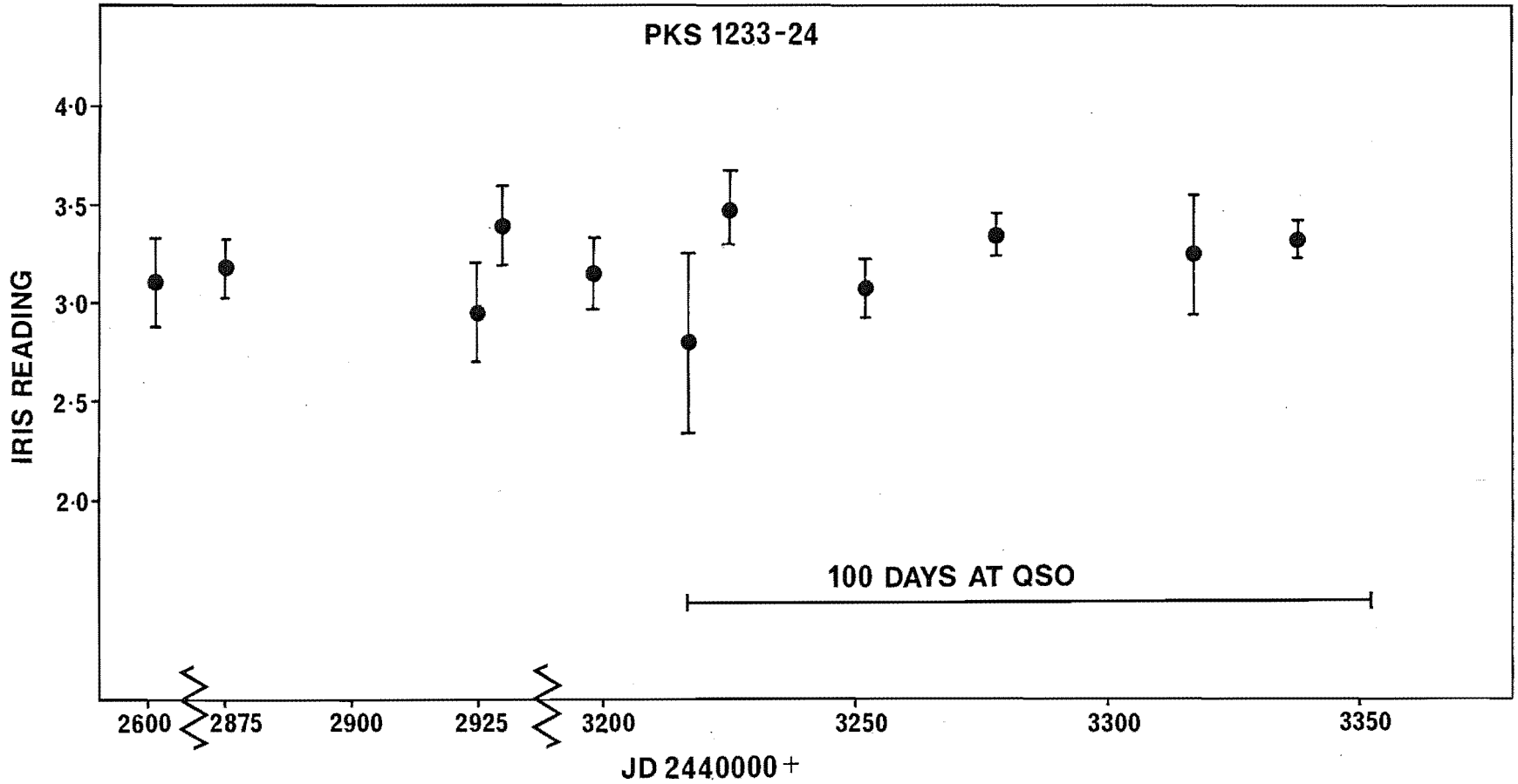
PKS 1233-24
IRIS READING
4·0
3·5
3·0
2·5
2·0
100 DAYS AT QSO
2600
2875
2900
2925
3200
3250
3300
3350
JD 2440000 +

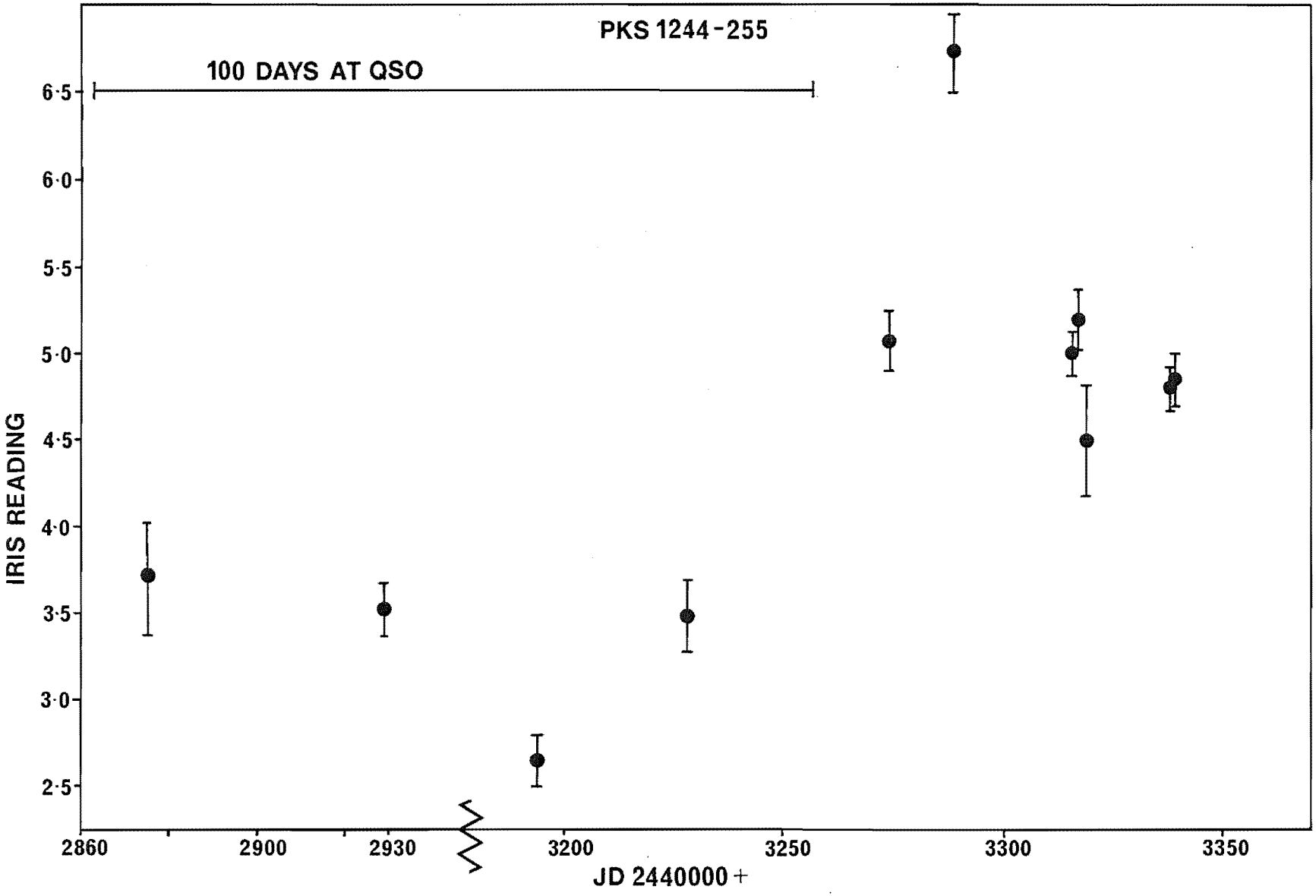
PKS 1244-255
100 DAYS AT QSO
IRIS READING
6·5
6·0
5·5
5·0
4·5
4·0
3·5
3·0
2·5
2860
2900
2930
3200
3250
3300
3350
JD 2440000+

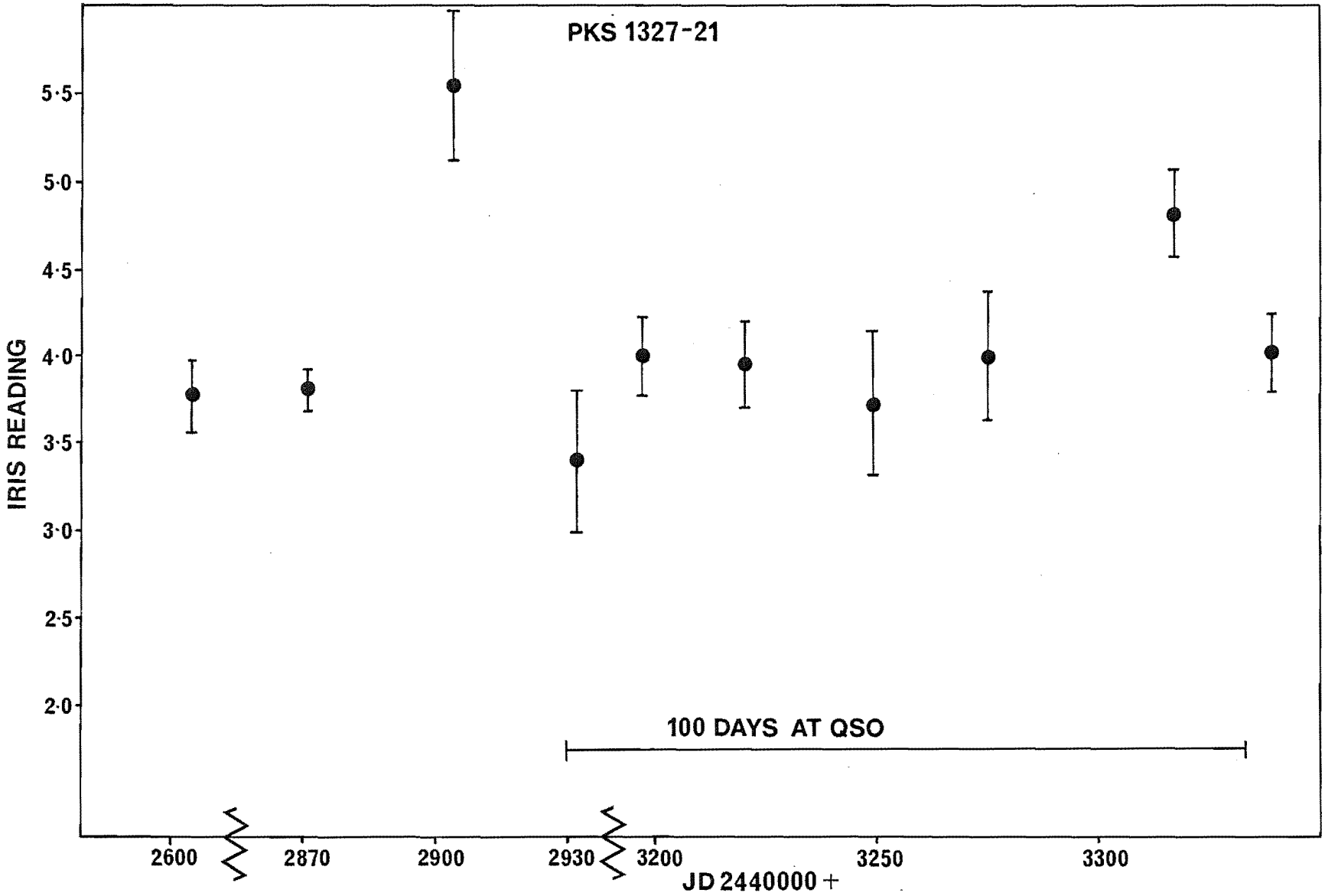
PKS 1327-21
IRIS READING
5·5
5·0
4·5
4·0
3·5
3·0
2·5
2·0
100 DAYS AT QSO
2600
2870
2900
2930
3200
3250
3300
JD 2440000 +

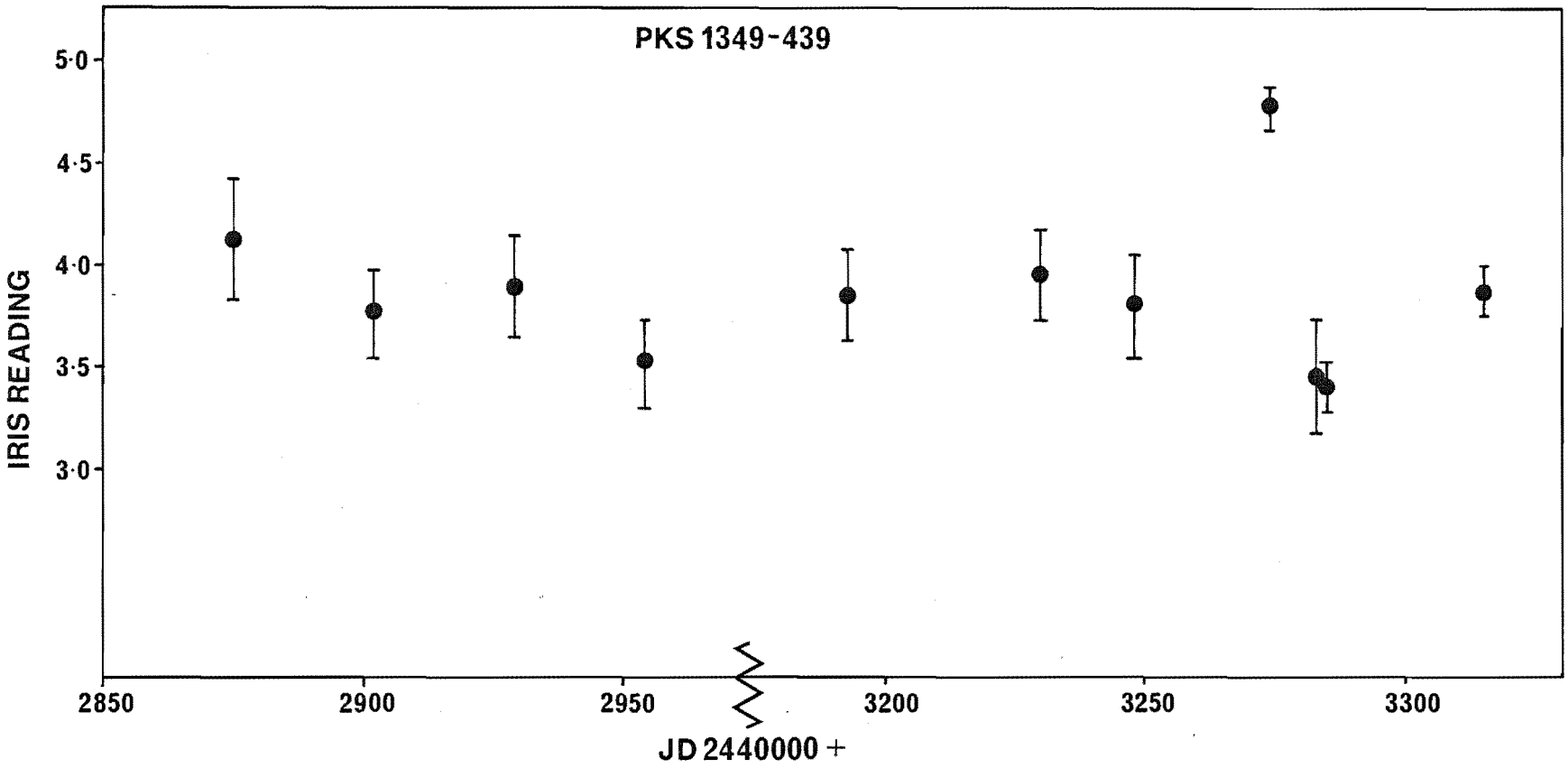
PKS 1349-439
IRIS READING
5·0
4·5
4·0
3·5
3·0
2850
2900
2950
3200
3250
3300
JD 2440000 +

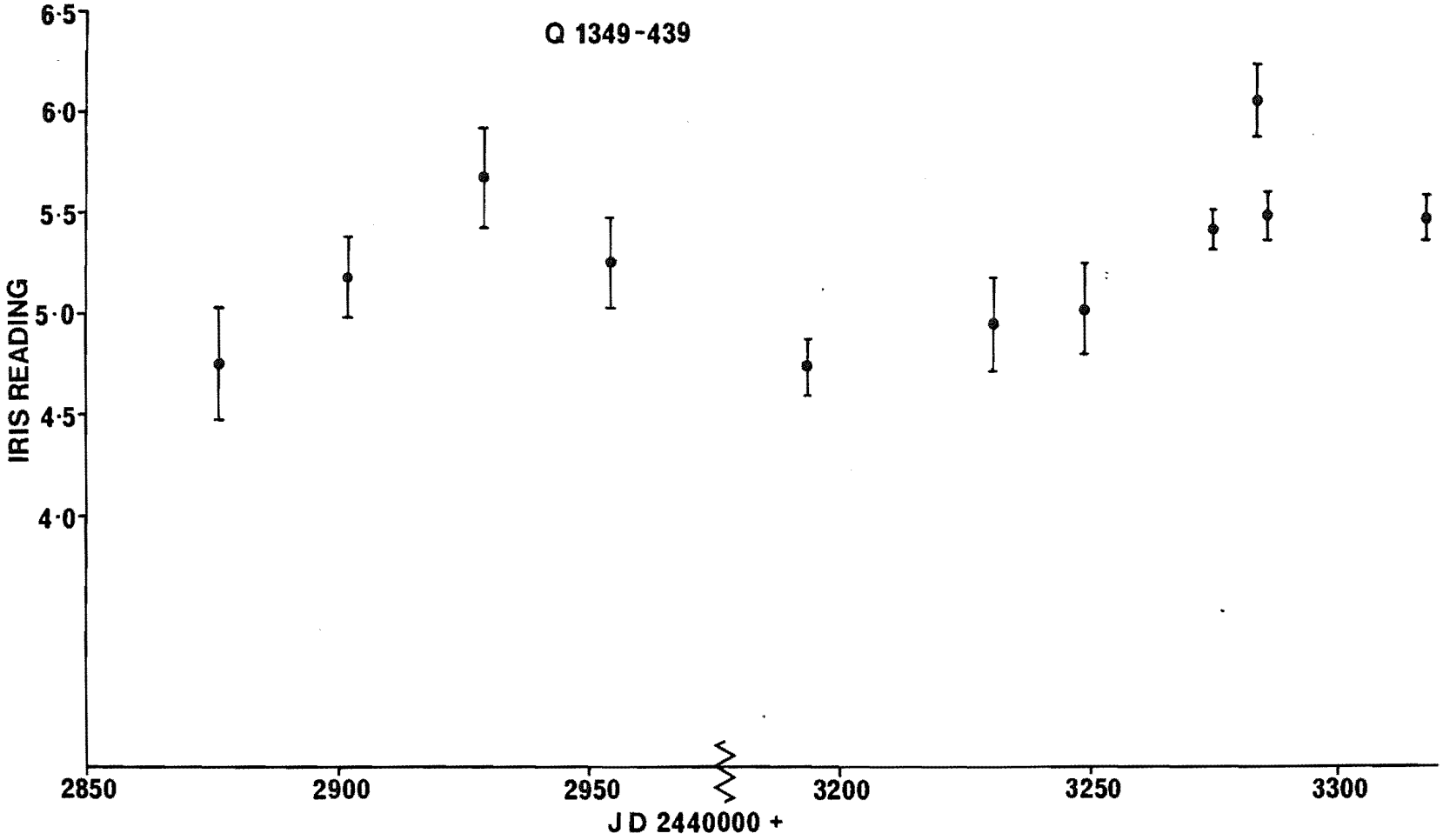
Q 1349-439
IRIS READING
6·5
6·0
5·5
5·0
4·5
4·0
2850
2900
2950
3200
3250
3300
J D 2440000 +

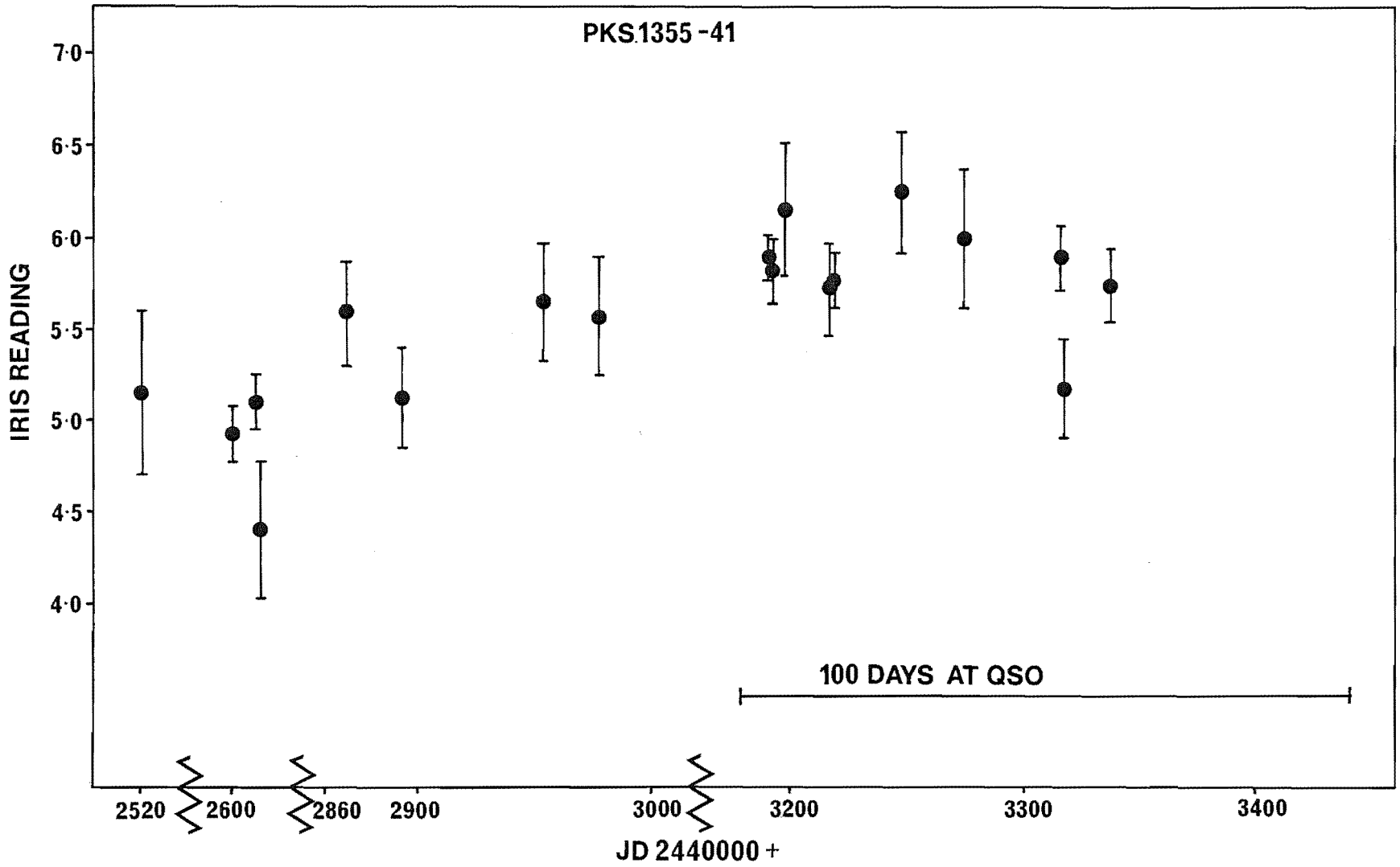
PKS 1355 -41
IRIS READING
7·0
6·5
6·0
5·5
5·0
4·5
4·0
100 DAYS AT QSO
2520
2600
2860
2900
3000
3200
3300
3400
JD 2440000 +

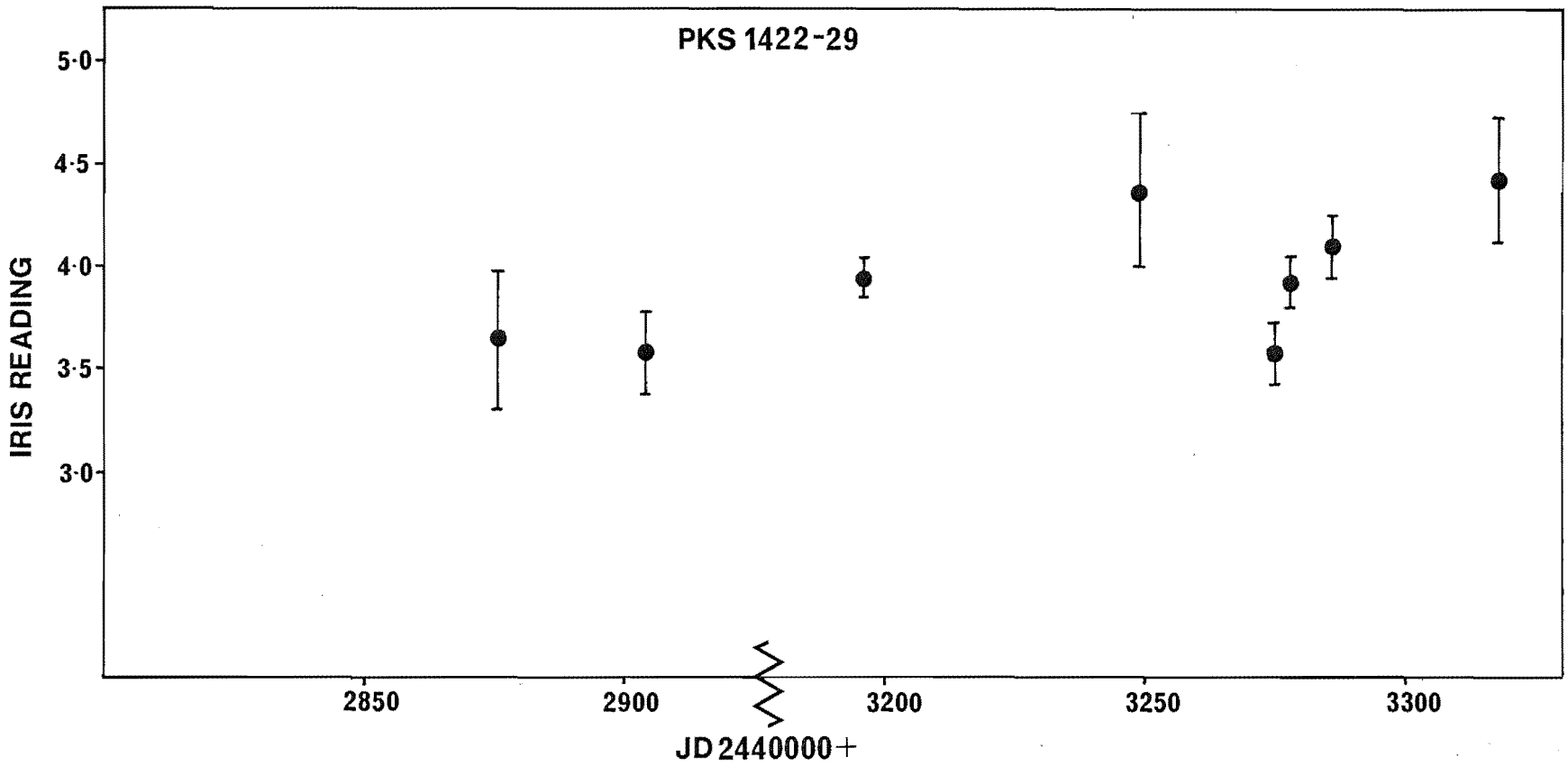
PKS 1422-29
IRIS READING
5·0
4·5
4·0
3·5
3·0
2850
2900
3200
3250
3300
JD 2440000+

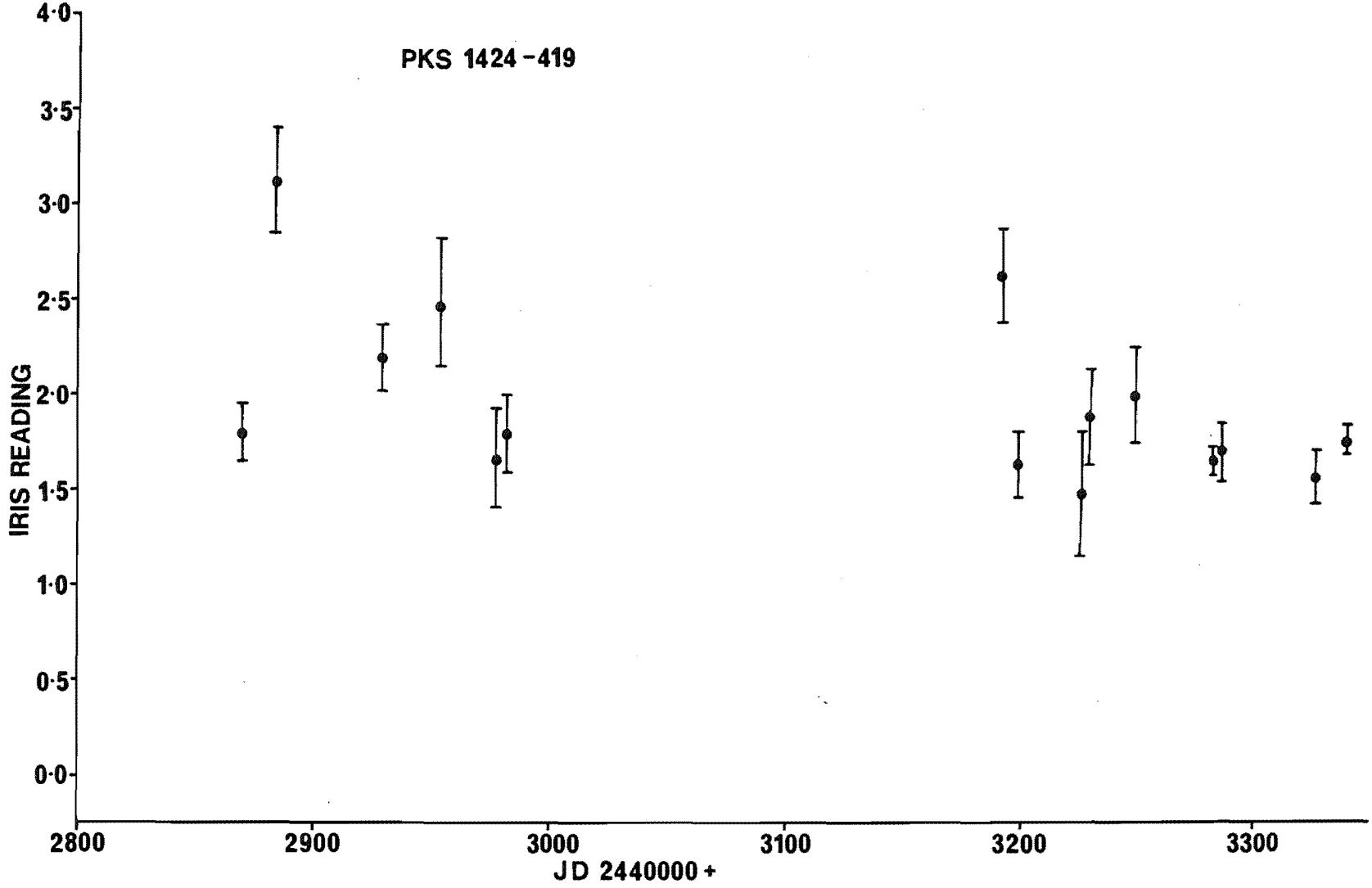
PKS 1424 -419
IRIS READING
4·0
3·5
3·0
2·5
2·0
1·5
1·0
0·5
0·0
2800
2900
3000
3100
3200
3300
JD 2440000 +

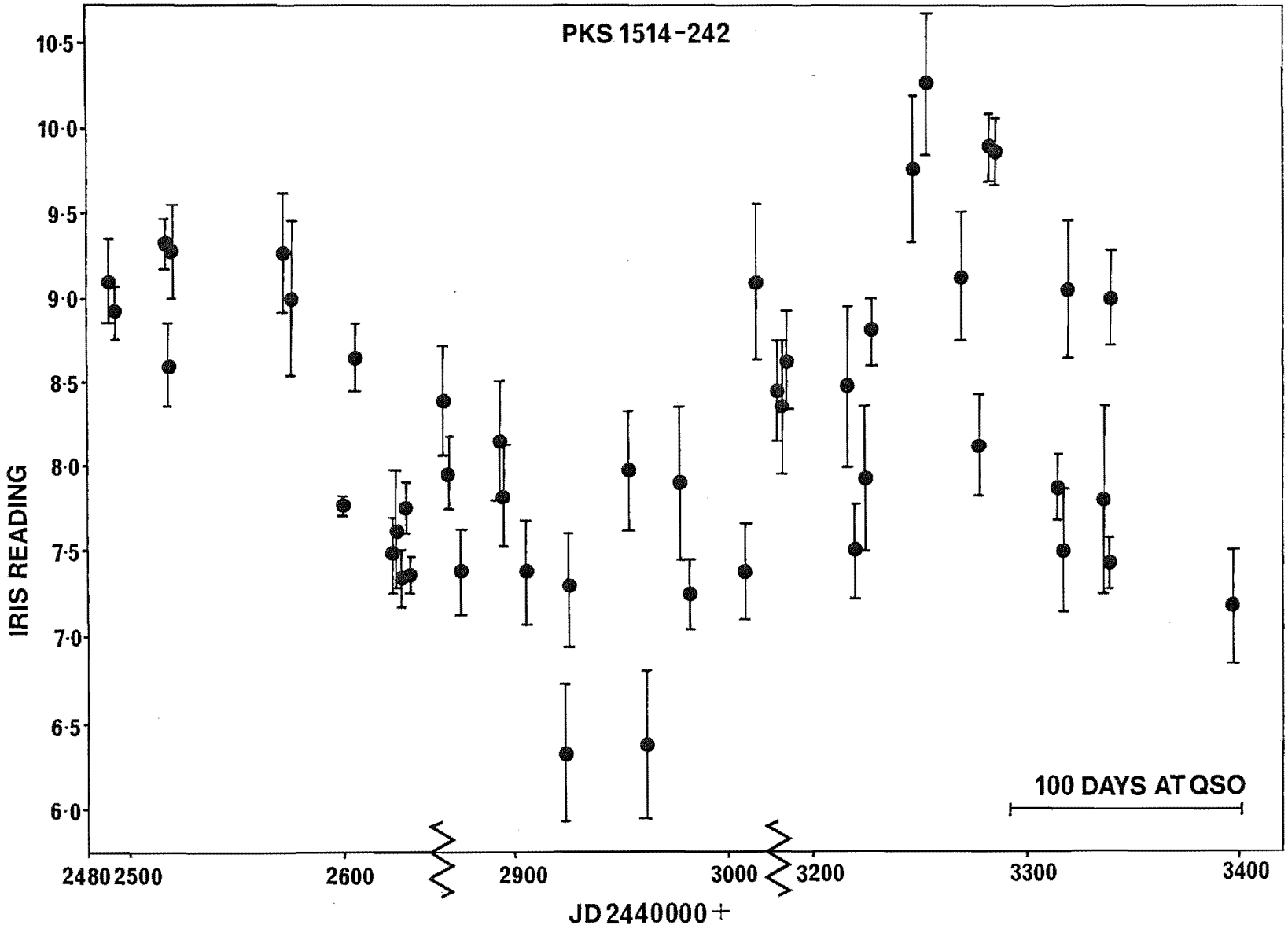
PKS 1514-242
IRIS READING
10·5
10·0
9·5
9·0
8·5
8·0
7·5
7·0
6·5
6·0
2480 2500
2600
2900
3000
3200
3300
3400
JD 2440000 +
100 DAYS AT QSO

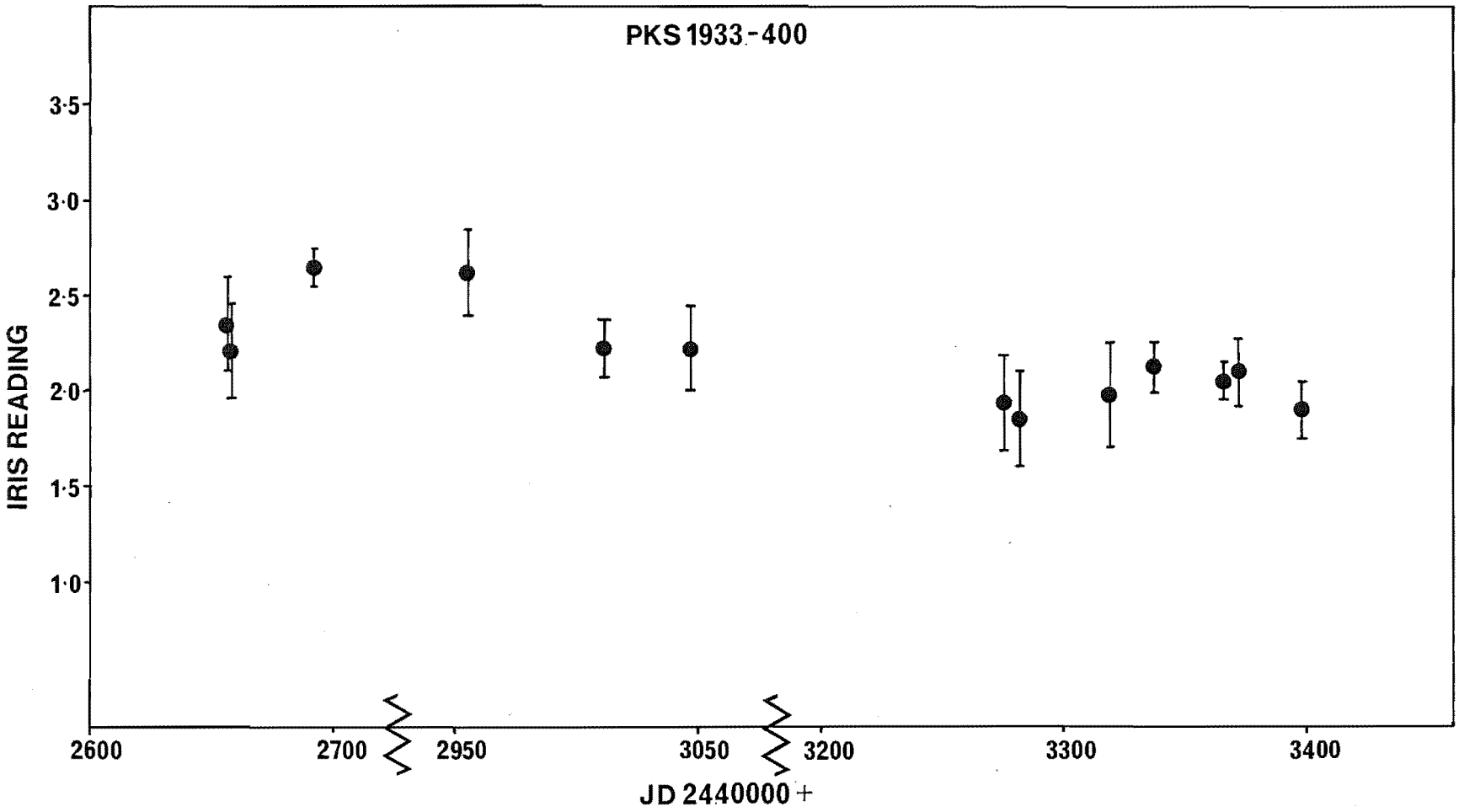
PKS 1933-400
IRIS READING
3·5
3·0
2·5
2·0
1·5
1·0
2600
2700
2950
3050
3200
3300
3400
JD 2440000+

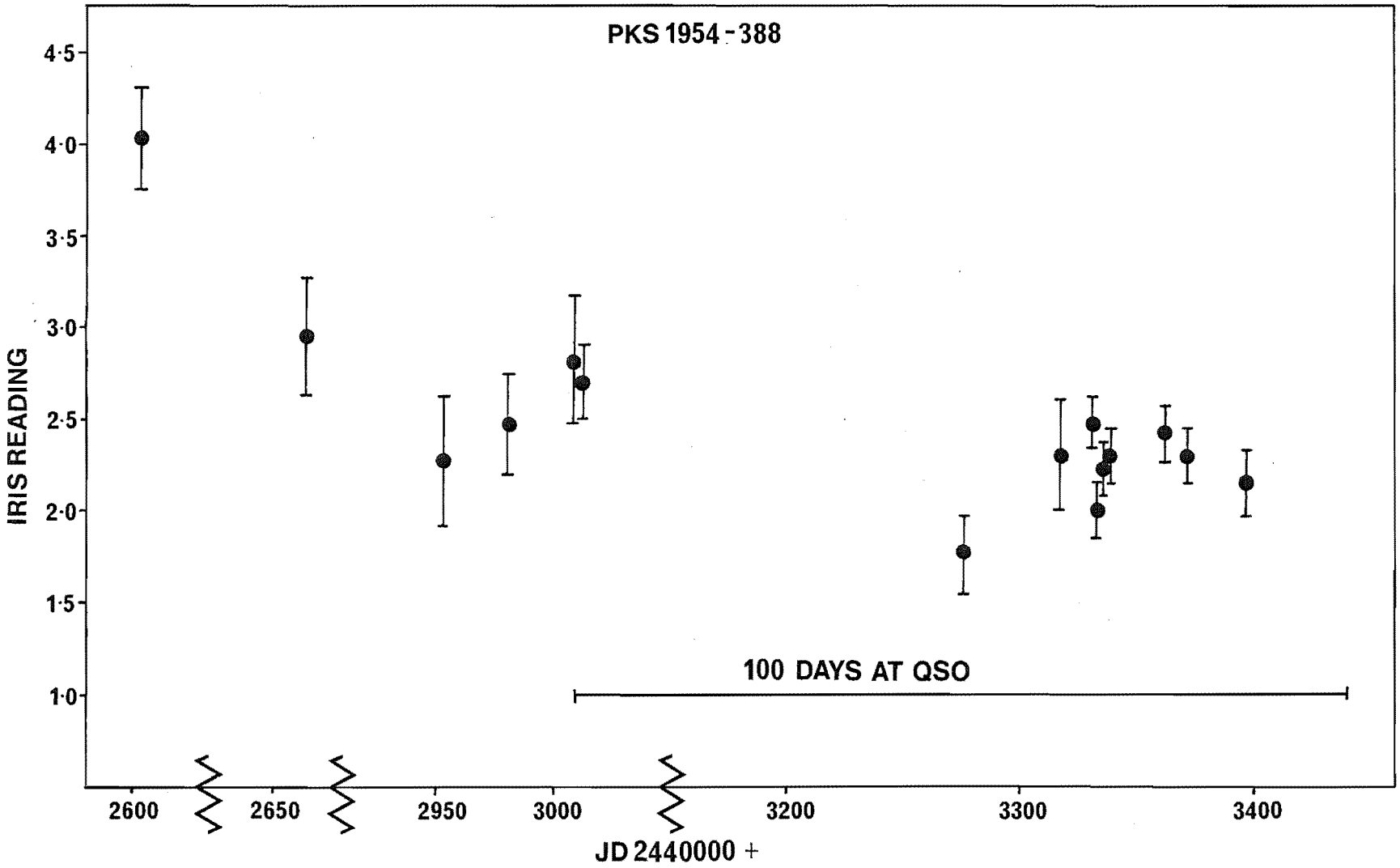
PKS 1954-388
IRIS READING
4·5
4·0
3·5
3·0
2·5
2·0
1·5
1·0
100 DAYS AT QSO
2600
2650
2950
3000
3200
3300
3400
JD 2440000 +

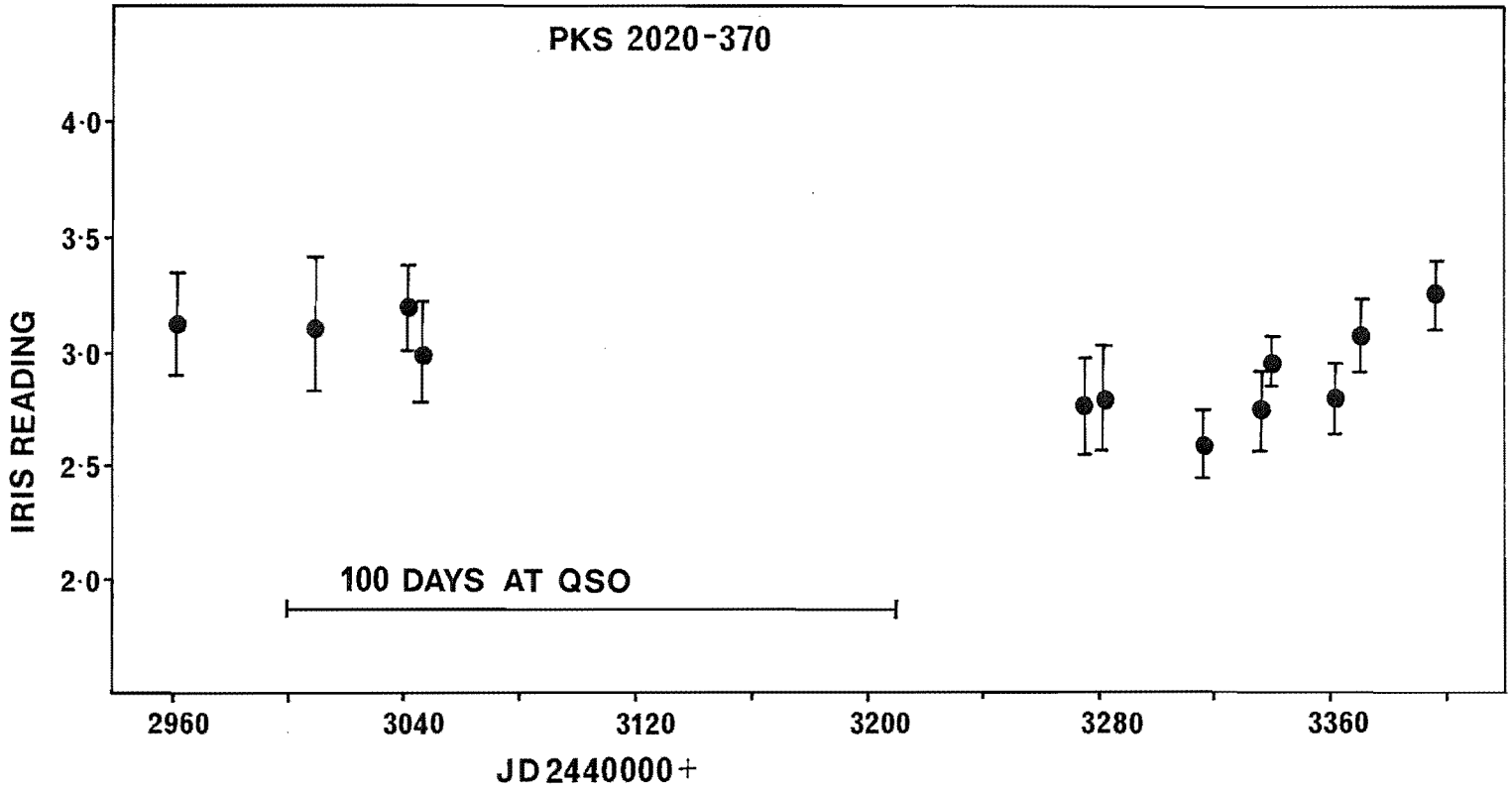
PKS 2020-370
IRIS READING
4·0
3·5
3·0
2·5
2·0
100 DAYS AT QSO
2960
3040
3120
3200
3280
3360
JD 2440000+

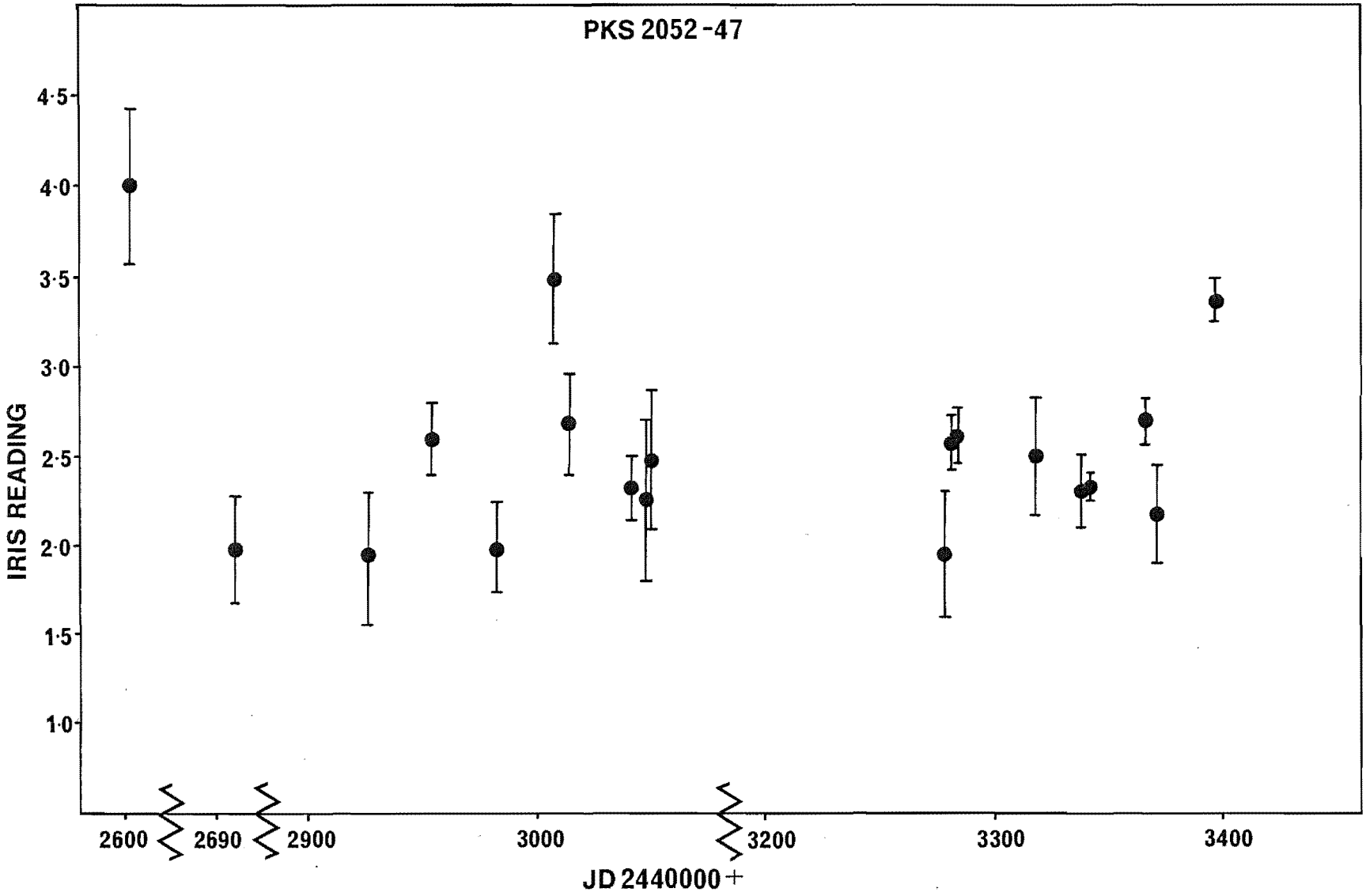
PKS 2052-47
IRIS READING
4·5
4·0
3·5
3·0
2·5
2·0
1·5
1·0
2600
2690
2900
3000
3200
3300
3400
JD 2440000+

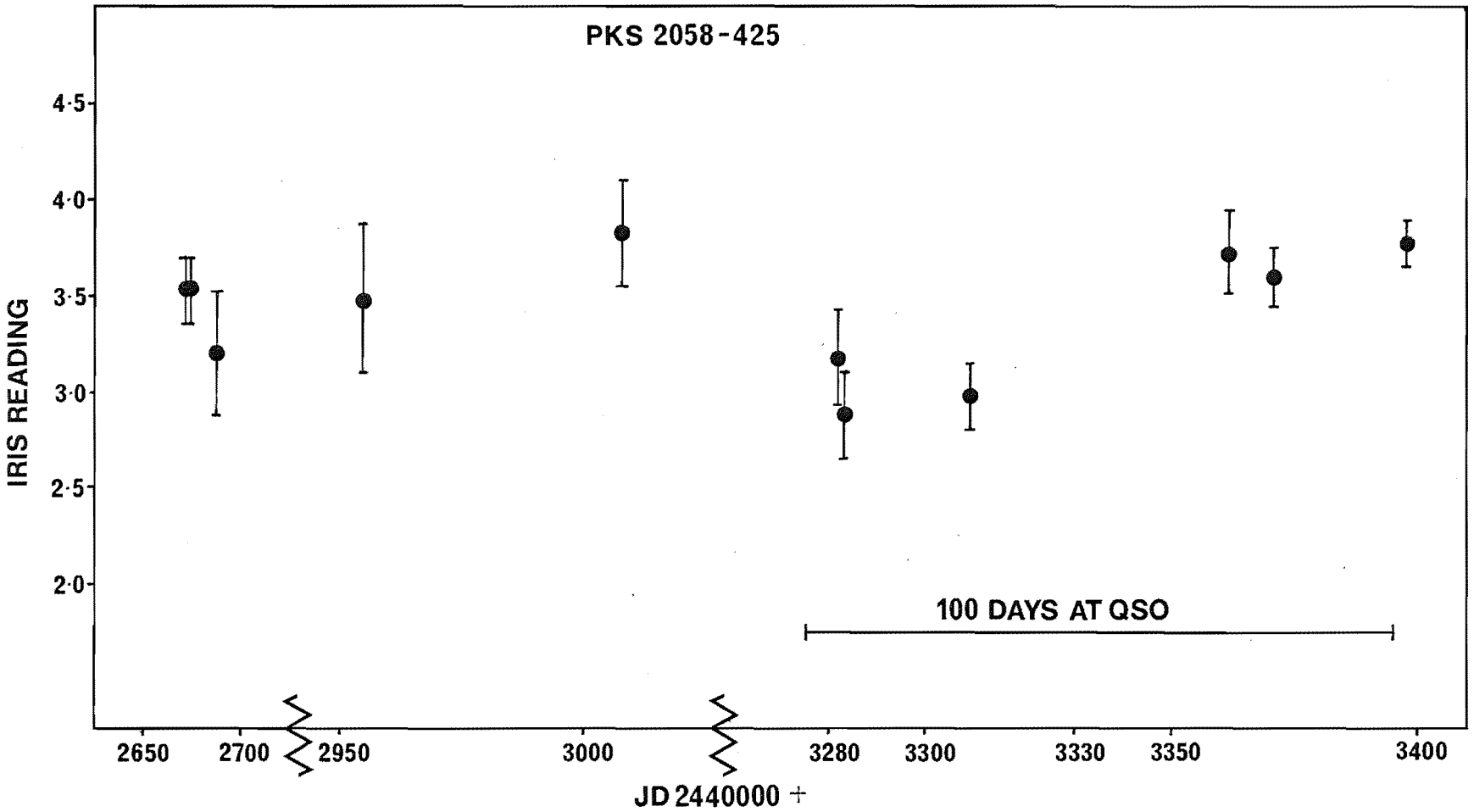
PKS 2058-425
IRIS READING
4·5
4·0
3·5
3·0
2·5
2·0
100 DAYS AT QSO
2650
2700
2950
3000
3280
3300
3330
3350
3400
JD 2440000 +

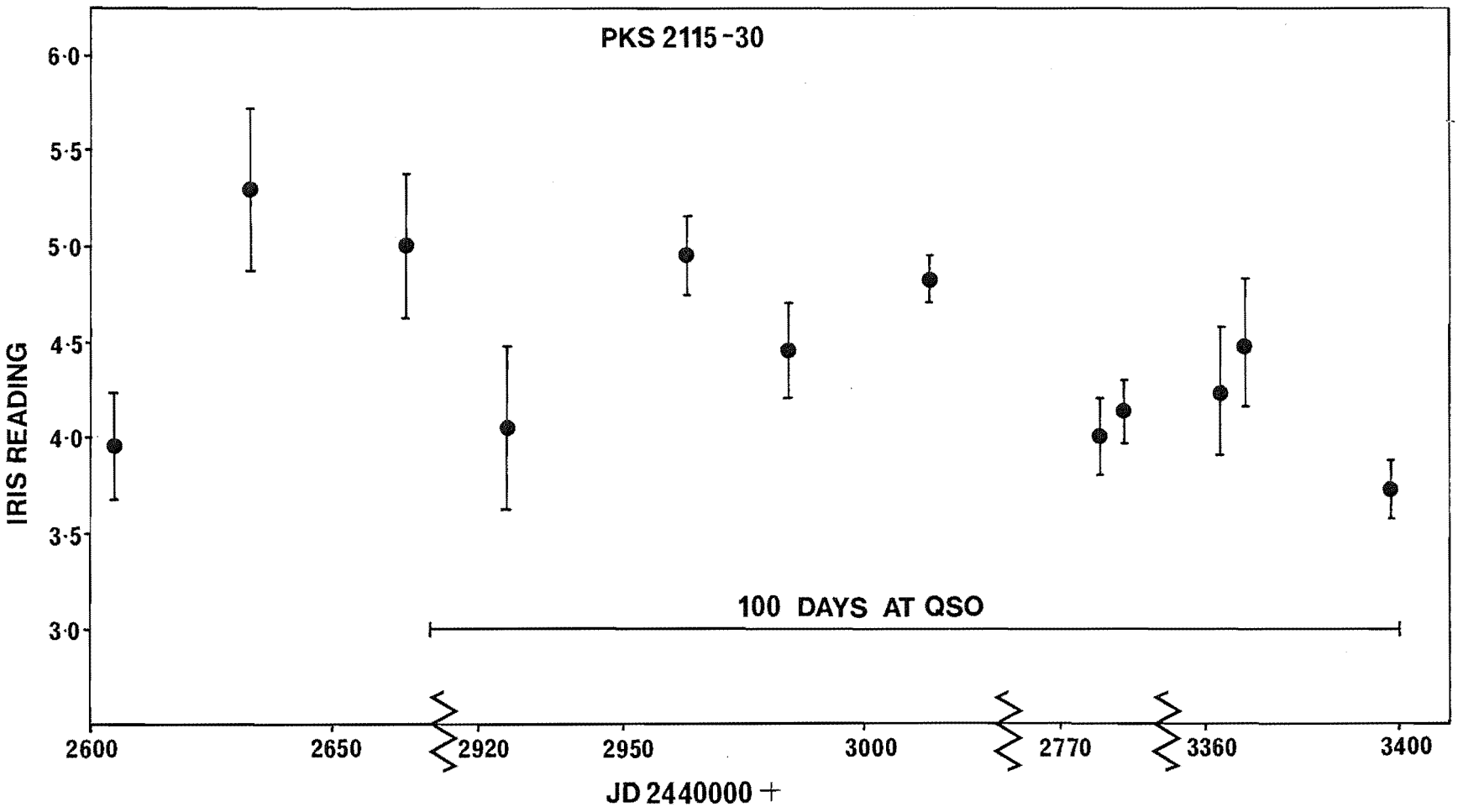
PKS 2115-30
IRIS READING
6·0
5·5
5·0
4·5
4·0
3·5
3·0
100 DAYS AT QSO
2600
2650
2920
2950
3000
2770
3360
3400
JD 2440000 +

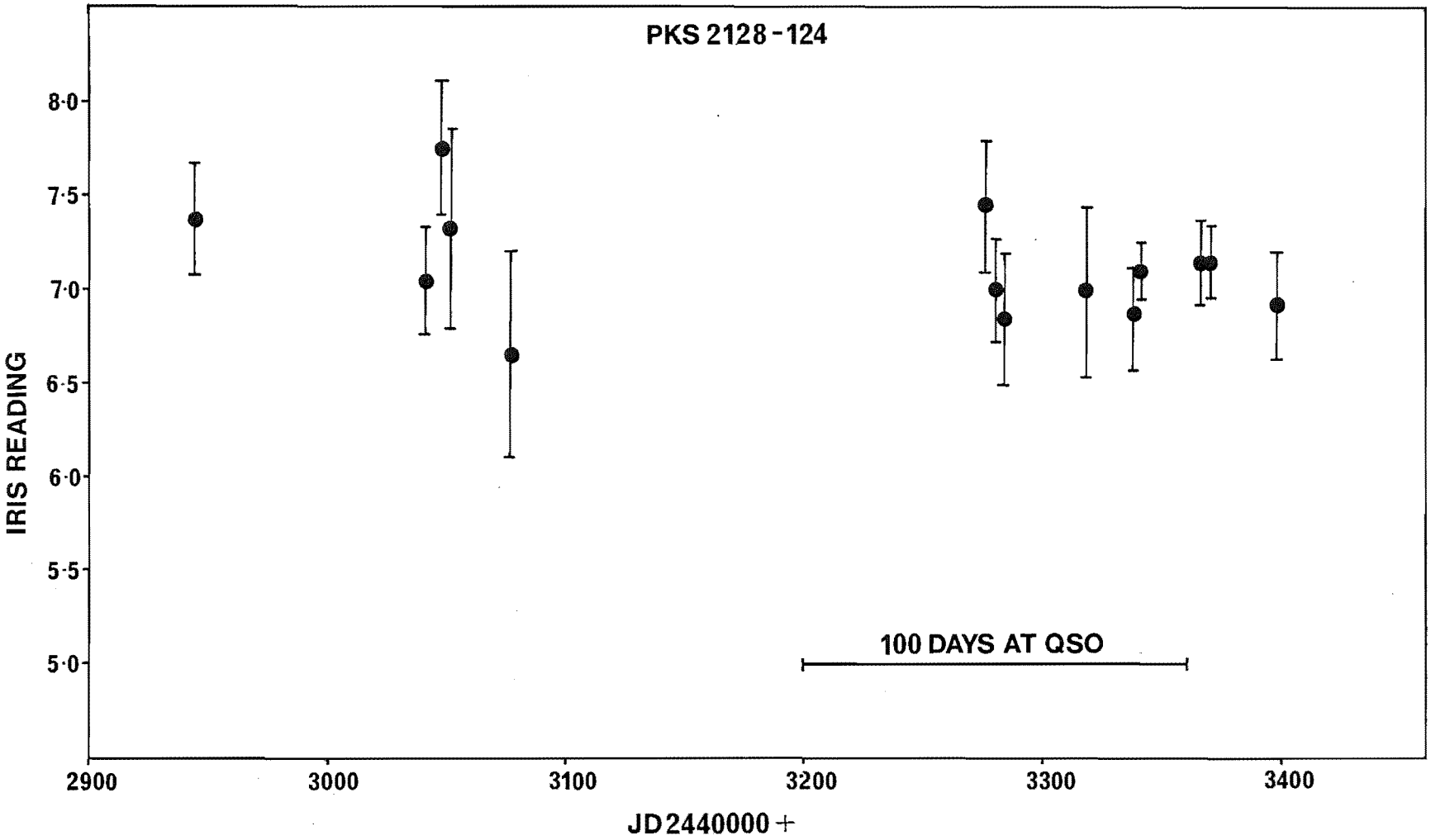
PKS 2128-124
8·0
7·5
7·0
6·5
6·0
5·5
5·0
IRIS READING
100 DAYS AT QSO
2900
3000
3100
3200
3300
3400
JD 2440000 +

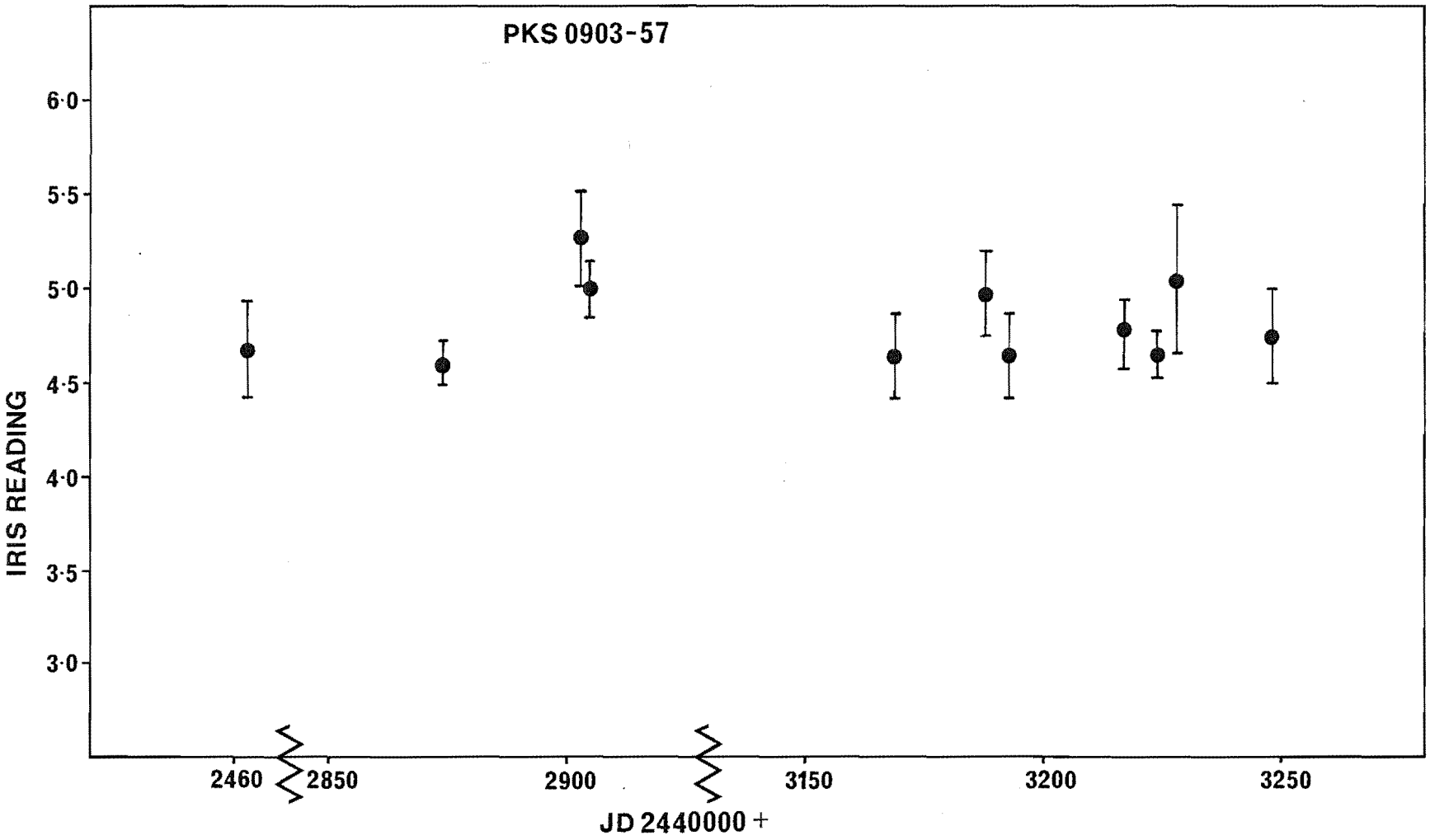
PKS 0903-57
IRIS READING
6·0
5·5
5·0
4·5
4·0
3·5
3·0
2460
2850
2900
3150
3200
3250
JD 2440000 +

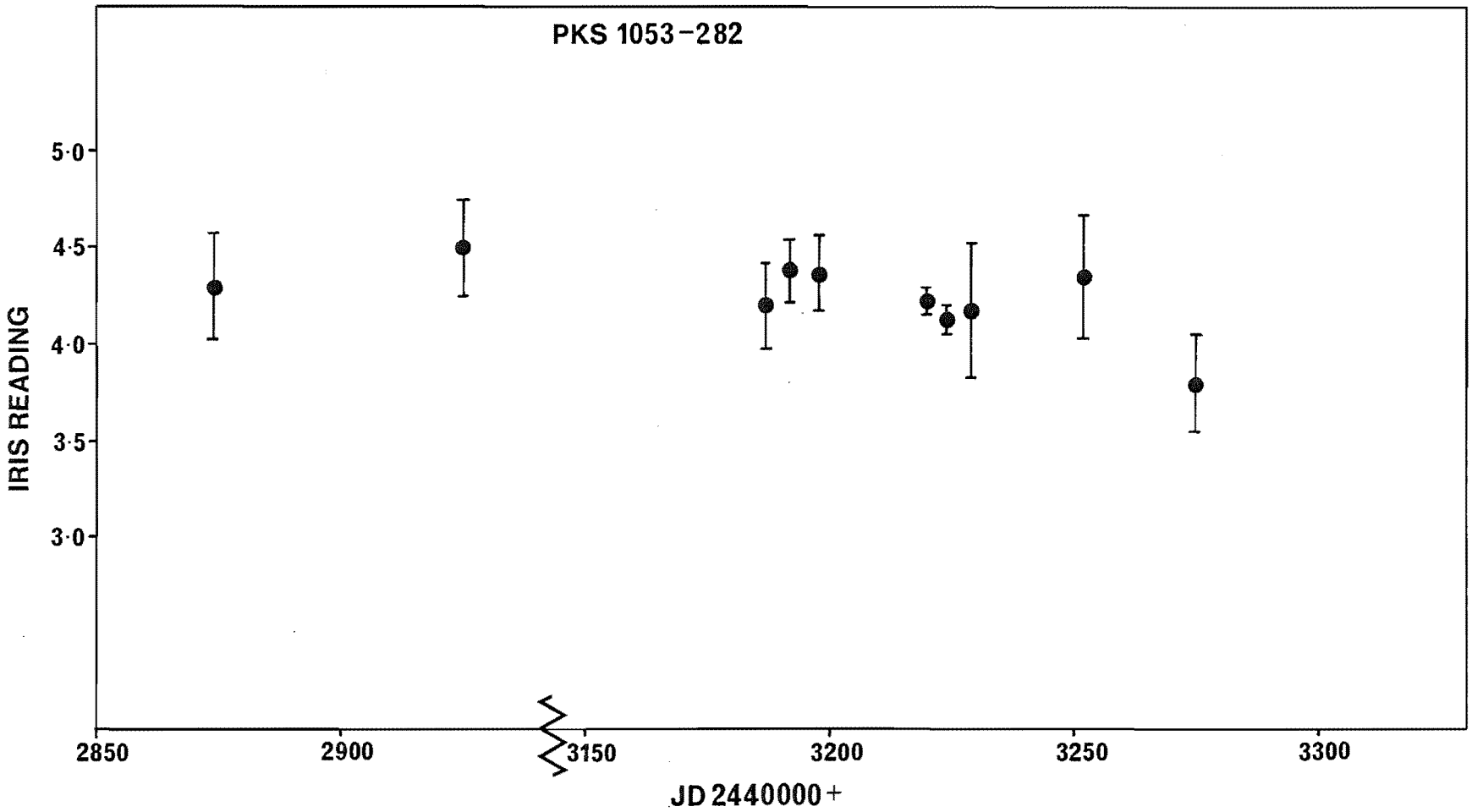
PKS 1053−282
IRIS READING
5·0
4·5
4·0
3·5
3·0
2850
2900
3150
3200
3250
3300
JD 2440000+

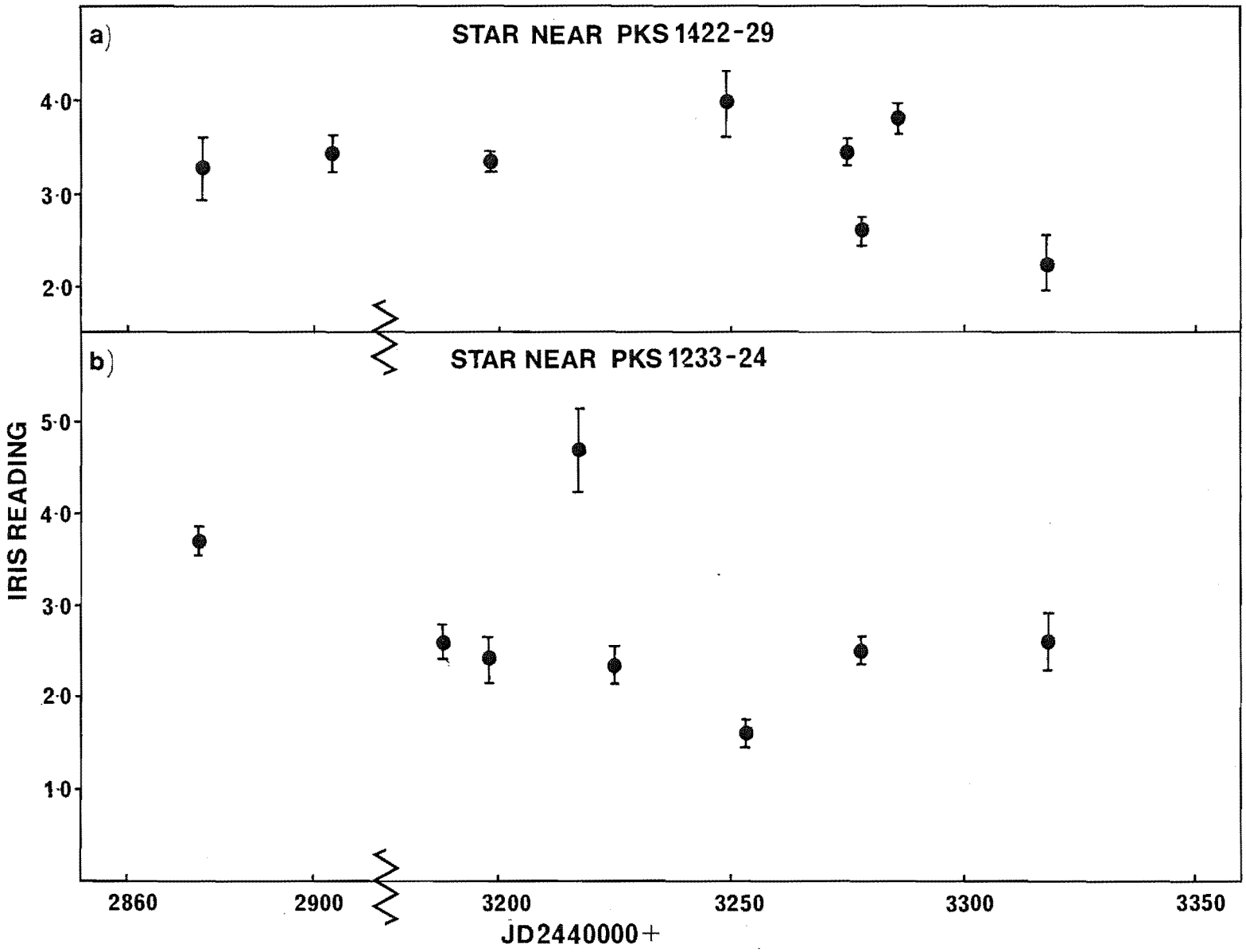
a)
STAR NEAR PKS 1422-29
4·0
3·0
2·0
b)
STAR NEAR PKS 1233-24
IRIS READING
5·0
4·0
3·0
2·0
1·0
2860
2900
3200
3250
3300
3350
JD2440000+

ACKNOWLEDGMENTS

A great many people have provided assistance above and beyond the call of duty. Outstanding among these are Mike Clark (Mt. John Observatory), Graham Kershaw (University of Canterbury) and John Hearnshaw (University of Canterbury). Alex Smith (University of Florida) provided the sequence for AP LIBRAE, John Bolton (CSIRO) provided substantial amounts of information on his quasar identifications, and Bruce McAdam (University of Sydney) donated his radio observations of the low frequency variables. Don Mathewson (Mt. Stromlo and Siding Spring Observatory) kindly made available the iris photometer, and extended the hospitality of his institution during its use.

A special mention is of course due to my supervisor, Ken Fea.

To all of those who have helped, especially those noted above, I extend a grateful thank you.

Two special notes of appreciation are in order. The first is to my parents, whose generosity has made my education possible. The second is to my wife, who cheerfully suffered my repeated absences, while always providing the help and encouragement which I have appreciated so much.

REFERENCES

Adam, G., 1978. Astron. Astrophys. Suppl. 31 151.

Allen, C.W., 1973. "Astrophysical Quantities". Athlone Press, London.

Aller, H.D., Oslen, E.T., and Aller, M.F., 1976. Astron. J. 81 738.

Altschuler, D.R., and Wardle, J.F.C., 1977. Mon. Not. R. Astr. Soc. 179 153.

Andrew, B.H., Macleod, J., Harvey, G.A., and Medd, W.J., 1978. Astron. J., 83 863.

Angione, R.J., 1971. Astron. J. 76 412.

Angione, R.J., 1973. Astron. J. 78 353.

Angione, R.J., and Smith, H.J., 1972. "External Galaxies and Quasi Steller Objects". ed. D.S. Evans p171.

Arons, I., Kulsrud, R.M., and Ostriker, J.P., 1975. Astrophys. J. 198 687.

Barbieri, G., Romano, G., Di Serego, S., Zambon, A., and Zambon, M., 1977. Astron. Astrophys. 59 419.

Barnothy, J.M., 1970. Astrophys. J. Lett. 159 L137.

Beall, J.H., Rose, W.K., Graf, W., Price, K.M., Dent, W.A., Conklin, E.K., Ulich, B.L., Dennis, B.R., Crannell, C.J., Dolan, J.F., Frost, K.J., and Orwing, L.E., 1978. Astrophys. J. 219 836.

Begelman, M.C., and Rees, M.J., 1978. Mon. Not. R. Astr. Soc., 185 847.

Bekenstein, J.D., and Rosenkratz, M.J., 1978. Astrophys. J. 224 812.

Belokon, E.T., Badadzanjanz., M.K., and Lyuty, V.M., 1978. Astron. Astrophys. Suppl. 31 383.

Blandford, R.D., and Königl, A., 1979. Preprint.

Blandford, R.D., and McKee, C.F., 1976. Phys. Fluids. 19 1130.

Blandford, R.D., and McKee, C.F., 1977. Mon. Not. R. astr. Soc. 180 343.

Blandford, R.D., and Rees, M.J., 1978. Phys. Scripta 17 265.

Blumenthal, G.R., and Gould, R.J., 1970, Rev. Mod. Phys. 42 237.

Bolton, J.G., 1977. Computer listing of Parkes catalogue as at 31/10/77.

Bolton, J.G., and Shimmins, A.J., 1973. Aust. J. Phys. Astrophys.Suppl. No. 30

Bond, H.E., Green, R.F., and Huchra, J.P., 1974. Publ. astr. Soc. Pacific 86 668.

Borra, E.F., 1975. Observatory 95 141.

Brandt, S., 1970. "Statistical and Computational Methods in Data Analysis". North Holland, Amsterdam.

Brown, D., 1955. U.S. Army Ballistics Research Laboratories, Report No. 937. Aberdeen Proving Ground. Maryland.

Burbidge, G.R., 1967. Nature 216 1287.

Burbidge, G.R., Crowne, A.H., and Smith, H.E. 1977. Astrophys. J. 33 113.

Burbidge, G.R., Jones, T.W., and O'Dell, S.L., 1974. Astrophys. J. 193 43(BJO).

Brück, M.T., Nandy, K., Caprioli, G., and Smriglio, F., 1969. Astrophys. Sp. Sci. 4 213.

Burkhead, M., and Seeds, M., 1971. AAS Photobulletin No.3 p15.

Cannon, R.D., and Penston, M.V., 1967. Nature 214 256.

Cannon, R.D., Penston, M.V., and Brett, R.A., 1971. Mon. Not. R. Astr. Soc. 152 79.

Cavaliere, A., Morrison, P., and Pacini, F., 1970 Astrophys. J. Lett. 162 L133.

Cavaliere, A., Pacini, F., and Setti, G., 1969. Astrophys. Lett. 4 103.

Cavallo, G., and Ventura, A., 1975. Nature 258 309.

Cayrel, R., 1953. Ann. d'Ap. 16 129.

Chertoprud, V.E., Gudzenko, L.I., and Ozernoy, L.M., 1973. Astrophys. J. Lett. 182 L53.

Christiansen, W.A., and Scott, J.S., 1977. Astrophys. J. Lett. 216 L1.

Christiansen, W.A., Scott, J.S., and Vestrand, W.T., 1978. Astrophys. J. 223 13.

Churms, J., and Evans, D.S., 1961. Observatory 81 25.

Cocke, W.J., and Pacholczyk, A.G., 1975. Astrophys. J. 195 279.

Cohen, M.H., Kellermann, K.I., Shaffer, D.B., Linfield, R.P., Moffett, A.J., Romney, J.D., Seielstad, G.A., Pauliny-Toth, I.I.K., Preuss, E., Witzel, A., Schilizzi, R.T. Geldzahler, B.J., 1977. Nature 268 405.

Colgate, S.A., 1967 Astrophys. J. 150 163.

Colgate, S.A., Lee, E.P., and Rosenbluth, M.N., 1970. Astrophys. J. 162 649.

Coleman, C.T., and Boksenberg, A., 1976. Contemp. Phys. 17 209.

Collin-Souffrin, S., 1978. Phys. Scripta. 17 293.

Colvin, J.D., 1974. Astrophys. J. 190 515.

Condon, J.J. and Dressel, L.L., 1973. Astrophys. Lett. 15 203.

Cromwell, R.H., 1969. Optical Sciences Centre, Tech. Rept. #38. Uni. of Arizona.

Cromwell, R.H., and Dyvig, R.R., 1973. Optical Sciences Centre Tech. Rept. No. 81. Uni. of Arizona.

Daltabuit, E., and Cantó, J., 1974. Riv. Mex. de Astron y Astrophys. 1 151.

Daltabuit, E., and Cox, D., 1972. Astrophys. J. Lett. 173 L13.

Daltabuit, E., MacAlpine, G.M., and Cox, D.P., 1978 Astrophys. J. 219 372.

Doughty, N.A., Shane, C.D., and Wood, F.B., 1972. Canterbury Sky Atlas (Australis).

De Bruyn, A.G., 1976. Astron. Astrophys. 52 429.

Deming, W.E., 1931. Phil. Mag. s7 11 146.

Dent, W.A., 1972. Astrophys. J. Lett. 175 L55.

Dent, W.A., Balonek, T.J., Smith, A.G., and Leacock, R.J., 1979. Astrophys. J. Lett. 227 L9.

De Veny, J.B., 1970. Publ. astr. Soc. Pacific 82 142.

Edwards, P.L., and Smith, A.G., 1977. Bull.A.A.S. 9 310.

Eggen, O.J., 1973. Astrophys. J. Lett. 186 L1.

Elliott, J.L., and Shapiro, S.L., 1974. Astrophys. J. Lett. 192 L3.

Elliot, K.H., Blades, J.C., Zealey, W.J., and Tritton, S., 1978. Nature 275 198.

Fabian, A.C., Maccagni, D., Rees, M.J., and Stoeger, W.R., 1976. Nature 206 683.

Fahlman, G.G., 1977. Astrophys. J. 211 649.

Fahlman, G.G., and Ulrich, T.J., 1975. Astrophys. J. 201 277.

Faulkner, J., and Gaskell, M., 1978. Nature 275 91.

Flasar, F.M., and Morrison, P., 1976. Astrophys. J. 204 352.

Gardner, F.F., Whiteoak, J.B., and Morris, D., 1975. Aust. J. Phys. Astrophys. Suppl. No. 35.

Gearhart, M.R., Kraus, J.D., Andrew, B.H., Blake, G., Scott, P., Ryle, M., Braude, S Ya., Sharykin, N.K., Zhouck, I.N., Bridle, A.H., Conklin, E.K., Douglas, J.N., Hachenberg, O., Thiel, M., Kauffmann, P., Purton, C.R., Feldman, P.A., Marsh, K.A., Stull, M.A., Price, K., Warner, J.W., Assousa, G., and Balick, B., 1974. Nature 249 743.

Gilmore, G., 1978.a. I.A.U. Circ. 3247.

Gilmore, G., 1978.b. I.A.U. Circ. 3221.

Gilmore, G., 1978.c. Southern Stars 27 144.

Gilmore, G., 1978.d. Southern Stars 27 155.

Gilmore, G., 1979. Mon. Not. R. Astr. Soc. in press.

Ginzburg, V.L., and Ozernoy, L.M., 1966. Astrophys. J. 144 599.

Ginzburg, V.L., and Ozernoy, L.M., 1977 Astrophys. Sp. Sci. 50 23.

Ginzburg, V.L., and Syrovatskii, S.I., 1965. Annu.Rev.Astron. Astrophys. 3 297.

Ginzburg, V.L., and Syrovatskii, S.I., 1969. Annu. Rev. Astron. Astrophys. 5 375.

Grandi, S.A., and Tifft, W.G., 1974. Publ. Astr. Soc. Pacific 86 873.

Green, R.F., Huchra, J.P., and Bond, H.E., 1977. Publ. Astr. Soc. Pacific. 89 255.

Grindlay, J.E. 1975. Astrophys. J. 199 49.

Gubbay, J., Legg, A.J. Robertson, D.S., Nicholson, G.D., Moffet, A.T., and Shaffer, D.B., 1977. Astrophys. J. 215 20.

Gudehus, D.H., 1970. Publ. Ast. Soc. Pacific. 82 1324.

Hackney, K.R., and Hackney, R.L., 1976. Astron. J. 81 7.

Hackney, R.L., 1972. Unpublished Ph.D. Thesis, University of Florida, Gainesville.

Hackney, R.L., Hackney, K.R., Smith, A.G., Folsom, G.H., Leacock, R.J., Scott, R.L., and Epstein, E.E. 1972. Astrophys. Lett. 12 147.

Harding, G.A., Harbour, R.S., and Tritton, R.D., 1971. Roy. Obs. Bull. No. 172.

Harris, W.E., and Racine, R., 1974. Astron. J. 79 472.

Harter, H.L. 1976. Int. Stat. Rev. 44 133.

Hartwick, F.D.A., Hesser, J.E., and McClure, R.D., 1972 Astrophys. J. 174 557.

Heckman, T.M. 1976. Publ. Astr. Soc. Pacific. 88 844.

Hoffmeister, C., 1964. Astr. Nacht. 288 49.

Hoyle, F., Burbidge, G.R., and Sargent, W.L., 1966. Nature 206 751.

Hoyle, F., and Fowler, W.A., 1963a Mon.Not.R. Astr. Soc. 125 169.

Hoyle, F., and Fowler, W.A., 1963b Nature 197 533.

Hunstead, R.W., 1972. Astrophys. Lett. 12 193.

Hunter, J.H., and Lü, P.K., 1969. Nature 223 1045.

Hunter, J.H., and Lü, P.K., 1970. Nature 225, 366.

Jones, T.W., and Burbidge, G.R., 1973. Astrophys. J. 186 791.

Jones, T.W., and Kellogg, P.J., 1972. Astrophys. J. 172 283.

Jones, T.W., and O'Dell, S.L., 1977. Astron. Astrophys. 61 291.

Jones, T.W., O'Dell, S.L., and Stein, W.A., 1974a. Astrophys. J. 188 353 (≡JOS I).

Jones, T.W., O'Dell, S.L., and Stein, W.A., 1974b. Astrophys. J. 192 261. (≡JOS II).

Jones, T.W., and Tobin, W., 1977. Astrophys. J. 215 474.

Kardashev, N.S., 1970. Soviet Astronomy - A.J. 14 375.

Kellerman, K.I., 1966. Astrophys. J. 146 621.

Kellerman, K.I. 1966. Aust. J. Phys. 19 195.

Kellerman, K.I., 1975 in "Physics of Nonthermal Radio Sources" ed. G. Setti. Reidel page 27.

Kellerman, K.I., 1978. Phys. Scripta. 17 257.

Kellerman, K.I., and Pauliny-Toth, I.I.K., 1969. Astrophys. J. Lett. 155 L71.

Kesteven, M.J.L., Bridle, A.H., and Brandie, G.W., 1977 Astron. J. 82 541.

Kinman, T.D., 1969. Nature 224 565.

Kinman, T.D., 1976. Astrophys. J. 205 1.

Kinman, T.D., Lamla, E., Ciurla, T., Harlan, E., and Wirtanen, C.A., 1968. Astrophys. J. 152 357.

Königl, A., 1978. Astrophys, J. 225 732.

Kormendy, J., 1973. Astrophys, J. 78 255.

Kronberg, P.P., and Clarke, J.N., Astrophys, J. Lett. 224 L51.

Levich, E.V., and Sunyaev, R.A., 1970. Astrophys. Lett. 7 69.

Lewin, W.H.G., and Joss, P.C., 1977. Nature 270 211.

Liller, M.H., and Liller, W., 1975. Astrophys. J. Lett. 199 L133.

Liller, W., 1974. Astrophys. J. Lett. 189 L101.

Locke, J.L., Andrew, B.H., and Medd, W.J., 1969. Astrophys. J. Lett. 157 L81.

Lü, P.K., 1972. Astron. J. 77 829.

Lynden-Bell, D., 1971. Pont. Acad. Sci. Scripta. Varia. No. 35 p527.

Lynden-Bell, D., 1978. Phys. Scripta 17 185.

Margon, B., Bowyer, S., Jones, T.W., Davidsen, A., Mason, K.O., and Sandford, P.W., 1976. Astrophys. J. 207 359.

Marscher, A.P., 1977. Astrophys. J. 216 244.

Marscher, A.P., 1978a. Astrophys. J. 219 392.

Marscher, A.P., 1978b. Astrophys. J. 224 816.

Matthews, W.G. 1972. Astrophys. J. 174 161.

Matthews, W.G., 1978. Astrophys. J. 219 408.

Mayer, B., 1976. Sky Telesc. 51 59.

McGimsey, B.Q., Smith, A.G., Scott, R.L., Leacock, R.J., Edwards, P.L., Hackney, R.L., and Hackney, K.R., 1975. Astrophys. J. 80 895.

McKay, B.J., 1972. Unpublished M.Sc. thesis University of Canterbury.

McVittie, G.C., 1974. Quart. J. Roy. Astr. Soc. 15 246.

Medd, W.J., Andrews, B.H., Harvey, G.A., and Locke, J.K., 1972. Mem. R. Astr. Soc. 77 109.

Medd, W.J., Locke, J.L., Andrew, B.H., and Van den Bergh, S., 1968. Astron. J. 73 293.

Miller, H.R., Clonts, S.L., and Folsom, G.H., 1974. Astron. J. 79 1352.

Miller, W.C., 1969. A.A.S. Photobulletin No. 1, p10.

Miller, W.C., 1975. A.A.S. Photobulletin No. 9, p3.

Millikan, A., 1972. A.A.S. Photobulletin No. 6, p18.

Moffett, A.T., 1975. in"Galaxies and the Universe" ed. A.M. Sandage. University of Chicago Press. Ch.7.

Morrison, P., 1969. Astrophys. J. Lett. 157 L73.

Morrison, P., and Cavaliere, A., 1971. Pont. Acad. Sci. Scripta Varia No. 35. p485.

Mufson, S., Moffett, T.J. and Ulrich, M-H., 1978. Astrophys. J. 224 22.

Mushotzky, R.F., Serlemitsos, P.J., Becker, R.H., Boldt, E.A., and Holt, S.S., 1978. Astrophys. J. 220 790.

Netzer, H., 1974. Mon. Not. R. Astr. Soc. 167 1P.

Nicolson, G.D., 1973. Nature Phys. Sci. 241 90.

Nicolson, G.D., 1978. Astrophys. Lett. 19 107.

O'Dell, S.L., Puschell, J.J., Stein, W.A., Owen, F., Porcas, R.W., Mufson, S., Moffett, T.J., and Ulrich, M-H., 1978. Astrophys. J. 224 22.

Opher, R., 1975. Astrophys. J. 201 526.

Osterbrock, D.E., 1971. Pont. Acad. Sci. Scripta Varia No. 35 p151.

Ozernoy, L.M., 1974 in Proc. First I.A.U. European Meeting 3 65.

Ozernoy, L.M., 1976. Soviet Phys. Usp. 19 863.

Ozernoy, L.M., and Sazanov, V.N., 1969. Astrophys. Sp. Sci. 3 395.

Ozernoy, L.M., and Sazonov V.N., 1971, Astrophys. Lett. 8 231.

Ozernoy, L.M., and Ulanovskii, L.E., 1974. Soviet. Astron.- A.J. 18 4.

Ozernoy, L.M., and Usov, V.V., 1973. Astrophys. Sp. Sci. 25, 149.

Ozernoy, L.M., and Usov, V.V., 1977. Astron. Astrophys. 56 163.

Peterson, F.W., and Dent., W.A. 1973. Astrophys. J. 186 421.

Pacholczyk, A.G., 1970. "Radio Astrophysics" Freeman.

Pauliny-Toth, I.I.K., and Kellerman, K.I., 1968. Astrophys. J. Lett. 152 L169.

Peach, J.V., 1969. Nature 222 439.

Penston, M.J., Penston, M.V., and Sandage, A., 1971. Publ. Astr. Soc. Pacific 83 783.

Penston, M.V., and Cannon, R.D., 1970. Roy. Obs. Bull. No. 159.

Peterson, B.A., and Bolton, J., 1972. Astrophys. Lett. 10 105.

Peterson, B.A., Jauncey, D.L., Wright, A.E., and Condon, J.J., 1976. Astrophys. J. Lett. 207, L5.

Peterson, F.W., and Dent, W.A., 1973. Astrophys. J. 186, 421.

Petschek, A.G., Colgate, S.A., and Colvin, J.D., 1976. Astrophys. J. 209 356.

Piddington, J.H., 1970. Mon. Not. R. Astr. Soc. 148 131.

Piirola, V., 1973. Astron. Astrophys. 27 283.

Piirola, V., 1975. Ann. Acad. Sci. Fennicae Ser.A. sect. VI. No. 418.

Pomphrey, R.B., Smith, A.G., Leacock, R.L., Olsson, C.N., Scott, R.L., Pollock, J.T., Edwards, P., and Dent, W.A., 1976. Astron. J. 81 489.

Press, W.H., 1978. Comments Astrophys. 7 103.

Purgathofer, A. Th., 1969. Lowell Obs. Bull. No. 147.

Readhead, A.C.S., Cohen, M.H., and Blandford, R.S., 1978. Nature 272 131.

Richter, L., Richter, N.B., Wenzel, W., 1972. Astr. Nacht. 293 119.

Rees, M.J., 1966. Nature 211 468.

Rees, M.J., 1967. Mon.Not.R.Ast.Soc. 135 345.

Rees, M.J., 1977. Ann. N.Y. Acad. Sci. 302 613.

Rees, M.J., 1978a. Mon. Not. R. Astr. Soc. 184 61P.

Rees, M.J., 1978b. Physica Scripta 17 193.

Robertson, J.W., 1974. Astron. Astrophys. Suppl. 15 261.

Ryle, M., and Longair, M.S., 1967. Mon. Not. R. Astr. Soc. 136 123.

Salpeter, E.E., 1971. Nature Phys. Sci. 233 5.

Sandage, A., 1972. Astrophys. J. 178 1.

Sanders, R.H., 1970. Astrophys. J. 162 791.

Sargent, W.L.W., Young, P.J., Boksenberg, A., Shortridge, K., Lynds, C.R., and Hartwick, F.D., 1978. Astrophys. J. 221 731.

Saslaw, W.C., Tyson, J.A., and Crane, P., 1978. Astrophys. J. 222 435.

Saslaw, W.C., Valtonen, M.J., and Aarseth, S.J., 1974. Astrophys. J. 190 253.

Savage, Ann., 1976. Mon. Not. R. Astr. Soc. 174 259.

Scheuer, P.A.G., and Readhead, A.C.S., 1979. Nature 277 182.

Schilizzi, R.T., Cohen, M.H., Romney, J.O., Shaffer, D.B., Kellerman, K.I., Swenson, G.W., Yen, J.L., and Rinehart, R., 1975. Astrophys. J. 201 263.

Schnopper, H.W., Epstein, A., Delvaille, J.P., Tucker, W., Doxey, R., and Jernigan, G., 1977. Astrophys. J. Lett. 215 L7.

Schoening, W.E., 1976. A.A.S. Photobulletin No. 11 p8.

Scott, R.L., Leacock, R.J., McGimsey, B.Q., Smith, A.G., Edwards, P.L., Hackney, K.R., and Hackney, R.L., 1976. Astron. J. 81 7.

Scott, R.L., and Smith, A.G., 1976. A.A.S. Photobulletin No. 12 p6.

Scott, R.L., Smith, A.G., and Leacock, R.L., 1977 A.A.S. Photobulletin No.15 p12.

Seielstad, G.A., 1974, Astrophys. J. 193 55.

Seielstad, G.A., and Berge, G.L., 1975. Astron. J. 80 271.

Shapiro, S.L., and Marchant, A.B., 1978. Astrophys. J. 225 603.

Shimmins, A.J., and Wall, J.V., 1973. Aust. J. Phys. 26 93.

Simon, M., 1969. Astrophys. J. 158 865.

Slee, O.B., 1977. Aust. J. Phys. Astrophys. Suppl. No. 43.

Slee, O.B., and Higgins, C.S., 1975. Aust. J. Phys. Astrophys. Suppl. No.36.

Smith, M.G., 1979. Vistas in Astronomy 22 321.

Stannard, D., Treverton, A.M., Porcas, R.W., and Davis, R.J., 1975 Nature 255 384.

Stock, J., and Williams, A.D., 1962 in "Astronomical Techniques" ed. W.A. Hiltner. University of Chicago Press p374.

Sturrock, P.A., 1965. Nature 205 861.

Sturrock, P.A., 1971. Astrophys. J. 170 85.

Ulmer, M.P., and Murray, S.S., 1976. Astrophys. J. 207 364.

Uomoto, A.K., Wills, B.J., and Wills, D., 1976. Astron. J. 81 905.

Usher, P.D., 1972. Astrophys. J. Lett. 172 L25.

Usher, P.D., 1978. Astrophys.J. 222 40.

Usher, P.D., and Mitchell, K.J., 1978. Astrophys. J. 223 1.

Van der Laan, H., 1971. "Nuclei of Galaxies" ed. D.J. O'Connell p245.

Vitello, P., and Pacini, F., 1977. Astrophys. J. 215 452.

Vitello, P., and Pacini, F., 1978. Astrophys. J. 220 756.

Von Hoerner, S., and Saslaw, W.C., 1976. Astrophys. J. 206 917.

Wagoner, R.V., 1969. Annu. Rev. Astron. Astrophys. 7 553.

Wall, J.V., 1974 in "ESO/SRC/CERN Conference on Research Programmes for the New Large Telescopes". ed. A. Reiz. p265.

Weaver, H., 1962. Handb. der Phys. LIV, 130.

Weistrop, D., 1973. Astron. Astrophys. 23 215.

West, R.M. and Heudier, J.L., 1978. "Modern Techniques in Astronomical Photography" published by E.S.O. Geneva, p304.

Williams, P.J.S., 1963. Nature 200 56.

Wills, D., 1976. Observatory 96 154.

Woltjer, L., 1966. Astrophys. J. 146 597.

Wooster, W.A., 1964. Acta. Cryst. 17 878.

Wlérick, G., LeLiévre, G., and Véron, P., 1971. Astron. Astrophys, 11 140.

Zwicky, F., 1957. "Morphological Astronomy" Julius Springer-Verlag p248.

APPENDIX I

SIR (PEL)

In reply please Quote Ref. No. PEL 131/18
All correspondence to be addressed to: THE DIRECTOR

DEPARTMENT OF SCIENTIFIC AND INDUSTRIAL RESEARCH
PHYSICS AND ENGINEERING LABORATORY JVN:0004F

Telephone: 666 919
Cables and Telegrams: PHYSICAL
Telex: PHYSICS NZ 3814

Private Bag,
Lower Hutt, New Zealand.

Report No. S 8374

Job No. 78/A/187

10 July, 1978

IMAGE INTENSIFIER SPECTRAL RESPONSE

Customer: Physics Department,
University of Canterbury,
Christchurch.

Sample: Varo Image Intensifier, Part No. 510.1248-303 and Serial No. 7332.

Object of Test: To determine the relative spectral response of the Image Intensifier at various positions on its detector surface.

Method of Test: A stable lamp and a monochromator with external optics was used to produce a parallel beam of monochromatic light. The beam diameter was 3 mm and the spectral bandwidth was 0.2 nm. The detector surface of the Image Intensifier was placed in the light path and the intensity of the image produced was monitored with a linear, stable photomultiplier tube and associated electronics. The response of the above for various wavelengths was compared to that of a previously calibrated photomultiplier tube and integrating sphere.

Three positions on the detector surface were investigated. They were:-

1. The centre of the detector;
2. The edge of the detector;
3. A second edge position at 90° to that of position 2.

contd/.....

The image intensifier voltage was 6.75 volts throughout the calibration procedure.

The calculated spectral response curves were normalised to give a response of 1.00 at 560 nm.

The room temperature was at 22°C through the calibration procedure.

Results:

	Relative Response		
Wavelength	Position 1	Position 2	Position 3
360	0.07	0.01	0.01
380	0.18	0.09	0.06
400	0.30	0.18	0.14
420	0.45	0.30	0.24
440	0.59	0.43	0.35
460	0.72	0.58	0.48
480	0.84	0.72	0.63
500	0.92	0.84	0.76
520	0.98	0.93	0.88
540	1.00	0.99	0.96
560	1.00	1.00	1.00
580	0.94	0.97	0.99
600	0.89	0.92	0.96
620	0.83	0.87	0.93
640	0.76	0.82	0.88
660	0.70	0.77	0.83
680	0.65	0.74	0.80
700	0.62	0.74	0.79
720	0.59	0.75	0.80
740	0.56	0.76	0.81
760	0.54	0.77	0.83
780	0.51	0.77	0.82
800	0.47	0.75	0.81
820	0.44	0.72	0.79
840	0.35	0.61	0.68
860	0.22	0.41	0.46

Errors: The errors in the relative response are estimated to be ±10%.

(J. V. Nicholas)
Scientist

(A. H. McIlraith)
for Director

APPENDIX II

TABLE II.1

Observational Results for 24 Quasars.

PKS 0135-247

Julian Date	Iris Reading	Julian Date	Iris Reading
244 2983.25	3.80 ± 0.28	244 3100.96	3.49 ± 0.21
3042.10	3.97 .10	3363.22	3.41 .32
3049.05	3.65 .41	3366.23	3.48 .46
3079.95	3.57 .10	3372.19	3.66 .23

PKS 0202-76

Julian Date	Iris Reading	Julian Date	Iris Reading
244 2460.99	2.47 ± 0.20	244 3009.22	3.16 ± 0.34
2574.22	2.52 .26	3045.13	2.55 .28
2665.14	2.90 .29	3079.99	3.21 .31
2692.10	2.63 .13	3098.97	2.45 .20
2694.08	3.07 .19	3363.24	3.18 .36
2717.01	2.44 .18	3368.23	3.24 .17
2781.03	2.22 .26		

PKS 0521-365

Julian Date	Iris Reading	Julian Date	Iris Reading
244 2394.09	7.36 ± 0.24	244 3049.16	7.83 ± 0.16
2394.10	7.73 .34	3099.05	6.77 .18
2400.02	7.72 .36	3103.05	8.38 .30
2487.96	7.07 .24	3106.09	7.65 .19
2517.85	7.83 .26	3109.08	8.14 .14
2518.86	7.98 .36	3128.00	8.42 .36
2668.20	7.69 .37	3157.93	9.44 .27
2695.18	6.98 .38	3187.90	8.68 .24
2717.09	8.88 .24	3192.93	7.75 .26

PKS 0521-365 (continued)

Julian Date	Iris Reading	Julian Date	Iris Reading
244 2781.06	9.16 ± 0.23	244 3216.87	8.01 ± 0.33
2834.94	8.32 .22	3219.87	7.03 .23
3042.17	7.82 .30	3224.87	7.98 .41
3045.18	6.96 .27	3229.85	6.54 .26

PKS 0537-441

Julian Date	Iris Reading	Julian Date	Iris Reading
244 2517.88	2.12 ± 0.23	244 3135.99	3.08 ± 0.26
2782.00	3.42 .26	3165.98	4.23 .29
2835.01	3.52 .18	3168.94	4.36 .23
3042.19	6.05 .08	3168.97	4.08 .28
3046.00	4.22 .41	3186.93	3.95 .17
3048.18	3.50 .20	3187.92	3.92 .20
3048.21	3.74 .23	3191.94	3.01 .19
3049.19	3.11 .22	3193.97	3.29 .21
3050.18	4.06 .25	3196.94	2.71 .18
3050.20	3.89 .15	3197.93	3.44 .18
3080.06	4.84 .18	3216.90	3.92 .15
3098.07	3.35 .18	3217.86	3.67 .09
3099.09	3.43 .15	3219.90	4.01 .24
3100.08	2.95 .21	3222.89	4.35 .20
3103.08	3.17 .17	3224.85	4.46 .12
3105.05	2.70 .22	3227.86	4.32 .27
3109.03	2.94 .16	3228.85	4.52 .24
3110.03	3.20 .19	3229.87	4.44 .28
3128.03	4.07 .16		
3135.97	3.22 .20	2518.88*	2.1 .5*

* - visual estimate

PKS 0548-322

Julian Date	Iris Reading	Julian Date	Iris Reading
244 2696.15	5.84 ± 0.16	244 3128.06	6.67 ± 0.30
2696.17	5.60 .15	3157.98	4.75 .22
2721.13	5.47 .16	3187.94	5.30 .33
2781.09	6.74 .43	3216.92	5.21 .16
2834.96	4.80 .21	3219.92	5.46 .28
3042.22	6.07 .41	3222.91	6.16 .27
3049.21	6.07 .29	3224.89	4.90 .23
3099.10	5.02 .24	3229.90	4.34 .21
3103.10	6.12 .21		

PKS 0743-67

Julian Date	Iris Reading	Julian Date	Iris Reading
244 2393.02	4.04 ± 0.37	244 2872.89	4.10 ± 0.23
2461.09	4.53 .26	2904.85	4.18 .20
2461.94	4.33 .31	3103.12	3.90 .25
2490.06	3.62 .16	3110.09	4.08 .20
2517.98	4.10 .33	3136.06	4.23 .27
2571.86	3.83 .26	3148.05	3.55 .30
2600.83	3.89 .26	3170.04	3.97 .15
2782.08	3.98 .19	3187.98	4.12 .20
2835.05	3.73 .18	3194.00	3.69 .31
2870.86	4.31 .28	3252.83	3.79 .39

PKS 1101-32

Julian Date	Iris Reading	Julian Date	Iris Reading
244 2870.97	4.70 ± 0.16	244 3217.96	4.53 ± 0.27
2925.81	4.28 .34	3222.96	4.76 .31
3169.09	5.11 .08	3227.97	4.56 .21

PKS 1101-32 (continued)

Julian Date	Iris Reading	Julian Date	Iris Reading
244 3188.05	4.76 ± 0.25	244 3252.93	4.31 ± 0.26
3197.00	4.80 .12	3282.85	4.47 .29

PKS 1117-248

Julian Date	Iris Reading	Julian Date	Iris Reading
244 2874.01	3.05 ± 0.23	244 3228.93	3.77 ± 0.35
3188.12	3.33 .14	3247.94	3.13 .42
3198.02	3.16 .25	3248.99	3.11 .20
3216.03	3.31 .20	3252.95	3.10 .14
3216.98	3.61 .21	3274.91	3.26 .25
3217.99	3.67 .21	3282.90	3.17 .13
3219.98	3.30 .19	3285.84	3.25 .16

PKS 1233-24

Julian Date	Iris Reading	Julian Date	Iris Reading
244 2601.83	3.17 ± 0.22	244 3225.05	3.48 ± 0.20
2874.97	3.18 .15	3252.99	3.08 .17
2925.84	2.95 .25	3277.95	3.35 .12
3188.15	3.40 .20	3317.85	3.33 .31
3198.09	3.16 .18	3338.85	3.33 .09
3217.06	2.80 .45		

PKS 1244-255

Julian Date	Iris Reading	Julian Date	Iris Reading
244 2875.01	3.72 ± 0.32	244 3316.84	4.99 ± 0.14
2929.87	3.52 .14	3316.86	5.21 .17
3193.09	2.66 .16	3317.83	4.50 .35
3228.04	3.49 .21	3338.81	4.80 .13
3275.93	5.08 .17	3339.80	4.84 .13
3289.82	6.74 .23		

PKS 1327-21

Julian Date	Iris Reading	Julian Date	Iris Reading
244 2605.85	3.78 ± 0.21	244 3220.05	3.95 ± 0.26
2871.07	3.81 .12	3249.02	3.72 .44
2904.93	5.54 .43	3275.95	4.01 .38
2932.84	3.40 .42	3317.88	4.83 .24
3197.13	4.01 .23	3339.82	4.02 .23

PKS 1349-439

Julian Date	Iris Reading	Julian Date	Iris Reading
244 2875.05	4.02 ± 0.27	244 3248.06	3.76 ± 0.23
2902.99	3.76 .20	3274.97	4.55 .12
2929.90	3.91 .26	3283.98	3.50 .18
2954.85	3.52 .21	3285.86	3.43 .13
3193.12	3.73 .16	3316.88	3.90 .19
3230.02	3.90 .21		

Q 1349-439

Julain Date	Iris Reading	Julian Date	Iris Reading
244 2875.05	4.73 ± 0.27	244 3248.06	5.04 ± 0.23
2902.99	5.18 .20	3274.97	5.43 .12
2929.90	5.67 .26	3283.98	6.08 .18
2954.85	5.25 .21	3285.86	5.50 .13
3193.12	4.74 .16	3316.88	5.49 .19
3230.02	4.95 .21		

PKS 1355-41

Julian Date	Iris Reading	Julian Date	Iris Reading
244 2521.20	5.15 ± 0.47	244 3192.14	6.08 ± 0.19
2600.93	4.93 .15	3198.12	6.17 .44
2605.89	5.11 .16	3217.11	5.74 .26
2606.90	4.42 .38	3218.02	5.78 .17

PKS 1355-41 (Continued)

Julian Date	Iris Reading	Julian Date	Iris Reading
244 2869.13	5.60 ± 0.27	244 3248.09	6.21 ± 0.34
2893.03	5.12 .27	3275.98	6.04 .38
2954.88	5.66 .33	3317.90	5.91 .18
2978.83	5.58 .33	3318.82	5.21 .28
3191.15	5.90 .17	3338.87	5.73 .20

PKS 1422-29

Julian Date	Iris Reading	Julian Date	Iris Reading
244 2876.15	3.65 ± 0.33	244 3275.02	3.58 ± 0.14
2904.03	3.59 .22	3277.98	3.98 .13
3198.15	3.94 .11	3285.93	4.10 .15
3249.08	4.39 .38	3317.92	4.43 .32

PKS 1424-419

Julian Date	Iris Reading	Julian Date	Iris Reading
244 2870.12	1.81 ± 0.14	244 3225.08	1.52 ± 0.31
2894.07	3.20 .30	3228.11	1.91 .23
2929.94	2.20 .18	3248.13	2.02 .24
2954.91	2.45 .32	3282.98	1.68 .10
2978.85	1.68 .22	3285.95	1.72 .16
2982.84	1.81 .21	3316.91	1.60 .14
3191.18	2.65 .22	3339.88	1.79 .09
3198.18	1.66 .18		

PKS 1514-242

Julian Date	Iris Reading	Julian Date	Iris Reading
244 2490.11	9.10 ± 0.25	244 2978.89	7.90 ± 0.46
2490.14	8.92 .17	2981.92	7.25 .21
2517.02	9.33 .18	3009.83	7.37 .28
2517.05	8.59 .24	3012.85	9.09 .46

PKS 1514-242 (continued)

Julian Date	Iris Reading	Julian Date	Iris Reading
244 2518.13	9.29 ± 0.28	244 3192.17	8.45 ± 0.30
2571.13	9.27 .35	3192.18	8.37 .39
2574.92	9.00 .48	3193.18	8.62 .30
2600.87	7.77 .06	3216.18	8.47 .47
2605.93	8.64 .20	3220.10	7.49 .27
2632.88	7.49 .22	3225.13	7.92 .43
2632.89	7.62 .34	3228.17	8.82 .20
2633.84	7.34 .18	3248.18	9.75 .42
2633.85	7.75 .16	3253.11	10.27 .42
2633.89	7.38 .11	3275.13	9.12 .38
2869.20	8.40 .32	3278.05	8.11 .30
2869.21	7.96 .23	3283.00	9.88 .21
2875.17	7.39 .24	3283.04	9.79 .21
2894.15	8.14 .35	3316.95	7.86 .20
2894.17	7.82 .30	3316.96	7.49 .35
2906.13	7.39 .31	3318.94	9.04 .39
2924.07	6.32 .39	3336.89	7.80 .55
2926.08	7.31 .36	3338.91	7.41 .18
2953.98	7.98 .35	3339.91	8.99 .28
2961.98	6.36 .43	3396.90	7.19 .33

PKS 1933-400

Julian Date	Iris Reading	Julian Date	Iris Reading
244 2656.86	2.35 ± 0.25	244 3282.10	1.86 ± 0.24
2657.85	2.22 .25	3319.06	1.98 .27
2692.88	2.66 .12	3337.95	2.13 .12
2955.04	2.62 .22	3366.94	2.04 .10
3011.91	2.23 .16	3372.89	2.11 .18
3047.84	2.23 .22	3398.88	1.89 .15
3276.16	1.94 .26		

PKS 1954-388

Julian Date	Iris Reading	Julian Date	Iris Reading
244 2657.89	3.05 ± 0.29	244 3336.94	2.41 ± 0.16
2604.99	4.03 .28	3337.98	2.02 .14
2953.09	2.22 .31	3338.98	2.23 .14
2981.95	2.48 .28	3339.97	2.31 .16
3009.89	2.77 .32	3362.93	2.43 .16
3012.94	2.47 .21	3371.92	2.29 .16
3278.17	1.80 .20	3397.95	2.15 .17
3317.07	2.31 .30		

PKS 2020-370

Julian Date	Iris Reading	Julian Date	Iris Reading
244 2962.07	3.13 ± 0.22	244 3317.09	2.61 ± 0.15
3010.94	3.12 .29	3337.04	2.76 .19
3041.89	3.20 .18	3339.99	2.93 .18
3047.89	3.01 .23	3362.95	2.80 .16
3276.18	2.77 .23	3371.95	3.21 .21
3282.13	2.80 .23	3397.98	3.24 .16

PKS 2052-47

Julian Date	Iris Reading	Julian Date	Iris Reading
244 2601.13	3.96 ± 0.43	244 3278.20	1.99 ± 0.34
2694.88	2.00 .29	3282.21	2.58 .16
2926.21	1.99 .40	3283.18	2.63 .14
2954.13	2.59 .20	3318.22	2.50 .33
2982.01	2.02 .27	3338.00	2.34 .18
3008.94	2.46 .36	3340.01	2.33 .09
3013.90	2.70 .28	3366.02	2.69 .13
3041.92	2.32 .19	3371.97	2.20 .21
3048.86	2.31 .36	3398.00	3.37 .12
3049.87	2.57 .41		

PKS 2058-425

Julian Date	Iris Reading	Julian Date	Iris Reading
244 2689.90	3.53 ± 0.17	244 3283.20	2.87 ± 0.22
2689.93	3.53 .18	3339.04	2.98 .19
2695.90	3.20 .34	3362.98	3.73 .20
2955.08	3.47 .40	3371.99	3.61 .16
3008.92	3.84 .29	3398.92	3.78 .14
3282.16	3.17 .22		

PKS 2115-30

Julian Date	Iris Reading	Julian Date	Iris Reading
244 2605.09	3.95 ± 0.28	244 3013.94	4.83 ± 0.13
2633.02	5.30 .42	3278.23	4.01 .20
2665.94	5.00 .38	3283.22	4.14 .17
2926.24	4.06 .44	3363.01	4.21 .37
2963.04	4.95 .22	3368.02	4.48 .35
2984.03	4.44 .26	3398.97	3.73 .15

PKS 2128-124

Julian Date	Iris Reading	Julian Date	Iris Reading
244 2954.17	7.39 ± 0.31	244 3283.24	6.86 ± 0.33
3041.96	7.06 .29	3318.24	6.99 .45
3048.89	7.77 .34	3338.13	6.89 .28
3049.90	7.30 .52	3339.06	7.07 .17
3078.90	6.71 .54	3366.05	7.14 .22
3278.25	7.50 .35	3368.04	7.15 .20
3281.23	7.01 .28	3399.00	6.93 .31

TABLE II.2

Observational Results for 2 Misidentified Stars.

The Incorrect Identification with PKS 0903-57

Julian Date	Iris Reading	Julian Date	Iris Reading
244 2463.05	4.67 ± 0.27	244 3193.02	4.65 ± 0.23
2874.91	4.60 .11	3217.93	4.79 .17
2903.86	5.28 .24	3224.93	4.65 .12
2905.89	5.00 .16	3228.90	5.06 .40
3169.01	4.63 .24	3248.88	4.74 .26
3188.01	4.98 .23		

The Incorrect Identification with PKS 1053-282

Julian Date	Iris Reading	Julian Date	Iris Reading
244 2873.96	4.30 ± 0.23	244 3219.95	4.23 ± 0.09
2925.82	4.50 .25	3224.99	4.12 .09
3187.07	4.20 .22	3228.96	4.18 .35
3192.06	4.41 .19	3252.89	4.34 .33
3197.99	4.34 .19	3275.83	3.81 .26

TABLE II.3

Observational Results for 2 Probably Variable Stars.

The Star 30 arc s west and 227 arc s south of PKS 1233-24

Julian Date	Iris Reading	Julian Date	Iris Reading
244 2874.97	3.70 ± 0.16	244 3225.05	2.36 ± 0.19
3188.15	2.61 .20	3252.99	1.58 .16
3198.09	2.42 .25	3277.95	2.49 .16
3217.06	4.72 .47	3317.85	2.61 .33

The Star 34 arc s south and 34 arc s east of PKS 1422-29

Julian Date	Iris Reading	Julian Date	Iris Reading
244 2876.15	3.27 ± 0.33	244 3275.02	3.46 ± 0.14
2904.03	3.43 .22	3277.98	2.59 .13
3198.15	3.35 .11	3285.93	3.79 .15
3249.08	3.94 .38	3317.92	2.24 .32

APPENDIX III

This appendix references all published data on the sources monitored in the Canterbury quasar programme. The information is listed in ten columns with the following divisions:

Column 1 - source name (IAU convention)
2 - position references
3 - finding chart references
4 - all references to the redshift or optical spectrum
5 - all references to apparent magnitude (optical and infra-red)
6 - all radio flux and radio spectral data
7 - X-ray and γ-ray data
8 - polarisation measurements
9 - structural studies
10 - all other information.

Many of the references simply reproduce data which is published elsewhere, but all known references are included here for completeness.

The reference list is presented in Table III.2. The references in that list are not included in the main references section, which refers only to the 5 chapters of text. In the interests of convenience the following non-standard journal title abbreviations have been used:

Aust.J.Phys.Astrophys.Suppl.Ser	≡	A.J.P.Ap.S.
Aust.J.Phys	≡	A.J.P.
Mem.Roy.astr.Soc.	≡	Mem R.A.S.
Mon.Not.Roy.astr.Soc.	≡	M.N.R.A.S.
Roy.Obs.Bull.	≡	R.O.B.

Publ.astr.Soc.Pacific	≡ P.A.S.P.
Astron.Astrophys	≡ Ast.Ap.
Astron.Astrophys.Suppl.Ser.	≡ Ast.Ap.Suppl.
Astron.J.	≡ A.J.
Astrophys.Lett.	≡ Ap.Lett
Astrophys.J.	≡ Ap.J.
Astrophys.J.Suppl.Ser.	≡ Ap.J.Suppl.

The numbering scheme has no significance, and was adopted for convenience only.

TABLE III. 1

Published references to the monitored quasars.

OBJECT	2	3	4	5	6	7	8	9	10
0000-398	181	181	181,188	59,181					
0000-412	181,60	181	181,188,60 240	181,59					
0003-06	160,1,85 102,84 133,12,115 116	116 102		85,102 241,133, 116	160,80,1 102,133,12 101,115			115	
0005-239	190,16,203 1,133,134	16	190,202,203 240,1,133, 134	190,202 16,203,1 240,133 134,12	190,16,1 133,134, 12				
0007-353	191	191	191	191	59,191				
0029-414	1,87,205 72,9,198	72,	240,1,198	240,1,87 205,72 198	1,72,9, 198				204
0046-315	184,203 1,87,74 11	74	184,203, 240,1	240,1,87, 74,11,184 203	184,1,74				
0048-097	179,30,16 122,38, 236,1,87 205,77 243,29 134,28 104	77 243	236,240 191,167	179,125 30,16,36 207,174 236,238,1, 87,77 243,29 134,28 125	30,127 122,16,123 128,103 80,38,36 174,238 1,13,77 243,29 134,28,37 98,104 222,223 257		179 38 207 180 242 13 257	123 192 223	77,257

OBJECT	2	3	4	5	6	7	8	9	10
0049-393	181	181	240,181,188	181,188	59,181				
0118-272	16,1,12 133,	16	184,202 240	202,1,12 134,133	16,1,12 133,134				
0122-379	195	195	195	195	195				
0130-403	181	181	181,188	181,188	181,59				
0135-247	163,16,14 1,87,105 133,198,18 12	12	240,1,133 198,	16,240,1, 87,105,133 198,	163,146,16 14,1,105 133,198,18 12			18	
0138-381	181	181	181,188	181,188	181,59				
0149-397	191,178,88	178	191,178	191,178	59,178				
0149-474U	58	58	240	58					
0150-334	11,1,8,7,74 203,190	74	11,1,240 203,190	11,1,89,87 74,240,203 190,	11,1,74,190				
0154-512U	58	58	240,58						
0202-76	1,87,53,34 198,43,6	34	240,1,198	92,1,87,53 34,198,89	15,92,1,13 53,34,198 43,6		13	15,34 6	204
0207-398	181	181	181,188	181,188	181,59				
0230-790	1,58	58		1	1				
0234-301	184,203,1 87,74	74	184,203,1	184,203,1 87,74	184,1,74				

OBJECT	2	3	4	5	6	7	8	9	10
0242-410	191	191	191	191	59,191				
0321-337	191	191	191	191	191,59				
0324-407	181,203	181	181,188,203	181,188,203	181,59				
0329-385	191	191	191	191	191,59				
0331-654	1,244,10	10		1,10	1,244,10 13		13		
0334-359	191,203	191	191,203	191,203	191,59				
0347-383	195	195	195	195	195				
0355-483	244,89,10 190,55,203 1,77,54,17	10,77	89,190,55 203,240,1	89,10,190 55,203,240 1,77,54,17	244,10,190 55,1,77 54,17				204
0420-388	195	195	195	195					
0427-435	1,87,9,74	74	1	1,87,9,74	1,9,74,				
0439-433	1,205,72 9,89	72	240,1	240,1,72 9,89	235,1,72,9				
0453-423	181,203,196	181	181,203,188 196	181,203,188 196	181,59				
0506-61	76,54,89 190, 203,1	76	89,190 240,203,1	76,54,89 190,240,203 1	76,54,89 190,36,1,13		13		204

OBJECT	2	3	4	5	6	7	8	9	10
0521-365	14,1,87,40 9,95,21,97 7,43,17	9	190,207,240 1,40,9,143 136	39,165,92,36 207,180,173 147,245,155 1,87,9,95 21,143,136,17	92,14,15,36 173,1,51,13 9,21,97,7 20,80,11 143,192,91 43,17		51,13 20	92,36 97,7 192	165,147
0524-433	1,87,9,74	74	1,87,9,74	1,9,74					
0537-441	184,14,203 1,87,205 53,72,89 18,	72	184,164,203 240,1,89 245,78	184,36,207 180,174,173 166,168,164 203,240,1 87,205,53 72,89,246 252,253,254	127,184,14 235,36,207 174,173,1 213,13,53 72,18,192 78	183,	13,	18, 192	168
0548-322	1,205,11	11,170 242	1,207,170 242,247	1,205,11 207,180,170 248	1,11,207	247 242			247,207 170,247 242
0551-366	191,203	191	191,203	191,203	191,59				
0609-609	1,57	57,	58	1,57,	1,57				
0622-441	190,203,1 87,53,9,74 89,	74,	190,203 240,1,89	190,203,240 1,87,53,9 74,89	190,1,13, 53,9,74		13		
0743-67	203,1,87 205,35,12 43	35	211,203,1 42,205	211,203,1 42,87,205 35,89,252	127,120,36 211,1,13 35,12,6,43		13,		

OBJECT	2	3	4	5	6	7	8	9	10
0925-203	1,208,89 12	12	240,1,208	240,1,208 89,12	1,208,12				208
0959-443	203,1,87 72,9,190	72	203,1,190	203,1,87 72,9,190	1,13,9,190 72		13		
1004-217	1,58,19	19	240,1,58 19,	240,1,58 19,	1,58,19				
1011-282	58,1,129	129	240,58,1	240,58,1 129	58,1,118,81			118	
1050-184	1,19,58	19,	240,1,19,58	240,1,19,58	1,19,58				
1101-264	203,195	195	203,195 178	203,195	195,249				
1101-325	190,201,14 203,1,87 74,18,11	74	190,203 240,1	190,203 240,1,87 74,11,89,254	190,201,14 1,74,18,11			18	
1104-445	1,87,205 9,75,69,244 208	69	240,1,208	36,240,1 87,205,9 75,69,244 208	235,36,1 13,9,75,69 244,192,208		13	192	
1116-46	203,1,87 205,40,34 35,93,114 244,97,43	35	127,187,36 203,42,205	203,36,42 87,205,40 35,114,244	127,120,15 36,1,13,34 35,244,97 43		13	36 34 244 97	
1117-248	55,57,19 81,12,1	12	55,202,240 1,19	89,55,202 240,1,57,19 12,	55,14,1 57,19,81 12				

OBJECT	2	3	4	5	6	7	8	9	10
1206-238	19,1	19	19,1,58	19,1	19,1				
1207-399	89,1,87 205,72,9 198	9,	1,240,198	89,1,240 87,205,9 198	1,13,205 72,9,198		13,		
1233-24	14,66,203 1,87,205 84,138,25, 29,95,19 18,81,7	95	127,161,211 66,203,1 205,84,67, 219,	91,161,211 66,203,1 87,205,84, 138,25,19, 67,	127,91,120 15,14,211, 1,6,13,118 81,138,25, 19,18,7		13,	15, 6, 118, 18,	
1240-294	190,203, 1,76	76	190,189,203 1,240	190,189 203,1,240 76	190,189,1				189,
1243-412	14,1,205 72,9	72		1,205,72 9,	14,1,13,72 9,		13,		
1244-255	55,1,76 133,19,81 12	76	55,1,240 19,12,	55,1,240 76,133,19 12,253,252, 254,	55,1,76 133,19,81, 12			133	
1256-229	1,19	19,	58,	1,19,	1,13,19		13		
1300-243	203,191,135	191	203,191	203,191,	59,191,				
1311-270	58,1,19,	19	58,1,240 19	58,1,240 19	58,1,19				
1327-21	94,40,22 21,66,203 1,87,19,18 43,7,8	22	44,161,56 248,211,66 203,1,19 67,41,137	92,44,161 94,40,22 28,21,211 210,66,203 1,87,19,67	92,120,15 49,13,22 21,211,1 19,18,41 43,150,7		171 49,13,	211 18 41 150 7,8	

OBJECT	2	3	4	5	6	7	8	9	10
1328-264 1349-439	58,1,19 1,87,9,74	19 74	58,1,19 240,189,1 74,	58,1,19 240,189,1 87,9,74,252	58,1,19 189,1,13, 9,74,6		13,		189,74
1355-41	14,203,1 87,205,72 9,84,95,18, 43,7,95	72, 95,	211,203,1, 42,205,72 9,	36,211,203, 1,42,87,205, 72,9,84 95,	127,120,14 36,211,1,13, 205,72,9 18,43,6,7		13,	36, 211, 18, 43,6 7,	204
1420-27	14,1,87,40 25,64,7 43,	25		92,1,87 40,25,29 64,	92,14,1,13 25,7,43		13	14,7 40,25	
1422-29	1,87,25 64,19,18 43,11	25		92,87,25 29,64,19	92,15,1 13,25,19, 18,43,7,11		13,	18 7,11	
1424-419	1,87,9,95 18,97	95		36,1,42,87 9,95,252 254,	235,36,1,13 9,18,97,6 7,192,78		13,	36,18 97,6 7,192	
1448-232	55,59,191 1,19,57,135	191	55,191,1 240,19,57	55,191,1 240,19,57	55,59,191 1,19,57				
1451-375	52,9,84 203,1,87, 205,72	72,	187,52,157 211,203, 1,240,205	52,157,36 9,84,211 203,1,240 87,205,72	127,52,157 36,142,9 211,1,13, 72		13		

OBJECT	2	3	4	5	6	7	8	9	10
1510-089	203,1,87 86,205,40 149,138,64 97,43,26	26	177,186,82, 38,193,161 211,203,1 213,87,205 138,200,137 78,	50,220 224,107 126,125,67 63,82,145, 36,175,161 211,203,1 213,205,40 149,138,29 64,200,26	63,127,120 232,121,90 235,154 144,15,221 123,128,68 103,117,80 38,36,211 1,213,86,49 112,13,205 249,156,214 192,37,97 109,43,36 91,153,142 144,148,217 218,78		121 38,86 49,112 169,13, 206, 141,	221 123 36 61,156 192 97, 153, 148, 217 218	154,144 70,200
1514-24	227,226,205 1,87,94,111 64,21,75,152 97,	152	158,187,207 172,185,1,94 143,228	92,158,124 38,207,180 174,173,170 234,182,159, 172,225,185 251,205,119 1,87,194,199 111,64,21,75 27,152,79	92,127,15,80 38,207,174 173,234,229 45,226,51, 205,1,13,21 75,2,5,27 192,230,231 91,78,97, 257	176 207, 183 227, 182,	158,38 207, 180,51 13,79, 257,	38,45 226,194, 185,172 199, 192,230 231,97	207,237 182,172,185 194,199,209 257
1814-519	1,87,34,35, 93,114,43	35,		1,87,35,114,	15,13,34,35 43,		13,	34,	
1834-436	1,87,96	96,		1,87,96	1,13,		13,		
1912-549	198,1,10,57	10	198	198,1,10,57	198,1,10,57				
1921-29	1,87,102 76	76	1,240	1,87,102 76	160,235,38 1,102,76 37,78		38		

OBJECT	2	3	4	5	6	7	8	9	10
1922-62	1,87,34,93 10,244,31 43	10,		1,10,244	15,1,13 34,10,244 31,43		51,13	34, 244,	204
1933-400	1,87,205 9.84,75,69 10,244	75	157	36,1,87,205 9,84,75 69,10,244	36,1,13,9 75,69,10 244,6		13,		
1934-63	1,87,54 34,10,244 31,24,43 215,	31,24	157,1	157,36,1,87 54,10,244 4,31,24	139,157,15, 36,1,13,54 34,10,244 2,4,24 32,43,215		13, 24 32,33 256	36,34 244 192,4 233 251	24,216
1950-613	1,87,205 69,244,10	69,	240,1,55	1,205,87 69,244,10	1,13,69 244,10		13		
1953-325	1,87,74	74	184,240,1	1,87,74	1,74			192	184,240 74
1954-388	52,203,1 87,205 9,75,69 10,244	69	52,203, 1,240	52,36,203 1,240,87 205,9,75 69,10,244 250,254	52,36,75 1,13,9,69 10,244,6 192		13	192	
2000-329	1,87,205 10,244,69	69		1,87,205 10,244,69	1,13,10,244 69		13		
2020-370	184,203,1 87,205,72 9,84,6	72	184,240,211 203,1,205 72,9,6	184,240,211 203,1,87 205,72,9 84,6,254	184,1 72,9,6,			192	184,204 72,
2039-51	87,47	47		87,47				47	

OBJECT	2	3	4	5	6	7	8	9	10
2040-374	203,191	191	203,191	203,191	59,191				
2049-368	1,87,54 9,96,43	96		1,87,54 9,96,43	1,13,54,9 96,43		13		54,43
2052-47	1,87,93 96,97,46	96		1,87,93 96,46	36,235,1 213,13,97		13,	36 97	
2054-377	1,87,9 74,	74	55,	1,87,9 74,	1,9,74				
2055-440	203,191	191,	203,191	203,191	59,191				
2058-297	1,76,133	76,		1,76,133,	1,76,133				
2058-425	1,87,72, 9,198,	72,	1,240,198	1,240,87 72,9,198,254	14,1,13,72 9,198,6		13,		
2112-407	203,181	181,	203,181, 188,240	203,181, 188,240	181,59				
2115-30	22,210,1 87,205 40,21,18 97,43,7 11,	22,95	44,161,1 211,66,205 143,66,41	22,92,44, 161,211,210 66,1,87 205,40 29,21,95 66,145,11	127,22,92 154,120,15 80,171,211 1,51,13,21 143,18,97 41,43,150 7,11,		171, 51,13,	162 211 97 41, 150 7, 11	
2116-358	203,191	191	203,191	203,191	59,191				

OBJECT	2	3	4	5	6	7	8	9	10
2128-124	66,203,1 87,205 29,83,140 134	29 140,	66,44,66,1 211,203,205 193,41,143	99,125,110 224,67,107 63,92,44 36,173,66 211,203,1 87,205,193 140,	224,63,127 92,154,120 15,14,80,36 173,130,171 211,6,1,49 13,205,29 18,140,150 134		171, 49,169 13	36,6 41 150 192	
2138-377	1,87,205, 72,9	72		1,87,205 72,9	1,72,9				
2144-362	1,87,9,74 198,	74	1,240,198	1,240,87 9,74,198	1,9,74,198				
2204-408	195	195	195	195	195				
2204-540	52,203 1,87,54 34,96,17 23,	96,73	52,203,1 17,	154,52,54 240,203,1 87,34,96 17,73,23	127,154 52,15,235 1,13,54,34 17,73,23		13	34 192,	23
2219-394	203,191 59,	191	203,191	203,191	191,59				
2222-396	191,	191,	191,	191,	59				
2225-404	203,191	191	203,191	203,191	59,191				
2226-41	1,87,9 96	95,	1,	1,87,9 96	1,13,9		13		
2227-399	197,52,1 203,87,88 9,74	74	197,52,1 203,240,87 88,	197,52,1 203,240 9,74	52,1,9 74				

OBJECT	2	3	4	5	6	7	8	9	10
2240-26	160,16,1 87,76,102 133,134,	76,		16,1,87 76,102 133,134,	160,16,14,1 76,102 133,134				
2245-328	189,1,87 74,		1,240	189,1,87 74,	189,1,74 78				189,74
2251-178	239,	239	239,258	239,258	239	239 251		239	239
2255-282	52,184,16, 203,1,76 133,134,	76,	52,184,203 1,240,133 134,	52,184,16, 203,1,240 76,133,134	52,184,16 1,76,133, 134				
2300-683	1,10,244 198,		1,240,198	1,240,10 198,	1,10,244, 198				204
2306-312	1,87,74	74		1,87,74	1,74				
2309-416	1,9,10 244,75	75		1,9,10 244,75	1,9,10,75 244,				
2310-322	52,203 1,87,88 74	74	52,203,1 240,	52,203 1,240,87 74	52,1,74				
2312-31	1,87,74	74		1,87,74	1,74				
2314-409	1,9,10 244,	10,		1,9,10,	1,9,10,244				
2315-404	1,87,9 24,10 244,	74		1,87,9 74,10,245	1,9,74 10,244,				

OBJECT	2	3	4	5	6	7	8	9	10
2321-375	1,87,9 74,244	74		1,87,9,74	1,9,74 244				
2326-477	190,203 1,87,205 75,69 10,244,17	69,	187,190 157,211, 203,1,240 205	190,157 211,203 1,240,87 205,75 10,244,17	190,157 235,13,75 69,10,244, 17		13		
2329-384	203,1,9, 87,205 84,75,69 10,244 198,	69,	187,157, 211,203,1 240,205 198	157,211, 203,1,240 87,205 9,84,75 69,10,244, 198,	157,1,13 9,75,69 10,244 198		13		
2331-24	65,202 16,66,1 87,205,12 102,133,134,	102,	65,202,1 12,	65,202, 16,66,1,87 205,102, 133,134,12	65,202, 16,1,102, 133,134, 12				
2340-567	1,10,244 17	10,		1,10,17,	1,10,244, 17				
2350-338	203,191	191	203,191	203,191	59,191				
2352-342	1,76,10 11,198,	76,	1,240 198,	1,240, 76,10,11 198,	1,76,10, 11,198				
2352-455	14,203,1 87,205 75,69,10 244,17	10	187,157 211,203,1 205,	157,211,1 203,87, 205,75 69,10,244 17	157,14,1 13,75,69 10,244 17		13		

OBJECT	2	3	4	5	6	7	8	9	10
2353-683	203,1 87,205 75,69,10 244,	69,	187,157, 211,203,205, 75,	157,211, 203,1,87 205,75, 69,10,244,	157,120 127,36,1, 13,205,75 69,10,244		13,		
2355-364	203,191	191	203,191	203,191	59,191				
2357-348	203,191	191,	203,191	203,191	59,191				
The following 3 sources are misidentified galactic stars.									
0903-57	1,40,34 114,43	114	42	1,42,40 114,	1,13,34 43,6		13,	34, 6	
1010-427	1,87,205 72	72	240,89	1,87,205 72,89	1,72				
1053-282	201,1,82 94,85,	94		1,87,94 85,	201,1,118 85,			118, 85	

TABLE III. 2

REFERENCE LIST.

1 Bolton, J.G., 1977 Unpublished listing of the Parkes Catalogue, updated to 31/10/1977.

2 Ekers, R.D., 1969 A.J.P.Ap.S.6.

3 Ekers, J.A., (ed) 1969 A.J.P.Ap.S.7.

4 Shimmins, A.J., Manchester, R.N., Harris, B.J., 1969 A.J.P.Ap.S.8.

5 Hoskins, D.G., and Murdoch, H.S., 1970 A.J.P.Ap.S.15.

6 Shimmins, A.J., and Bolton, J.G., 1972 A.J.P.Ap.S.23.

7 Slee, O.B., and Higgins, C.S., 1973, A.J.P.Ap.S.27.

8 Davies, I.M., Little, A.G., and Mills, B.Y., 1973 A.J.P.Ap.S.28.

9 Bolton, J.G., and Shimmins, A.J., 1973 A.J.P.Ap.S.30.

10 Wall, J.V., and Cannon, R.D., 1973 A.J.P.Ap.S.31.

11 Shimmins, A.J., and Bolton, J.G., 1974 A.J.P.Ap.S. 32

12 Bolton, J.G., Shimmins, A.J., Wall, J.V., and Butler, P.W., 1975 A.J.P.Ap.S. 34.

13 Gardner, F.F., Whiteoak, J.B., and Morris, D., 1975, A.J.P.Ap.S. 35.

14 Slee, O.B., and Higgins, C.S., 1975 A.J.P.Ap.S.36.

15 Wills, B.J., 1975 A.J.P.Ap.S. 38.

16 Wall, J.V., Bolton, J.G., Wright, A.E., Savage, A., and Van der Hagen, J., 1976 A.J.P.Ap.S. 39.

17 Bolton, J.G., Savage, A., and Wright, A.E., 1977 A.J.P.Ap.S. 41.

18 Slee, O.B., 1977 A.J.P.Ap.S.43.

19 Savage, A., Bolton, J.G., and Wright, A.E., 1977 A.J.P.Ap.S. 44.

20 Bolton, J.G., Gardner, F.F., and Mackey, M.B., 1964 A.J.P. 17 340.

21 Bolton, J.G., Clarke, M.E., and Ekers, R.D. 1965 A.J.P. 18 627

22 Ekers, R.D., and Bolton, J.G., 1965 A.J.P. 18 669

23 Westerlund, B.E., and Smith, L.F., 1966 A.J.P. 19 181

24 Kellermann, K.I., 1966 A.J.P. 19 195

25 Bolton, J.G., and Ekers, J., 1966 A.J.P. 19 275

26 Bolton, J.G., and Ekers, J., 1966 A.J.P. 19 559

27 Shimmins, A.J., Clarke, M.E., and Ekers, R.D., 1966 A.J.P. 19 649

28 Shimmins, A.J., Day, G.A., Ekers, R.D., and Cole, D.J., 1966 A.J.P. 19 837

29 Bolton, J.G., and Ekers, J., 1967 A.J.P. 20 109

30 Bolton, J.G., Shimmins, A.J., and Merkelijn, J., 1968 A.J.P. 21 81

31 Sutton, J.M. 1968 A.J.P. 21 221

32 Morris, D., and Whiteoak, J.B., 1968 A.J.P. 21 493

33 Gardner, F.F., Morris, D., and Whiteoak, J.B. 1969 A.J.P. 22 79

34 Ekers, R.D. 1970 A.J.P. 23 217

35 Hunstead, R.W., Lasker, B.M., Mintz, B., and Smith, M.G., 1971 A.J.P. 24 601

36 Shimmins, A.J., and Wall, J.V., 1973 A.J.P. 26 93

37 Medd, W.J., Andrew, B.H., Harvey, G.A., and Locke, J.L., 1972 Mem.R.A.S. 77 109.

38 Altschuler, D.R., and Wardle, J.F.C., 1976 Mem.R.A.S. 82 1

39 Cannon, R.D., Penston, M.V., and Brett, R.A., 1971 M.N.R.A.S. 152 79

40 Hunstead, R.W., 1971 M.N.R.A.S. 152 277

41 Miley, G.K., 1971 N.N.R.A.S. 152 477

42 Tritton, K.P., 1971 M.N.R.A.S. 155 1P

43 Hunstead, R.W., 1972 M.N.R.A.S. 157 367

44 Evans, A., 1972 M.N.R.A.S. 160 407

45 Conway, R.G., and Stannard, D., 1972 M.N.R.A.S. 160 31P

46 Tritton, K.P., and Whitworth, D.P.D., 1973 M.N.R.A.S. 165 253

47 Tritton, K.P., and Schilizzi, R.T., 1973 M.N.R.A.S. 165 245

48 Fanaroff, B.L., 1974 M.N.R.A.S. 166 1P

49 Haves, P., Conway, R.G., and Stannard, D., 1974 M.N.R.A.S. 169 117

50 Selmes, R.A., Tritton, K.P., and Wordsworth, R.W., 1975 M.N.R.A.S. 170 15

51 Haves, P., 1975 M.N.R.A.S. 173 553

52 Browne, I.W.A., Savage, A., and Bolton, J.G., 1975 M.N.R.A.S. 173 87P.

53 Savage, A., 1976 M.N.R.A.S. 174 259.

54 Savage, A., Bolton, J.G., and Wright, A.E., 1976. M.N.R.A.S. 175, 517.

55 Savage, A., Browne, I.W.A., and Bolton, J.G., 1976 M.N.R.A.S. 177 77P.

56 Baldwin, J.A., 1977 M.N.R.A.S. 178 67P

57 Savage, A., Bolton, J.G., and Wright, A.E., 1977 M.N.R.A.S. 179, 135.

58 Browne, I.W.A., and Savage, A., 1977 M.N.R.A.S. 179 65P.

59 Murdoch, H.S., and Crawford, D.F., 1977 M.N.R.A.S. 180 41P.

60 Whelan, J.A.J., Carswell, R.F., and Smith, M.G., 1977 M.N.R.A.S. 181 81P.

61 Hawkins, M.R.S., 1978 M.N.R.A.S. 182 361.

62 Penston, M.V., and Cannon, R.D. 1970 R.O.B. 159.

63 Basu, D., 1973 Observatory 93 184.

64 Bolton, J.G., 1968 P.A.S.P. 80 5.

65 Andrew, B.H., Van den Bergh, S., Conklin, E.K., and Kraus, J.D., 1971 P.A.S.P. 83 87.

66 De Veny, J.B., Osborn, W.H., and Janes, K. 1971 P.A.S.P. 83 611.

67 Grandi, S.A., and Tifft, W.G., P.A.S.P. 86 873.

68 Grahl, B.H., and Grewing, M., 1969 Ap.Lett. 4 107.

69 Shimmins, A.J., Bolton, J.G., Peterson, B.A., and Wall, J.V., 1971 Ap.Lett. 8 139.

70 De Young, D.S., 1971 Ap.Lett. 9 43.

71 Kellermann, K.I., and Pauliny-Toth, I.I.K., 1971 Ap.Lett. 8 153.

72 Peterson, B.A., and Bolton, J.G., 1972 Ap.Lett. 10 105

73 Tritton, K.P., and Nicolson, G.D. 1972 Ap.Lett. 11 187

74 Peterson, B.A., and Bolton, J.G., 1973 Ap.Lett. 13 187

75 Wall, J.V., 1973 Ap.Lett. 15 101.

76 Peterson, B.A., Bolton, J.G., and Shimmins, A.J., 1973 Ap.Lett. 15 109.

77 Peterson, B.A., Bolton, J.G., and Savage, A., 1976 Ap.Lett. 17 137.

78 Nicolson, G.D., 1978 Ap.Lett. 19 107

79 Capps, R.W., and Knacke, R.F., 1978 Ap.Lett. 19 113.

80 Gorshkov, A.G., and Konnikova, V.K., 1976 Soviet Astronomy 19 716.

81 Braccesi, A., Ceccarelli, M., Fanti, R., Gelato, G., Giovannini, C., Harris, D., Rosatelli, C., Sinigaglia, G., and Volders, L., 1965 Nuovo Cimento 40B 267.

82 Lari, C., and Setti, G., 1967 Nuovo Cimento 52B 507

83 Véron, M.P., and Véron, P., 1973 Ast.Ap. 28 319.

84 Véron, M.P., and Véron, P., 1975 Ast.Ap. 42 1.

85 Véron, P.M., Véron, P., Adgie, R.L. and Gent, H., 1976 Ast.Ap. 47 401.

86 Weiler, K.W., and Raimond, E., 1976 Ast.Ap.52 397.

87 Véron, M.P., and Véron, P., 1974 Ast.Ap.Suppl. 18 309.

88 Véron, M.P., and Véron, P., 1977 Ast.Ap.Suppl. 29 149

89 Adam, G., 1978 Ast.Ap.Suppl. 31 151

90 Medd, W.J., Locke, J.L., Andrew, B.H., and Van den Bergh, S. 1968 A.J. 73 293.

91 Pauliny-Toth, I.I.K., and Kellermann, K.I., 1968 A.J. 73 953.

92 Westerlund, B.E., and Wall, J.V., 1969 A.J. 74 335.

93 Bajaja, E., 1970 A.J. 75 669.

94 Moseley, G.F., Brooks, C.C., and Douglas, J.N., 1970 A.J. 75 1015.

95 Lü, P.K., 1970 A.J. 75 1161.

96 Lü, P.K., 1970 A.J. 75 1164.

97 Fomalont, E.B., and Moffet, A.T., 1971 A.J. 76 5.

98 Stull, M.A. 1971 A.J. 76 1.

99 Angione, R.J. 1971 A.J. 76 25.

100 Angione, R.J., 1971 A.J. 76 412.

101 Bell, M.B., Seaquist, E.R., and Braun, L.D., 1971 A.J. 76 524.

102 Radivich, M.M., and Kraus, J.D., 1971 A.J. 76 683.

103 Stull, M.A., 1972 A.J. 77 13.

104 Jauncey, D.L., and Hunstead, R.W., 1972 A.J. 77 345

105 Gearhart, M.M., Lund, J.M., Frantz, D.J., and Kraus, J.D., 1972 A.J. 77 557.

106 Berge, G.L., and Seielstad, G.A. 1972 A.J. 77 810.

107 Lü, P.K. 1972 A.J. 77 829.

108 Douglas, J.N., Bash, F.N., Ghigo, F.D., Moseley, G.F., and Torrence, G.W., 1973 A.J. 78 1.

109 Dent, W.A., and Hobbs, R.W., 1973 A.J. 78 163.

110 Angione, R.J., 1973 A.J. 78 353.

111 Wills, B.J., Wills, D., and Douglas, J.N., 1973 A.J. 78 521.

112 Bignell, R.C., and Seaquist, E.R., 1973 A.J. 78 536.

113 Bignell, R.C., 1973 A.J. 78 557.

114 Lü, P.K., 1974 A.J. 79 453.

115 Adgie, R.L., 1974 A.J. 79 846.

116 Johnson, K.H., 1974 A.J. 79 1006.

117 Dent, W.A., Kapitzky, J.E., and Kojoian, G., 1974 A.J. 79 1232.

118 Bash, F.N., Cotton, W.D., and Douglas, J.N., 1974 A.J. 79 1341.

119 Miller, H.R., Clonts, S.L., and Folsom, G.H., 1974 A.J. 79 1352.

120 Kraus, J.D., and Gearhart, M.M., 1975 A.J. 80 1.

121 Seielstad, G.A., and Berge, G.L., 1974 A.J. 80 271.

122 Sharp, J.R., and Bash, F.N., 1975 A.J. 80 335.

123 Cotton, W.D., Owen, D.N., and Ghigo, F.D., A.J. 80 353.

124 McGimsey, B.Q., Smith, A.G., Scott, R.L., Leacock, R.J., Edwards, P.L., Hackney, R.L., and Hackney K.R., 1975 A.J. 80 895.

125 Scott, R.L., Leacock, R.J., McGimsey, B.Q., Smith, A.G., Edwards, P.L., Hackney, K.R., and Hackney, R.L., 1976 A.J. 81 7.

126 Pomphrey, R.B., Smith, A.G., Leacock, R.J., Olsson, C.N., Scott, R.L., Pollock, J.T., Edwards, P., and Dent, W.A., 1976 A.J. 81 489.

127 Pacht, E., 1976 A.J. 81 489.

128 Kesteven, M.J.L., Bridle, A.H., and Jauncey, D.L., 1976 A.J. 81 929.

129 Wills, B.J., 1976 A.J. 81 1031.

130 Bridle, A.H., Kesteven, M.J.L., and Brandie, G.W., 1977 A.J. 82 21.

131 Anguita, C., and Pedreros, M., 1977 A.J. 82 102.

132 Kronberg, P.P., and Wardell, J.F.C., 1977 A.J. 82 688.

133 Condon, J.J., Hicks, P.D., and Jauncey, D.L., 1977 A.J. 82 692.

134 Condon, J.J., Jauncey, D.L., and Wright, A.E. 1978 A.J. 83 1036.

135 Nieto, J.L., 1978 A.J. 83 1141.

136 Westerlund, B.E., and Stokes, N.R., 1966 Ap.J. 145 354.

137 Burbidge, E.M., and Kinman, T.D., 1966 Ap.J. 145 654.

138 Bolton, J.G., and Kinman, T.D., 1966 Ap.J. 145 951.

139 Kellermann, K.E., 1966 Ap.J. 146 621.

140 Kinman, T.D., Bolton, J.G., Clarke, R.W., and Sandage, A., 1967 Ap.J. 147 848.

141 Appenzeller, I., and Hiltner, W.A., 1967 Ap.J. 149 L17.

142 Kellermann, K.I., and Pauliny-Toth, I.I.K., 1968 Ap.J. 152 639.

143 Searle, L., and Bolton, J.G., 1968 Ap.J. 154 L101.

144 Locke, J.L., Andrew, B.H., and Medd, W.J., 1969 Ap.J. 157 L81.

145 Oke, J.B., Neugebauer, G., and Becklin, E.E., 1970 Ap.J. 159 341.

146 Kraus, J.D., and Andrew, B.H., 1970 Ap.J. 159 L41.

147 Eggen, O.J., 1970 Ap.J. 159 L95.

148 Kellerman, K.I., Clark, B.G., Jauncey, D.L., Cohen, M.H., Shaffer, D.B., Moffet, A.T., and Gulkis, S., 1970 Ap.J. 161 803.

149 Kristian, J., and Sandage, A., 1970 Ap.J. 162 391.

150 Macdonald, G.H., and Miley, G.K. 1971 Ap.J. 164 237.

151 Wills, B.J., Kraus, J.D., and Andrew, B.H., 1971 Ap.J. 169 L87.

152 Bond, H.E. 1971 Ap.J. 167 L79.

153 Kellermann, K.I., Jauncey, D.L., Cohen, M.H., Schaffer, B.B., Clark, B.G., Broderick, J., Rönnäng, B., Rydbeck, O.E.H., Matveyenko, L., Moiseyev, I., Vitkevitch, V.V., Cooper, B.F.C., and Batchelor, R., 1971 Ap.J. 169 1.

154 Wills, B.J., 1971 Ap.J. 169 221.

155 Shen, B.S.P., Usher, P.D., and Barrett, J.W., 1972 Ap.J. 171 457.

156 Broderick, J.J., Kellermann, K.I., Shaffer, D.B., and Jauncey, D.L., 1972 Ap.J. 172 299.

157 Peterson, B.A., and Bolton, J.G., 1972 Ap.J. 173 L19.

158 Strittmatter, P.A., Serkowski, K., Carswell, R., Stein, W.A., Merrill, K.M., and Burbidge, E.M., 1972 Ap.J. 175 L7.

159 Rieke, G.H., 1972 Ap.J. 176 L61.

160 Conklin, E.K., Andrew, B.H., Wills, B.J., and Kraus, J.D., 1972 Ap.J. 177 303.

161 Sandage, A., 1972 Ap.J. 178 25.

162 Kristian, J., 1973 Ap.J. 179 L61.

163 Andrew, B.H., Ehman, J.R., Gearhart, M.R., and Kraus, J.D. 1973 Ap.J. 185 137.

164 Eggen, O.J., 1973 Ap.J. 186 L1.

165 Adams, T.F., 1974 Ap.J. 188 463.

166 Liller, W., 1974 Ap.J. 189 L101.

167 Strittmatter, P.A., Carswell, R.F., Gilbert, G., and Burbidge, E.M., 1974 Ap.J. 190 509.

168 Elliott, J.L., and Shapiro, S.L., 1974 Ap.J. 192 L3.

169 Vallée, J.P., and Kronberg, P.P., 1974 Ap.J. 193 303.

170 Disney, M.J., 1974 Ap.J. 193 L103.

171 Wardle, J.F.C., and Kronberg, P.P., 1974 Ap.J. 194 249.

172 Disney, M.J., Peterson, B.A., and Rodgers, A.W., 1974 Ap.J. 194 L79.

173 Usher, P.D., 1975 Ap.J. 198 L57.

174 Pollock, J.T., 1975 Ap.J. 198 L53.

175 Liller, M.H., and Liller, W., 1975 Ap.J. 199 L133.

176 Grindlay, J.E., Helmken, H.F., Hanbury Brown, R., Davis, J., and Allen, L.R., 1975 Ap.J. 201 82.

177 Burbidge, E.M., and Burbidge, G.R., 1975 Ap.J. 202 287.

178 Smith, M.G., 1975 Ap.J. 202 591.

179 Tapia, S., Craine, E.R., and Johnson, K., 1976 Ap.J. 203 291.

180 Kinman, T.D., 1976 Ap.J. 205 1.

181 Smith, M.G., 1976 Ap.J. 206 L125.

182 Margon, B., Bowyer, S., Jones, T.W., Davidsen, A., Mason, K.O., and Sanford, P.W., 1976 Ap.J. 207 359.

183 Ulmer, M.P., and Murray, S.S. 1976 Ap.J. 207 364.

184 Peterson, B.A., Jauncey, D.L., Wright, A.E., and Condon, J.J., 1976 Ap.J. 207 L5.

185 Peterson, B.A., Rodgers, A.W., Wampler, E.J., and Disney, M.J., 1976 Ap.J. 207 L17.

186 Weedman, D.W., 1976 Ap.J. 208 30.

187 Green, R.F., and Richstone, D.O., 1976 Ap.J. 208 639.

188 Osmer, P.S., and Smith, M.G., 1976 Ap.J. 210 267.

189 Bolton, J.G., Peterson, B.A., Wills, B.J., and Wills, D., 1976 Ap.J. 210 L1.

190 Wright, A.E., Jauncey, D.L., Peterson, B.A., and Condon, J.J., 1977 Ap.J.211 L115.

191 Osmer, P.S., and Smith, M.G., 1977 Ap.J. 213 607.

192 Gubbay, J., Legg, A.J., Robertson, D.S., Nicolson, G.D., Moffet, A.T., and Shaffer, D.B., 1977 Ap.J. 215 20.

193 Phillips, M.M., 1977 Ap.J. 215 746.

194 Visvanathan, N., and Griersmith, D., 1977 Ap.J. 215 759.

195 Osmer, P.S., and Smith, M.G., 1977 Ap.J. 215 L47.

196 Carswell, R.F., Smith, M.G., and Whelan, J.A.J., 1977 Ap.J. 216 351.

197 Hoag, A.A., and Smith, M.G., 1977 Ap.J. 217 362.

198 Jauncey, D.L., Wright, A.E., Peterson, B.A., and Condon, J.J., 1978 Ap.J. 219 L1.

199 McGimsey, B.Q., and Miller, H.R., 1978 Ap.J. 219 387

200 Stockton, A., 1978 Ap.J. 223 747.

201 Gearhart, M.R., Kraus, J.D., and Andrew, B.H., 1976 Ap.J. Suppl. 30 337.

202 Wills, D., and Wills, B.J., 1976 Ap.J. Suppl. 31 143

203 Burbidge, G.R., Crowne, A.H., and Smith, H.E., 1977 Ap.J. Suppl. 33 113.

204 Duus, A., and Newell, B., 1977 Ap.J.Suppl. 35 209.

205 Barbieri, C., and Zambon, M., 1977 Unpublished Catalogue of Quasi Stellar Objects.

206 Stockman, H.S. Preprint.

207 Stein, W.A., O'Dell, S.L., and Strittmatter, P.A., 1976 Ann.Rev.Ast. and Ap. 14 173.

208 Peterson, B.A., Wright, A.E., Jauncey, D.L., and Condon, J.J. 1978 Preprint.

209 Kinman, T.D., 1975 in "Variable Stars and Stellar Evolution" IAU Symposium 67. ed V.E. Sherwood and L. Plaut p573.

210 Barbieri, C., and De Felici, F., 1966. Pub. Dell'Osservatorio Astronomico di Padova Number 133.

211 Setti, G., and Woltjer, L., 1973. Ann.N.Y.Acad.Sci. 224 8.

212 Ashbrook, M.D., 1942 Harvard Annals 109 Number 7.

213 McAdam, W.B., and Turtle, A.J., 1978 private communication.

214 Andrew, B.H., MacLeod, J.M., and Feldman, P.A., 1979 I.A.U. Circ. 3328.

215 Bolton, J.G., Gardner, F.F., and Mackey, M.B., 1963 Nature 199 682.

216 Shklovsky, J. 1965 Nature 206 176.

217 Palmer, H.P., Rowson, B., Anderson, B., Donaldson, W., Miley, G.K., Gent, H., Adgie, R.L., Slee, O.B., and Crowther, J.H., 1967 Nature 213 789.

218 Gubbay, J., Legg, A.J., Robertson, D.S., Moffet, A.T., and Seidel, B., 1969 Nature 222 730.

219 Burbidge, G.R., and Burbidge, E.M., 1969 Nature 222 735.

220 Hunter, J.H., and Lü, P.K., 1969 Nature 223 1045.

221 Gubbay, J., Legg, A.J., Robertson, D.S., Moffet, A.T., Ekers, R.D., and Seidel, B., 1969 Nature 224 1094.

222 Stull, M.A., 1970 Nature 225 832.

223 Ross, H.N., 1970 Nature 226 431.

224 Folsom, G.H., Smith, A.G., Hackney, R.L., and Hackney, K.R., 1971 Nature P.S. 230 199.

225 Biraud, F., 1971 Nature 232 178

226 Hunstead, R.W., 1971 Nature 233 401.

227 Frye, G.M., Albats, P.A., Zych, A.D., Staib, J.A., Hopper, V.D., Rawlinson, W.R., Thomas, J.A., 1971 Nature 233 466.

228 Rodgers, A.W., 1971 Nature P.S. 233 75.

229 Nicolson, G.D., 1971 Nature P.S. 233 155.

230 Kapahi, V.K., 1971 Nature P.S. 234 49.

231 Ananthakrishnan, S., Pramesh Rao, A., and Bhandari, S.M., 1972 Nature P.S. 235 167.

232 Andrew, B.H., Medd, W.J., Harvey, G.A., and Locke, J.L., 1972 Nature 236 445.

233 Roberts, J.A., Ribes, J.C., Murray, J.D., and Cooke, D.J., 1972 Nature P.S. 236 3.

234 Hall, D.L., and Usher, P.D. 1973 Nature P.S. 241 31.

235 Nicolson, G.D., 1973 Nature P.S. 241 90.

236 Carswell, R.F., Strittmatter, P.A., Disney, J.J., Hoskins, D.G., and Murdoch, H.S., 1973 Nature P.S. 246 89.

237 Shapiro, S.L., and Elliott, J.L., 1974 Nature 250 111.

238 Usher, P.D., Kolpanen, D.R., and Pollock, J.T., 1974 Nature 252 365.

239 Ricker, G.R., Clarke, G.W., Doxsey, R.E., Dower, R.G., Jernigan, J.G., Delvaille, J.P., MacAlpine, G.M., and Hjellming, R.M., 1978 Nature 271 35.

240 Bolton, J.G., 1977 Private Communication.

241 Kurochkin, N.E., 1973 I.A.U. Circ. 2593.

242 Schwartz, D.S., Doxsey, R.E., Griffiths, R.E. Johnston, M.D., and Schwartz, J., 1979 Preprint.

243 Hoskins, D.G., Murdoch, H.S., Adgie, R.L., Crowther, J.H., and Gent, H., 1974. M.N.R.A.S. 166 235.

244 Shimmins, A.J., 1971 A.J.P. Ap.S. 21.

245 Wall, J.V., 1974 in Proceedings of the ESO/SRC/CERN Conference on Research Programmes for the New Large Telescopes ed. A. Reiz p265.

246 Riegler, G.R., Agrawal, P.C., and Rosker, M.J., 1978 I.A.U. Circ. 3261.

247 Fosbury, R.A.E., and Disney, M.J., 1976 Ap.J. 207 L75.

248 Burbidge, G.R., and O'Dell, S.L., 1972 Ap.J. 178 583.

249 Hunstead, R.W., 1972 Ap.Lett. 12 193.

250 Gilmore, G., 1978 I.A.U. Circ. 3247.

251 Soifer, B.T., Neugebauer, G., and Matthews, K., 1979 Nature 278 231.

252 Gilmore, G., 1978 Paper presented at I.A.U. Regional Meeting, Asian-South Pacific Region, Wellington, N.Z. December 1978 (Proceedings in press).

253 Gilmore, G., 1978 at I.A.U. Colloquium 46 (in press).

254 Gilmore, G., 1979 M.N.R.A.S. in press.

255 Gubbay, J.S., Legg, A.J., Robertson, D.S., Craske, N., and Nicolson, G.D., 1971 A.J. 76 965.

256 Pacholczyk, A.G., and Swihart, T.L., 1974. Ap.J. 192 591.

257 Altschuler, D.R., and Wardle, J.F.C., 1975 Nature 255 306.

258 Canizares, C.R., McClintock, J.E., and Ricker, G.R., 1978 Ap.J. 226 L1.